National Library
of Canada

Acquisitions and
Bibliographic Services Branch

395 Wellington Street
Ottawa, Ontario
K1A 0N4

Bibliothèque nationale
du Canada

Direction des acquisitions et
des services bibliographiques

395, rue Wellington
Ottawa (Ontario)
K1A 0N4

Your file Votre référence

Our file Notre référence

NOTICE

The quality of this microform is heavily dependent upon the quality of the original thesis submitted for microfilming. Every effort has been made to ensure the highest quality of reproduction possible.

If pages are missing, contact the university which granted the degree.

Some pages may have indistinct print especially if the original pages were typed with a poor typewriter ribbon or if the university sent us an inferior photocopy.

Reproduction in full or in part of this microform is governed by the Canadian Copyright Act, R.S.C. 1970, c. C-30, and subsequent amendments.

AVIS

La qualité de cette microforme dépend grandement de la qualité de la thèse soumise au microfilmage. Nous avons tout fait pour assurer une qualité supérieure de reproduction.

S'il manque des pages, veuillez communiquer avec l'université qui a conféré le grade.

La qualité d'impression de certaines pages peut laisser à désirer, surtout si les pages originales ont été dactylographiées à l'aide d'un ruban usé ou si l'université nous a fait parvenir une photocopie de qualité inférieure.

La reproduction, même partielle, de cette microforme est soumise à la Loi canadienne sur le droit d'auteur, SRC 1970, c. C-30, et ses amendements subséquents.

Canada

The University of Alberta

Flow in Ice Covered Channels

by ©

Nathan Philip Schmidt

A thesis submitted to the Faculty of Graduate Studies and Research in partial fulfillment of the requirements for the degree of Master of Science

Department of Civil Engineering

Edmonton, Alberta

Fall,1992

National Library
of Canada

Canadian Theses Service

Ottawa, Canada
K1A 0N4

Bibliothèque nationale
du Canada

Service des thèses canadiennes

The author has granted an irrevocable non-exclusive licence allowing the National Library of Canada to reproduce, loan, distribute or sell copies of his/her thesis by any means and in any form or format, making this thesis available to interested persons.

The author retains ownership of the copyright in his/her thesis. Neither the thesis nor substantial extracts from it may be printed or otherwise reproduced without his/her permission.

L'auteur a accordé une licence irrévocable et non exclusive permettant à la Bibliothèque nationale du Canada de reproduire, prêter, distribuer ou vendre des copies de sa thèse de quelque manière et sous quelque forme que ce soit pour mettre des exemplaires de cette thèse à la disposition des personnes intéressées.

L'auteur conserve la propriété du droit d'auteur qui protège sa thèse. Ni la thèse ni des extraits substantiels de celle-ci ne doivent être imprimés ou autrement reproduits sans son autorisation.

ISBN 0-315-77112-7

Canadä

The University of Alberta

RELEASE FORM

NAME OF AUTHOR: Nathan Philip Schmidt
TITLE OF THESIS: Flow in Ice Covered Channels
DEGREE: Master of Science
YEAR THIS DEGREE GRANTED: 1992

Permission is hereby granted to the University of Alberta to reproduce single copies of this thesis and to lend or sell such copies for private, scholarly or scientific research purposes only.

The author reserves all other publication and other rights in association with the copyright in the thesis, and except as hereinbefore provided neither the thesis nor any substantial portion thereof may be printed or otherwise reproduced in any material form whatever without the author's prior written permission.

Nathan Schmidt

Nathan Philip Schmidt
8312 - 42 Avenue
Edmonton, Alberta
Canada T6K 1E1

October 6, 1992
Submission Date

The University of Alberta

Faculty of Graduate Studies and Research

The undersigned certify that they have read, and recommended to the Faculty of Graduate Studies and Research for acceptance, a thesis entitled Flow in Ice Covered Channels submitted by Nathan Philip Schmidt in partial fulfillment of the requirements for the degree of Master of Science in Water Resources Engineering.

R. Gerard - Supervisor (deceased)

N. Rajaratnam - Supervisor

Faye Hicks

F. Hicks - Committee Member

John Shaw

J. Shaw - Committee Member

ABSTRACT

This study reviews previous studies on the topic of flow in ice covered channels, and presents the results of experiments done to examine the phenomenon. Measurements were made on floating cover and open channel flows in a laboratory flume using various combinations of rough and smooth boundaries. A Preston tube apparatus was used to gather velocity profiles and provide boundary shear velocities. Roughness characteristics of the bed and cover materials were also examined. The data set was then applied to equations presented in previous studies to examine their accuracy.

The Preston tube technique for determining boundary shears was found to be quite useful. Boundary shear velocities were found to be substantially higher for the rough boundary than for the smooth in runs combining these surfaces. For flows with similar cover and bed roughnesses, the zero shear plane was found to be coincident with the plane of maximum velocity, at the center of the velocity profile. For flows with dissimilar boundary roughnesses, the zero shear plane was found to be closer to the smooth boundary than the plane of maximum velocity. Also, for this situation, the average velocity in the smooth boundary zone was found to be higher than that in the rough boundary zone.

Equations for determining composite channel roughnesses were examined, with several found to provide reasonable accuracy. Other equations developed to quantify other flow characteristics were found to agree well with the experimental data.

ACKNOWLEDGEMENTS

The author would like to express his deepest gratitude to Dr. R. Gerard who provided great support and guidance even to his last days. His example was always one to follow, and his dedication to his work even while coping with illness was inspiring. He would also like to thank Dr. N. Rajaratnam who made the transition between supervisors as smooth as was possible and provided new perspective on the study.

The author thanks S. Lovell, M. Jasek and A. Mainali for help given in supplying and setting up materials and equipment and for help in analysis and presentation.

Financial support for this study was provided by the Natural Sciences and Engineering Research Council in the form of a postgraduate scholarship, and is greatly appreciated.

TABLE OF CONTENTS

Page

List of Tables ....
List of Figures ....
List of Plates ....
List of Symbols ....

1.0 Introduction 1
  1.1 Theoretical Analyses of Ice Covered Flows 2
    1.1.1 Pavlovskiy (1931) 2
    1.1.2 Lotter (1933) 6
    1.1.3 Belokon (1938) 8
    1.1.4 Sabaneev (1948) 9
    1.1.5 Levi (1948) 10
    1.1.6 Konovalov (1952) 13
    1.1.7 Trufanov (1954) 15
    1.1.8 Shiperko (1961) 16
    1.1.9 Dul'nev (1962) 17
    1.1.10 Carey (1966) 17
    1.1.11 Larsen (1966) 19
    1.1.12 Hancu (1967) 21
    1.1.13 Yu, Graf and Levine (1968) 23
    1.1.14 Summary 24
  1.2 Experimental Investigations into Covered Flows .. 25
    1.2.1 Hanjalic and Launder (1972) 26
    1.2.2 Ismail and Davar (1978) 27
    1.2.3 Gogus and Tatinclaux (1980, 1981) 28
    1.2.4 Lau and Krishnappan (1981, 1982) 30
    1.2.5 Calkins (1982) 31
    1.2.6 Gerard (1982) 31
    1.2.7 Tatinclaux and Gogus (1983) 32
    1.2.8 Chee (1985) 35
    1.2.9 Hendriksen and Davar (1986) 37
    1.2.10 Wuebben (1986) 37
    1.2.11 Gerard and Beltaos (1987) 38
    1.2.12 Summary 39
  1.3 Goals of This Study 40

2.0 Experimental Apparatus and Procedure 42
  2.1 Experimental Apparatus 43

2.2 Experimental Procedure 45
    2.2.1 Discharge Measurement 47
    2.2.2 Velocity Profile Measurement 47
    2.2.3 Flume Surveys 50
    2.2.4 Boundary Shear Measurement 50
    2.2.5 Roughness Measurement 53
    2.2.6 Summary of Experiments 55

3.0 Analysis of Experimental Results 56
  3.1 Verification of Fully Developed Flow 56
  3.2 Averaging of Velocity Profiles 58
  3.3 Location of Virtual Origin 92
  3.4 Average Velocities 93
  3.5 Shear Stresses 96
  3.6 Boundary Roughnesses 100
  3.7 Summary of Results 113

4.0 Application of Experimental Data to Previous Work 116
  4.1 Composite Roughness Equations 116
    4.1.1 Equal Bed and Cover Roughnesses 116
    4.1.2 Unequal Bed and Cover Roughnesses 119
    4.1.3 Summary 121
  4.2 Comparison with Selected Empirical Equations 121
  4.3 Summary 126

5.0 Conclusions and Recommendations 128
  5.1 Conclusions 128
  5.2 Recommendations 132

References 133

Additional Reading 137

Appendix A - The Preston Tube Technique for Boundary Shear Measurement 138
Appendix B - Velocity Profile Data After Averaging 147
Appendix C - Determinations of Bed and Energy Slopes 178

LIST OF TABLES

Table Page

3.1 Development lengths to test section 57
3.2 Average velocities and ratios of zones 95
3.3 Calculated boundary shears 97
3.4 Effect of cover on bed shear 99
3.5 Calculated smooth boundary viscous roughnesses 101
3.6 Calculated rough boundary sand grain roughnesses 107
4.1 Predicted and experimental composite roughnesses (like boundaries) 117
4.2 Predicted and experimental composite roughnesses (unlike boundaries) 119
4.3 Performance of equation 1.81 122
4.4 Performance of equation 1.83 123
4.5 Performance of equation 1.95 125
C.1 Bed and energy slopes 180

LIST OF FIGURES

Figure Page

1.1 Parameters influencing ice covered flows 3
2.1 Experimental flume 44
3.1 Average velocity profiles for run S/R/70 at test section and 1.0 m upstream of test section 59
3.2 Average velocity profiles for run S/R/40 before and after adjustment 61
3.3(a) Averaged velocity profiles for runs S/O/10, 20, 40 and 70 62
3.3(b) Component velocity profiles for run S/O/10 63
3.3(c) Component velocity profiles for run S/O/20 64
3.3(d) Component velocity profiles for run S/O/40 65
3.3(e) Component velocity profiles for run S/O/70 66
3.4(a) Averaged velocity profiles for runs R/O/10, 20, 40 and 70 67
3.4(b) Component velocity profiles for run R/O/10 68
3.4(c) Component velocity profiles for run R/O/20 69
3.4(d) Component velocity profiles for run R/O/40 70
3.4(e) Component velocity profiles for run R/O/70 71
3.5(a) Averaged velocity profiles for runs S/S/10, 20, 40 and 70 72
3.5(b) Component velocity profiles for run S/S/10 73
3.5(c) Component velocity profiles for run S/S/20 74
3.5(d) Component velocity profiles for run S/S/40 75
3.5(e) Component velocity profiles for run S/S/70 76
3.6(a) Averaged velocity profiles for runs R/R/10, 20, 40 and 70 77
3.6(b) Component velocity profiles for run R/R/10 78
3.6(c) Component velocity profiles for run R/R/20 79
3.6(d) Component velocity profiles for run R/R/40 80
3.6(e) Component velocity profiles for run R/R/70 81
3.7(a) Averaged velocity profiles for runs S/R/10, 20, 40 and 70 82
3.7(b) Component velocity profiles for run S/R/10 83
3.7(c) Component velocity profiles for run S/R/20 84
3.7(d) Component velocity profiles for run S/R/40 85
3.7(e) Component velocity profiles for run S/R/70 86
3.8(a) Averaged velocity profiles for runs R/S/10, 20, 40 and 70 87
3.8(b) Component velocity profiles for run R/S/10 88

3.8(c) Component velocity profiles for run R/S/20 89
3.8(d) Component velocity profiles for run R/S/40 90
3.8(e) Component velocity profiles for run R/S/70 91
3.9 Determination of depth of virtual origin 94
3.10 Distribution of shear stress across channel depth 100
3.11(a) Semi-logarithmic velocity profiles for S/O/bed runs 102
3.11(b) Semi-logarithmic velocity profiles for S/S/bed runs 103
3.11(c) Semi-logarithmic velocity profiles for S/S/cover runs 104
3.11(d) Semi-logarithmic velocity profiles for S/R/bed runs 105
3.11(e) Semi-logarithmic velocity profiles for R/S/cover runs 106
3.12(a) Semi-logarithmic velocity profiles for R/O/bed runs 108
3.12(b) Semi-logarithmic velocity profiles for R/R/bed runs 109
3.12(c) Semi-logarithmic velocity profiles for R/R/cover runs 110
3.12(d) Semi-logarithmic velocity profiles for R/S/bed runs 111
3.12(e) Semi-logarithmic velocity profiles for S/R/cover runs 112
3.13 Variation of measured roughness with R/k_{mean} 113
4.1 Predicted vs. experimental composite roughnesses (like boundaries) 118
4.2 Predicted vs. experimental composite roughnesses (unlike boundaries) 120
4.3 Performance of equation 1.81 123
4.4 Performance of equation 1.82 124
4.5 Performance of equation 1.95 125

LIST OF PLATES

Plate Page

2.1 3M Nomad cushion plus floor matting used to simulate ice cover and bed roughness 42
2.2 Experimental flume in T. Blench Hydraulics Laboratory at the University of Alberta 43
2.3 Velocity measurement apparatus 48
2.4 Typical chart recorder output 49

LIST OF SYMBOLS

A	-	flow cross sectional area (L^2)
a	-	wetted perimeter ratio (-)
	-	intermediate variable in Larsen analysis
B	-	top width of channel (L)
b	-	intermediate variable in Larsen analysis
C	-	Chezy coefficient ($L^{1/2}/T$)
C_*	-	dimensionless Chezy coefficient (-)
D_p	-	diameter of Preston tube (L)
D^+	-	intermediate value in Preston tube calculations (-)
f	-	Darcy-Weisbach friction factor (-)
g	-	gravitational constant (L/T^2)
H	-	total distance between boundaries (L)
H_e	-	depth of water: bed to free surface (L)
h	-	roughness height (L)
K	-	constant describing character of ice cover (-)
k	-	boundary roughness (L)
k_m	-	mean boundary roughness (L)
k_s	-	equivalent sand grain roughness (L)
k_v	-	viscous roughness (L)
m	-	Bazin-Boussinesq coefficient (-)
n	-	Manning coefficient (-)
P	-	wetted perimeter (L)
	-	piezometric head (L)
Q	-	discharge (L^3/T)
q	-	unit discharge (L^2/T)

R - hydraulic radius (L)
R_e - Reynolds number based on hydraulic radius (-)
R_H - Reynolds number based on flow depth (-)
r - pipe radius (L)
S_f - friction slope of channel (-)
S_0 - bed slope of channel (-)
u - flow velocity at a given streamline (L/T)
u' - turbulent component of flow velocity (L/T)
u_* - shear velocity (L/T)
V - average sectional velocity (L/T)
v' - turbulent component of flow normal to bed (L/T)
w - power of R in Chezy-Manning relation (-)
x - longitudinal distance in streamwise direction (L)
x^* - intermediate value in Preston tube calculations (-)
y - distance from boundary (L)
y^* - intermediate value in Preston tube calculations (-)
α - ratio of n_1/n_2 (-)
γ - unit weight of water (M/L^2T^2)
η - variable defining position of maximum velocity plane (-)
κ - von Karman's constant (-)
λ - friction coefficient (-)
- ratio of hydraulic radii in Chee analysis (-)
m - fluid viscosity (M/LT)
ν - kinematic viscosity (L^2/T)
ν_t - turbulent eddy viscosity (L^2/T)
Φ - function in the modified law of the wall

Ψ - function in the modified law of the wall

ρ - density of water (M/L^3)

τ - boundary shear stress (M^2/L^2T^2)

0 - subscript denoting open channel condition

1 - subscript denoting lower zone of influence

2 - subscript denoting upper zone of influence

- no subscript denotes bulk flow value

1.0 Introduction

The study of flow in an ice covered channel is a challenging one, as it requires the application of principles of fluid mechanics and turbulence to a field normally governed in practice by empirical equations such as those of Manning and Chezy. The imposition of an additional boundary on the open channel flow causes it to resemble that in a closed conduit, though the fact that the cover floats on the surface removes the complication of having to deal with large pressure gradients which might be associated with duct flows.

The increase in wetted perimeter associated with the appearance of an ice cover results in a radical change in the velocity profile and shear stress distribution. Differences between the ice and bed roughness can add complexity to any analysis of the flow. The additional boundary tends to make the flow slower, with an obvious increase in stage for a given discharge. In modelling channel flow, especially in the case of flow under ice jams, an assessment of the effects of such a cover is crucial to an accurate prediction of water levels.

To investigate the phenomenon of ice covered flows, a review of previous work, both theoretical and experimental, has been performed. A look at the history of the study of flows in ice covered channels reveals two distinct stages in the development of the present body of knowledge. Early studies, starting approximately seventy years ago, involved theoretical analyses of the phenomenon with occasional observations of natural streamflow used to gauge the validity of conclusions. Advances in theory and technology facilitated later work, beginning in the 1970's, in which the thrust was more empirical. Laboratory experiments and computational analyses dominated this second phase of development in providing further insight into the factors governing ice covered flow.

1.1 Theoretical Analyses of Ice Covered Flows

The earliest attempts at establishing the effects of an ice cover on flow in a channel appear in Soviet literature and date back to the 1930's. A comprehensive review of the first three decades of analysis is contained in a 1964 paper by Nezhikovskiy. In the years following this, several papers by Americans and one by a Hungarian were published. These first analyses tended to be strictly theoretical, with a non-existent or negligible experimental component. The solutions presented attempt to provide a value of composite roughness, based on some combination of the channel bed and ice cover roughnesses, that can be used in flow calculations. Most of them divide the stream cross-section into two zones, one influenced by the bed and the other by the cover, and use the characteristics of each zone to arrive at a representative value.

1.1.1 Pavlovskiy (1931)

This was the first published attempt at determining a composite channel roughness based on the physical characteristics of the channel. These parameters are detailed on Figure 1.1. Pavlovskiy equated the stream's average driving force per unit width

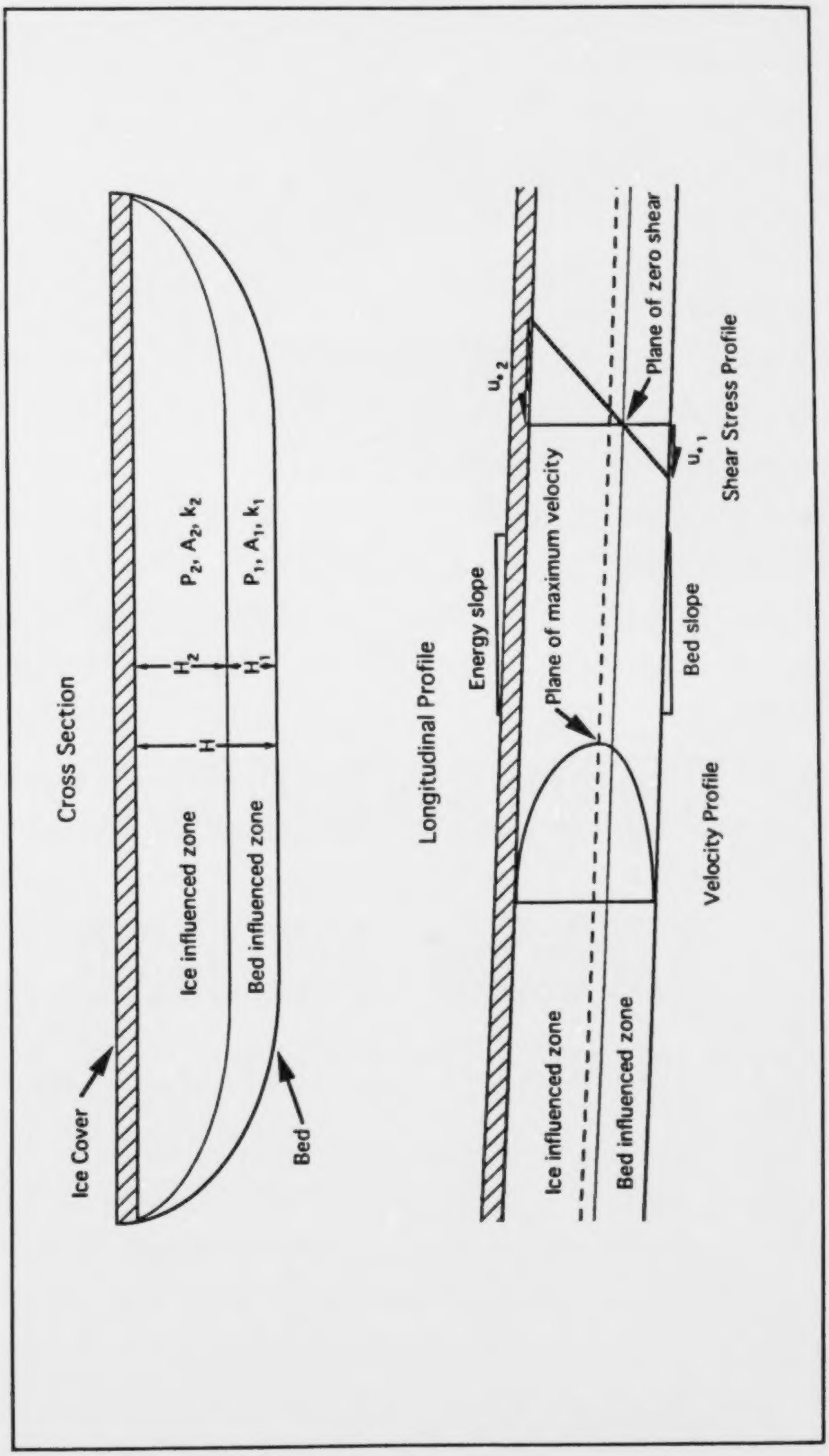
Cross Section
Ice Cover
Bed
Ice influenced zone
Bed influenced zone
H
H_2
H_1
P_2, A_2, k_2
P_1, A_1, k_1
Longitudinal Profile
Energy slope
Bed slope
Plane of maximum velocity
Plane of zero shear
Ice influenced zone
Bed influenced zone
Velocity Profile
Shear Stress Profile
u_{*2}
u_{*1}

Figure 1.1 - Parameters influencing ice covered flows

of wetted perimeter, $\gamma H S_f$, to its average boundary shear per unit width, τ:

$$\gamma H\, S_f = \tau = \frac{\tau_1\, P_1 + \tau_2\, P_2}{P_1 + P_2} \qquad (1.1)$$

Here γ represents the unit weight of fluid and S_f the friction or energy slope, while P_i is the wetted perimeter of the zone of influence. The subscripts 1 and 2 represent the bed and ice influenced zones, respectively. It was taken that the depth of a zone of influence, H_i, was equal to its hydraulic radius, a valid assumption for wide rectangular channels. The values of boundary shear were computed as:

$$\tau_i = g\, R_i\, S_f = \frac{V^2}{C_i^2} = \frac{V^2}{\left(\frac{1}{n_i} R_i^{1/6}\right)^2} \qquad (1.2)$$

Here R_i represents the hydraulic radius of the zone of influence, with n_i the roughness coefficient from the Manning equation and V the average flow velocity. C_i is the Chezy coefficient based on the Chezy-Manning relation:

$$C_i = \frac{1}{n_i} R_i^{1/6} \qquad (1.3)$$

Pavlovskiy was unable to compute the values of R_i, as they are based on the undetermined values of A_i as well as the related wetted perimeters. Therefore, he assumed that $R_1 = R_2 = R$. Thus, his basic equation reduces to:

$$\frac{P_1 + P_2}{\left(\frac{1}{n}\right)^2} = \frac{P_1}{\left(\frac{1}{n_1}\right)^2} + \frac{P_2}{\left(\frac{1}{n_2}\right)^2} \qquad (1.4)$$

$$\text{So,} \quad n^2 = \frac{n_1^2 P_1 + n_2^2 P_2}{P_1 + P_2} \qquad (1.5)$$

If the parameter a is arbitrarily defined as $\frac{P_2}{P_1}$, then:

$$n = \sqrt{\frac{n_1^2 + a\, n_2^2}{1 + a}} \qquad (1.6)$$

The assumption that $R_1 = R_2 = R$ is obviously invalid as it requires that:

$$\frac{A_1}{P_1} = \frac{A_2}{P_2} = \frac{A_1 + A_2}{P_1 + P_2} \qquad (1.7)$$

which in turn means that:

$$\frac{P_1}{P_2} = \frac{A_1}{A_2} \qquad (1.8)$$

regardless of the relative roughness of the boundaries. This is refuted by simple laboratory or field measurements which show that rougher boundaries influence a larger portion of the flow cross section.

Pavlovskiy computes boundary shear as a function of the properties of the entire section, while roughnesses of the surfaces are accounted for separately. His assumption that $R_1 = R_2 = R$ would be valid for a single value of roughness, bed and cover, but fails for differing roughnesses. Pavlovskiy did, though, only intend his method to provide "a first approximation" to the solution of the problem [Nezhikovskiy, 1964].

1.1.2 Lotter (1933)

This work was based on the knowledge that the total discharge, Q, must equal the sum of the bed-influenced and cover-influenced flows:

$$Q = Q_1 + Q_2 \tag{1.9}$$

$$\text{where} \quad Q_i = V_i\, A_i \tag{1.10}$$

And, by the Chezy equation:

$$V_i = C_i \sqrt{R_i\, S_f} \tag{1.11}$$

$$\text{So} \quad A\, C \sqrt{R\, S_f} = A_1\, C_1 \sqrt{R_1\, S_f} + A_2\, C_2 \sqrt{R_2\, S_f} \tag{1.12}$$

Dividing out S_f and letting $A_i = R_i\, P_i$,

$$C\, P\, R^{3/2} = C_1\, P_1\, R_1^{3/2} + C_2\, P_2\, R_2^{3/2} \tag{1.13}$$

Following Pavlovskiy's method in defining a,

$$C(P_1 + a\,P_1)\,R^{3/2} = C_1\,P_1\,R_1^{3/2} + a\,C_2\,P_1\,R_2^{3/2} \qquad (1.14)$$

Which reduces to:

$$C = \frac{C_1\,R_1^{3/2} + a\,C_2\,R_2^{3/2}}{(1+a)\,R^{3/2}} \qquad (1.15)$$

Now the same problem that Pavlovskiy had appears, in that R_1 and R_2, and therefore C_1 and C_2, are unknown. Lotter again assumed, falsely, that $R_1 = R_2 = R$. Thus, his formula reduces to:

$$C = \frac{C_1 + a\,C_2}{(1+a)} \qquad (1.16)$$

Substituting the Chezy-Manning relation, the following is obtained:

$$n = \frac{(1+a)}{\left(\frac{1}{n_1} + a\,\frac{1}{n_2}\right)} \qquad (1.17)$$

This formula, different than Pavlovskiy's but based on similar assumptions, is also then incorrect [Nezhikovskiy, 1964]. It is noted that for a wide channel, where the parameter a is equal to unity, this equation may be manipulated to yield:

$$n = \frac{2n_1n_2}{n_1 + n_2} \qquad (1.18)$$

Thus, when one zone of influence has a Manning's n which is much greater than that of the other, the composite n will approach a value of two times the lesser, while never exceeding it. In fact, one would expect the composite value to tend towards the larger of the two.

1.1.3 Belokon (1938)

Here the cross-section was split into two parts in which the dividing plane was that of the maximum velocity. The velocity profile was approximated by a parabolic curve of exponent 1.5, and the average velocities in each section were assumed to be equal. A further assumption was that the shear stress at the dividing plane was zero. He proposed that:

$$n = n_1 \left(1 + a\,\alpha^{1.5}\right)^{2/3} \tag{1.19}$$

where α represents the ratio of the ice cover Manning's n to that of the bed, and a is as before.

Nezhikovskiy points out a basic flaw in Belokon's formula, in that since a and α must always be greater than zero, the composite Manning's n must always be greater than n_2 where it should seemingly lie between n_1 and n_2. Also, for the case of a wide channel ($P_1 = P_2 = B$) with equal roughnesses, bed and cover, this formula yields:

$$n = n_1\, 2^{2/3} = 1.58\, n_1 \tag{1.20}$$

which seems somewhat unrealistic. The main problem with Belokon's relation is that it assumes a shear stress of zero at the plane of maximum velocity, which is noted as being unrealistic for a turbulent system [Nezhikovskiy, 1964].

1.1.4 Sabaneev (1948)

This formula was based on Belokon's work but corrected a mistake it contained. Nezhikovskiy states that Sabaneev also introduced a new assumption related to the existence of minimum energy losses for given boundary stresses. He arrived at the equation:

$$n = n_1 \left(\frac{1 + a\,\alpha^{(2/(2w+1))}}{1 + a} \right)^{w + 1/2} \qquad (1.21)$$

Where w is the exponent of R in the Chezy-Manning relation. Using Manning's value of 1/6 for w and the wide-channel approximation, this reduces to:

$$n = 0.63\, n_1 \left(1 + \alpha^{1.5}\right)^{2/3} \qquad (1.22)$$

which is essentially the same as for the Belokon formulation but with an additional multiplier of 0.63. This is stated as being more general and correct as it yields a value of $n = n_1 = n_2$ for $\alpha = 1.0$, and n will always lie between n_1 and n_2. However, the problem of non-coincident zero shear and maximum velocity planes, as in Belokon's original derivation, persists [Nezhikovskiy, 1964]. An alternate form of the Sabaneev equation, perhaps more descriptive in its form, also exists [Gerard, 1989]:

$$n = \left(\frac{n_1^{3/2} + n_2^{3/2}}{2}\right)^{2/3} \qquad (1.23)$$

1.1.5 Levi (1948)

Here a wide channel and a logarithmic velocity distribution in each zone of influence were assumed. The respective velocity profile equations are:

$$u_1 = \frac{1}{\kappa}\sqrt{\frac{g\,H\,S_f}{2}}\,\ln\frac{y}{k_1} \qquad (1.24a)$$

$$u_2 = \frac{1}{\kappa}\sqrt{\frac{g\,H\,S_f}{2}}\,\ln\frac{H - y}{k_2} \qquad (1.24b)$$

Here u_i represents the flow velocity at a given distance y from the boundary, and κ is von Karman's constant, equal to 0.42. The parameter k_i is the equivalent sand grain roughness of the boundary. These equations were taken as equal at the plane of maximum velocity, producing the relation:

$$u_1 H_1 = u_2 H_2 \qquad (1.25)$$

From which it is revealed that:

$$H_2\, k_1 = H_1\, k_2 \tag{1.26}$$

Knowing that $H = H_1 + H_2$, it is shown that:

$$H_1 = H \frac{k_1}{k_1 + k_2} \tag{1.27a}$$

$$H_2 = H \frac{k_2}{k_1 + k_2} \tag{1.27b}$$

Mean velocities for each zone of influence are obtained by integrating over the depth and the following result:

$$V_1 = \frac{1}{\kappa} \sqrt{\frac{g\, H\, S_f}{2}} \left[\ln \frac{H_1}{k_1} - 1 \right] \tag{1.28a}$$

$$V_2 = \frac{1}{\kappa} \sqrt{\frac{g\, H\, S_f}{2}} \left[\ln \frac{H_2}{k_2} - 1 \right] \tag{1.28b}$$

Now, the total unit discharge for the section may be taken as:

$$q = V\, H = C\, H^{3/2} \sqrt{\frac{S_f}{2}} \tag{1.29}$$

and this may be placed in the continuity equation:

$$q = C\, H^{3/2} \sqrt{\frac{S_f}{2}} = V_1\, H_1 + V_2\, H_2 = q_1 + q_2 \tag{1.30}$$

to yield:

$$C\,H^{3/2}\sqrt{\frac{S_f}{2}} = \frac{1}{\kappa}\sqrt{\frac{g\,H\,S_f}{2}}\left[H_1\left(\ln\frac{H_1}{k_1} - 1\right) + H_2\left(\ln\frac{H_2}{k_2} - 1\right)\right] \qquad (1.31)$$

which reduces to:

$$C = \frac{\sqrt{g}}{\kappa}\left[\frac{H_1}{H}\left(\ln\frac{y_1}{k_1}\right) + \frac{H_2}{H}\left(\ln\frac{y_2}{k_2}\right) - 1\right] \qquad (1.32)$$

Recalling that $H_2\,k_1 = H_1\,k_2$, this further reduces to:

$$C = \frac{\sqrt{g}}{\kappa}\left[\ln\left(\frac{H}{k_1 + k_2}\right) - 1\right] \qquad (1.33)$$

And if it is taken that the mean roughness is a simple average of the two boundary roughnesses:

$$k_m = \frac{k_1 + k_2}{2} \qquad (1.34)$$

The equation reduces to:

$$C = \frac{\sqrt{g}}{\kappa}\left[\ln\left(\frac{H}{2\,k_m}\right) - 1\right] \qquad (1.35)$$

Levi uses an exponent of 1/4 in the Chezy-Manning equation to produce a composite Manning's n of:

$$n = \frac{\kappa\left(\frac{H}{2}\right)^{1/4}}{\sqrt{g}\left[\ln\left(\frac{H}{2\,k_m}\right) - 1\right]} \qquad (1.36)$$

Which can be rearranged to solve for k_m:

$$k_m = \frac{H}{2} \exp\left[-1 - \frac{\kappa \left(\frac{H}{2}\right)^{1/4}}{n\sqrt{g}}\right] \tag{1.37}$$

The recommended procedure for using this equation is to use the Manning's n values of each surface to solve for its roughness, k_i, and then combine these roughnesses to produce k_m. Then, this value is placed in equation (1.36) to solve for the composite Manning's n [Uzuner, 1975].

Some drawbacks of this method include the need to know the location of the plane of maximum velocity to use equation (1.37), necessitating some assumption as to its location. As well, equation (1.26) is somewhat suspect when it is considered that the bed and cover roughness may vary over orders of magnitude.

1.1.6 Konovalov (1952)

Here a solution to the problem was derived in a slightly different fashion. Again considering two distinct zones of influence in the stream, with the dividing plane at the point of maximum velocity, the analysis was begun by taking a velocity distribution defined by the Bazin-Boussinesq formula. Equating the maximum velocities at the dividing plane, as did Levi, it was determined that:

$$C_1\sqrt{H_1} + \frac{H_1^2\, m}{3\, H^{3/2}} = C_2\sqrt{H_2} + \frac{H_2^2\, m}{3\, H^{3/2}} \tag{1.38}$$

where a typical value of m would be 23. As both H_1 and H_2 would be unknown, the equation is necessarily solved iteratively by first assuming that $V_1 = V_2$. Then the following equation could be solved for H_1, yielding H_2 in the process:

$$\frac{1}{n_1} H_1^{2/3} = \frac{1}{n_2} (H - H_1)^{2/3} \tag{1.39}$$

Then, from the determined values of H_1 and H_2, the respective section velocities may be calculated:

$$V_1 = C_1 \sqrt{H_1 S_f} = \frac{1}{n_1} H_1^{1/6} \sqrt{H_1 S_f} \tag{1.40a}$$

$$V_2 = C_2 \sqrt{H_2 S_f} = \frac{1}{n_2} H_2^{1/6} \sqrt{H_2 S_f} \tag{1.40b}$$

The solution process would then proceed iteratively until a reasonable convergence occurred. The mean velocity in the channel could then be calculated as a simple weighted mean, and a composite conveyance determined. In his review of the formula, Nezhikovskiy questions the validity of the method due to the fact that the Bazin-Boussinesq equations are known to be applicable to open channel flow situations, but little is known about their applicability to closed channels. It was further noted that this set of equations has its greatest use in solving for the location of the plane of maximum velocity, and should not be used to solve for an ice cover roughness based on open water roughness and closed channel depth measurements [Nezhikovskiy, 1964].

1.1.7 Trufanov (1954)

This formula which varies greatly from those already seen:

$$V = \left(0.75\ \sqrt{1-K}\right) V_0 \tag{1.41}$$

Here, V_0 is the theoretical average velocity of the channel given an open channel condition, but with the winter depth and channel slope. K is a variable which covers the range 0.20 - 0.88, depending on the ice cover roughness.

In analyzing this equation, Nezhikovskiy substitutes Manning's equation for V and V_0, and assumes that H = 2R (the wide channel approximation taking a cover into account):

$$\frac{1}{n}\left(\frac{H}{2}\right)^{2/3} S_f^{1/2} = \left(0.75\ \sqrt{1-K}\right)\frac{1}{n_2} H^{2/3} S_f^{1/2} \tag{1.42}$$

This reduces to:

$$\frac{1}{n}\left(\frac{1}{2}\right)^{2/3} = \left(0.75\ \sqrt{1-K}\right)\frac{1}{n_2} \tag{1.43}$$

Which, rearranged, yields:

$$n = 0.84\,\frac{n_2}{\sqrt{1-K}} \tag{1.44}$$

One criticism of this equation is that at the extreme values of the range of K, this equation tends to yield unrealistic results

[Nezhikovskiy, 1964]. Additionally, the choice of the value of K to be used is very subjective, not measurable as a physical roughness would be.

1.1.8 Shiperko (1961)

This method is based on the assumption that for a given cross-section and given values of Manning's n for bed and cover a minimum head loss, and therefore a maximum average velocity and discharge, must occur. His analysis yielded the equation:

$$C^2 = a_1 C_1^2 + a_2 C_2^2 \tag{1.45}$$

He then assumed as others had, incorrectly, that $R_1 = R_2 = R$ and from this determined that:

$$n = \sqrt{\frac{1}{\frac{a_1}{n_1^2} + \frac{a_2}{n_2^2}}} \tag{1.46}$$

Which, based on a familiar false assumption, must be incorrect [Nezhikovskiy, 1964]. Also, as with Lotter's formula, where there are disparate bed and cover Manning's n's, the composite value will tend to be much closer to the lower value of the two.

1.1.9 Dul'nev (1962)

This followed a similar procedure to the one Lotter had used thirty years previously, including the false assumption that $R_1 = R_2 = R$. From this, the subsequent expression is obtained:

$$n = \frac{1}{\frac{a_1}{n_1} + \frac{a_2}{n_2}} \tag{1.47}$$

Nezhikovskiy notes that if we assign the values:

$$a_1 = \frac{1}{1 + a} \tag{1.48a}$$

$$a_2 = \frac{a}{1 + a} \tag{1.48b}$$

the result is the same as Lotter's [Nezhikovskiy, 1964].

1.1.10 Carey (1966)

This equation arose from an analysis of ice covered flow in the St. Croix river. This included a component which examined the form of the underside of the ice cover and suggested that flow turbulence was responsible for the formation of bedforms on the upper boundary. A technique for determining a composite Manning's n was also presented. It was based on the Karman-Prandtl resistance equation for turbulent pipe flow:

$$\frac{1}{\sqrt{f}} = 2 \log \frac{r_0}{k} + 1.74 \qquad (1.49)$$

Here f is the friction factor of the flow. The value for pipe radius, r_0, was taken as equal to twice the hydraulic radius, yielding:

$$\frac{1}{\sqrt{f}} = 2 \log \frac{2R}{k} + 1.74 \qquad (1.50)$$

Carey assumed that the cross-section was divided into two parts, and that flow equations could be applied independently to each one. The dividing point was taken as the plane of zero shear, and it was assumed, falsely, that the average velocity in each section, and therefore the entire cross-section, was the same. Recognizing that:

$$f = \frac{8\, g\, R\, S_f}{V^2}, \qquad (1.51)$$

the equation then becomes:

$$\frac{V_1}{\sqrt{8\, g\, R_1\, S_f}} = 2 \log \frac{2\, R_1}{k_1} + 1.74 \qquad (1.52)$$

Since k_1 is known from open water calibrations, R_1 may then be solved for. Then values of n and f for the bed and cover regions may be calculated by assuming that S_f remains the same for the upper zone and determining R_2 based on R_1 and the section dimensions.

The assumption of equal average velocities in the bed and ice influenced sections appears to be the major drawback of this derivation [Carey, 1966]. The assumption that the friction slopes are the same in each zone is also something that might require investigation.

1.1.11 Larsen (1966)

This method for computing a composite Manning's n considered a logarithmic velocity distribution. It was based on the assumption that the flow could be divided into two sections with the dividing plane coincident with those of maximum velocity and zero shear. He started from the following equations:

$$u_1 = 2.5\, u_{*1} \ln \frac{30\ y}{k_1} \tag{1.53a}$$

$$u_2 = 2.5\, u_{*2} \ln \frac{30\ y}{k_2} \tag{1.53b}$$

Equating these at the plane of maximum velocity, where y is equal to H_1 and H_2, respectively, for the two equations, the following results:

$$\frac{u_{*1}}{u_{*2}} = \sqrt{\frac{\tau_1}{\tau_2}} = \frac{\ln \dfrac{30\ H_2}{k_2}}{\ln \dfrac{30\ H_1}{k_1}} = \frac{a}{b} \tag{1.54}$$

Here a and b are intermediate variables in the derivation. The mean velocities in each section may be found by integrating the velocity equations over the depth:

$$V_1 = 2.5\, u_{*1} \left(\ln \frac{30\ H_1}{k_1} - 1 \right) \tag{1.55a}$$

$$V_2 = 2.5\, u_{*2} \left(\ln \frac{30\ H_2}{k_2} - 1 \right) \tag{1.55b}$$

Dividing one by the other, another expression is created:

$$\frac{u_{*1}}{u_{*2}} = \frac{V_1 \left(\ln \frac{30\ H_2}{k_2} - 1 \right)}{V_2 \left(\ln \frac{30\ H_1}{k_1} - 1 \right)} = \frac{V_1\,(a - 1)}{V_2\,(b - 1)} \tag{1.56}$$

Using the wide channel approximation and substituting in the Manning equation for velocity, the following results:

$$\frac{V_1}{V_2} = \frac{n_2}{n_1} \left(\frac{H_1}{H_2} \right)^{2/3} \tag{1.57}$$

This equation may be combined with the one previously derived to yield:

$$\frac{H_1}{H_2} = \left(\frac{a\,(b - 1)\, n_1}{b\,(a - 1)\, n_2} \right)^{3/2} \tag{1.58}$$

Introducing the continuity equation and considering that a, b >> 1, Larsen's equation becomes:

$$\frac{1}{n} = \frac{\left[\left(\frac{H_1}{H_2}\right)^{5/3}\frac{1}{n_1}\right] + \frac{1}{n_2}}{\left(\frac{1}{2}\right)^{2/3}\left(\frac{H_2}{H_1} + 1\right)^{5/3}} \qquad (1.59)$$

This may be further simplified to:

$$\frac{n}{n_2} = \frac{1}{2^{2/3}}\left[\left(\frac{n_1}{n_2}\right)^{3/2} + 1\right]^{2/3} \qquad (1.60)$$

It is noted that this formula is only valid over a relative roughness range of between 0.2 and 1.0, and for depths of flow of greater than 1.5 m [Larsen,1966].

1.1.12 Hancu (1967)

Here an equation was introduced which was based on the velocity defect law:

$$u_{max} - u_i = \sqrt{\frac{\tau_i}{\rho}}\,\frac{1}{\kappa}\ln\frac{y}{H_i} \qquad (1.61)$$

It should be noted that here a value for von Karman's constant of 0.246 was used instead of today's generally accepted value of 0.42. Here it is taken that:

$$\tau_i = \frac{\rho}{2}\lambda_i V_i^2 \qquad (1.62)$$

where λ_i is a friction coefficient equal to one quarter of the Darcy-Weisbach friction factor.

Integrating the velocity defect equations over the flow depth for each section and then subtracting one from the other yields:

$$V_2 - V_1 = \frac{\kappa}{\sqrt{2}}\left(\sqrt{\lambda_1}V_1 - \sqrt{\lambda_2}V_2\right) \tag{1.63}$$

It is also taken that the friction slope in each zone of influence is equal to that for the entire flow, yielding:

$$\frac{\tau_1}{H_1} = \frac{\tau_2}{H_2} = \frac{dP}{dx} \tag{1.64}$$

So:

$$\lambda_1 V_1^2 H_2 = \lambda_2 V_2^2 H_1 \tag{1.65}$$

Hancu then made use of the Karman-Prandtl resistance equation:

$$\lambda_i^{-1/2} = 4 \log \frac{H_i}{k_i} + 4.25 \tag{1.66}$$

An equation for the composite friction coefficient was combined with the continuity equation to arrive at:

$$\lambda = \frac{1}{2}\left[\left(\frac{V_1}{V}\right)^2 \lambda_1 + \left(\frac{V_2}{V}\right)^2 \lambda_2\right] \tag{1.67}$$

Recalling that:

$$n^2 = \frac{R^{1/3}\lambda}{2\,g} \tag{1.68}$$

the previous equation may be manipulated to yield:

$$\left(\frac{n}{n_1}\right)^2 = \left(\frac{1}{2}\right)^{4/3}\left(\frac{H}{H_1}\right)^{1/3}\left[\left(\frac{V_1}{V}\right)^2 + \left(\frac{V_2}{V}\right)^2\left(\frac{n_2}{n_1}\right)^2\left(\frac{H_1}{H_2}\right)^{1/3}\right] \tag{1.69}$$

In a 1975 review of covered channel flow analysis techniques, it was recommended that of the methods presented, those of Larsen and Hancu are "the most complete and rigorous" and are therefore the most advisable to use [Uzuner, 1975].

1.1.13 Yu, Graf and Levine (1968)

This work was involved in an analysis on flow in the St. Clair River in the Great Lakes system. The investigators developed a semi-empirical relation based on the assumption of two flow sections of equal velocity and using a modified form of the Manning equation:

$$V_i = \frac{1}{n_i}\left(\frac{A_i}{P_i^{\,k}}\right)^{w+1/2} S_f^{\,0.5} \tag{1.70}$$

which when rearranged yields:

$$A_i = \left(\frac{n_i\,V_i}{S_{fi}^{\,0.5}}\right)^{2/(2w+1)} P_i^{\,k} \tag{1.71}$$

Using the noted assumptions, it is possible to obtain the following equation:

$$n = n_1 \left[\frac{1 + \left(\frac{P_2}{P_1}\right)^k \left(\frac{n_2}{n_1}\right)^{2/(2w+1)}}{\left(1 + \frac{P_2}{P_1}\right)^k} \right]^{w + 0.5} \qquad (1.72)$$

Using the wide channel approximation and Manning's value for w of 1/6, this in turn reduces to:

$$n = 0.63^k \, n_1 \left[1 + \left(\frac{n_2}{n_1}\right)^{1.5} \right]^{2/3} \qquad (1.73)$$

$$\text{where } k = \left(\frac{n_2}{n_1}\right)^{1/6} \qquad (1.74)$$

Assuming n_2 is close to n_1, k approaches unity and Yu's equation breaks down to exactly that of Sabaneev [Yu, 1968].

1.1.14 Summary

The preceding derivations display several common characteristics. Virtually all divide the flow into two zones which are considered to exert no influence on one another. The location of the boundary was initially chosen as midway between the bed and cover, but as more was learned about the phenomenon the plane of maximum velocity gained favor as the division. Many also assumed that this coincided with the plane of zero shear, something which will be shown later to be invalid for unequal boundary roughnesses.

Most chose an equation to describe the velocity profile in each zone of influence, matching them together at some point. This technique would be valid if the zones were in fact independent, but it will be seen that later studies exhibit significant interaction between the zones of influence.

It seems that many of the equations presented up to this point have similarities to each other. Many would appear to be more valid for situations where bed and cover roughnesses are close, and their greatest weaknesses become apparent in situations involving disparate roughnesses. The greatest component lacking in these derivations would appear to be the verification of the analytical solutions by experimentation.

1.2 Experimental Investigations into Covered Flows

Later studies tend to have a more experimental thrust in an attempt to more fully determine the structure of the flow, rather than depending on empirical open channel concepts which are adapted for use on closed channels. The development of more advanced measurement and computational techniques, as well as the application of knowledge from other fields, allowed greater insight into the principles governing ice covered flows.

1.2.1 Hanjalic and Launder (1972)

Here an investigation was performed into the characteristics of a fully developed asymmetric flow in a plane channel. The asymmetry was achieved by roughening one of the parallel plates, through which an air flow was passed, by attaching vertical ribs to it. Only fully developed flows were examined so that all flow characteristics at a section were functions only of the normal distance to the wall. A large aspect ratio was used (6:1 in one case, 12:1 in another) to minimize sidewall effects.

It was shown that velocity profiles adjacent to both the smooth and rough walls agreed with their respective laws of the wall. However, in the central area of the channel, the velocity profile exhibited evidence of interaction between the two zones, deviating from the logarithmic distribution. It was noted that the planes of maximum velocity and zero shear stress were not coincident, something which was previously assumed to be true in many analyses, and that the zero-shear plane was considerably closer to the smooth wall than that of the maximum velocity. It was seen that the effective origin of the velocity profiles was not at the root of the rib for the rough surface, but instead four-tenths of the rib height below its top. The turbulence characteristics of the flow were also examined in detail [Hanjalic and Launder, 1972].

1.2.2 Ismail and Davar (1978)

Here the phenomenon of covered flow with very rough boundaries was investigated. It was believed that here the flow resistance was a function of both skin friction and form resistance. Their investigation began with the law of the wall for rough turbulent flow:

$$\frac{u}{u_*} = \frac{1}{\kappa} \ln \frac{y}{k_s} + 8.5 \qquad (1.75)$$

Here it was thought that von Karman's constant was not in fact a constant value as the assumption of parallel flow at the boundary is not realistic for very rough surfaces. In addition, the parameter k_s has no real physical significance and should be replaced by the roughness height (h) in describing the roughness, and the value of κ would also vary with roughness shape and distribution characteristics. The equation then presented was:

$$\frac{u}{u_{*a}} = \psi(A) \ln \frac{y}{h} + \Phi(B) \qquad (1.76)$$

where $\Psi(A)$ and $\Phi(B)$ are functions of the relative roughness height, spacing and relative location of the velocity profile, and u_{*a} is taken as the virtual average shear velocity.

In the course of the experiments, it was found that a relationship existed which defined the plane of maximum velocity for a smooth bed channel:

$$\frac{H_1}{H} = 0.45\,\frac{h}{H} + 0.69 \qquad (1.77)$$

Ismail and Davar include in their paper a method for estimating a composite roughness coefficient based on measured velocity profiles. However, the analysis continues in the tradition of being based on the existence of two independent zones of influence [Ismail and Davar, 1978].

1.2.3 Gogus and Tatinclaux (1980, 1981)

These experimenters investigated the characteristics of flow beneath a rough floating cover. Their apparatus consisted of a flume with a suspended plywood cover connected to a direct force measurement device. Profiles were determined using a 1 cm diameter propeller velocity meter, calibrated physically and using a laser doppler anemometer. Shear measurements determined from the measured force were also checked against those calculated from velocity profiles.

Using two forms of the law of the wall, for smooth and rough boundaries, respectively,

$$\frac{u}{u_*} = \frac{2.30}{\kappa} \log \frac{y}{k_s} + 8.5 \qquad (1.78)$$

$$\frac{u}{u_*} = \frac{2.30}{\kappa} \log \frac{u_* y}{\nu} + 5.5 \qquad (1.79)$$

$$\text{where } u_* = V\sqrt{\frac{f}{8}} \qquad (1.80)$$

it was shown mathematically that the the assumption $V_1 = V_2 = V$ is false as it implies that $u_{*1} = u_{*2}$ and $f_1 = f_2$.

The following relations were also derived:

$$V_i = u_{max} - \frac{u_{*i}}{\kappa} \qquad (1.81)$$

$$u_{*i} = \kappa\, V_i \left(\frac{u_{max}}{V_i} - 1\right) \qquad (1.82)$$

As with Ismail and Davar, a relation between boundary roughnesses and the position of the plane of maximum velocity was developed:

$$\frac{H_1}{H_e} = 0.26 \log \frac{f_1}{f_2} + 0.5 \qquad (1.83)$$

Here H_e represents the depth to the piezometric head line. A relation, based on a linear shear distribution, was also derived to determine the value of shear at the point of maximum velocity:

$$\tau_i = \frac{\tau_2 H_1 + \tau_1 H_2}{H_1 + H_2} \qquad (1.84)$$

Among their conclusions was that the open channel flow value of bed friction factor is significantly changed by the presence of a rough cover on the surface. It seems to increase with increasing flow constriction (H_e/H) and with decreasing relative roughness (k_{s1}/k_{s2}) [Gogus and Tatinclaux, 1980].

In another publication one year later, these two authors further discuss the effects of a cover on channel flow. A formula is presented which relates ice and composite friction factors to flow depths:

$$\sqrt{\frac{1}{f_2}} - \sqrt{\frac{1}{f_o}} = 2 \log \frac{H_2}{H_o} \tag{1.85}$$

Here the subscript o denotes the open channel flow case. A discussion on relative and absolute flow depths in the boundary zones is presented, and curves for problem solutions are included. The effect of sediment entrainment, and its variation through the seasons, on the value of von Karman's constant is also noted. It was noted that lower bed shears which were expected to occur under covered flows would result in less sediment entrainment in the winter. Water with less sediment load would be expected to have a higher value of κ [Gogus and Tatinclaux, 1981].

1.2.4 Lau and Krishnappan (1981, 1982)

The first paper here discusses the effects of an ice cover on flow behavior. It analyzes both free surface and ice covered flows using the k-ε model [Lau and Krishnappan, 1981]. A later paper concentrates on a k-ε analysis of velocity distributions under floating covers. Results of model runs here note that velocity profiles follow a logarithmic distribution for typically only 60% of the thickness of the bed or cover influenced layer. This further supports the findings of Hanjalic and Launder and others which point to interaction between the two parts of the cross section [Lau, 1982].

1.2.5 Calkins (1982)

Here problems involved in field studies to determine the relevant parameters involved in covered channel flows are discussed, and solutions to aid in such research are provided. Calkins also provides a fairly complete summary of the equations necessary in a practical analysis. One of the difficulties in gathering data which is noted involves the use of propeller velocity meters in very shallow flows [Calkins, 1982].

1.2.6 Gerard (1982)

In the same year, a review of the fundamentals of ice covered flow was published. One of the more pertinent issues discussed was the existence of, particularly in ice covered flows which tend to resemble duct flows, secondary currents. These flows, caused by "gradients in transverse Reynolds normal stresses", sometimes reach magnitudes of three percent of the maximum downstream velocity for smooth wall conduits. They can be further increased by lateral variations in roughness which would be seen more often in nature. These secondary flows can result in a significant redistribution of boundary shear stresses [Gerard, 1982].

1.2.7 Tatinclaux and Gogus (1983)

Based on data from previous experiments, these investigators definitively stated that the bed and cover influenced zones, for situations with a non-unity value of relative roughness, had different average velocities with:

$$V_{rough} < V < V_{smooth} \tag{1.86}$$

They also discussed the assumption of where to divide the two zones. It was noted that using the plane of maximum velocity as a division implied that the shear stress at the interface was zero, an assumption that comes from turbulent flow models based on mixing length or eddy viscosity theories, shown respectively below:

$$-\rho\,\overline{u'\,v'} = \rho\, l^2 \frac{du}{dy}\left|\frac{du}{dy}\right| \tag{1.87}$$

$$\tau = \rho\,(\nu + \nu_t)\frac{du}{dy} \tag{1.88}$$

In these equations ρ represents the fluid density, l the mixing length and ν_t the turbulent eddy viscosity. The parameters u' and v' describe the turbulent components of the flow velocities u and v at a given position. It is assumed that at the plane of maximum velocity,

$$\frac{du}{dy} = 0 \tag{1.89}$$

$$\text{therefore} \quad \rho\,\overline{u'\,v'} = \tau = 0 \tag{1.90}$$

However, the work of Tennekes and Lumley is quoted in casting doubt on this. They say "Mixing length and eddy viscosity models should be used only... in turbulent flows characterized by a single length scale and a single velocity scale." In an ice covered flow there exist two length scales (boundary roughnesses) and two velocity scales (average velocities). It should be noted that the use of the plane of maximum velocity as an interface was questioned as early as 1964 by Nezhikovskiy, but this greatly enhances the understanding of why is should not be used.

Tatinclaux and Gogus felt that there was no momentum transfer across the plane of zero shear, and therefore that it should be used as an interface in any analysis. This is undoubtedly more correct than using the plane of maximum velocity, but the observations of Hanjalic and Launder (1972) and Lau (1982) still suggest that there is significant interaction across this boundary.

Several empirical formulae for ice covered flow analysis were provided:

$$\text{smooth boundary:} \quad \frac{1}{\sqrt{f_s}} = 1.71 \left(\frac{4\,H_s\,V}{\nu}\right)^{1/8} \tag{1.91}$$

$$\text{rough boundary:} \quad \frac{1}{\sqrt{f}} = -1.86 \log\left(\frac{k}{H}\right) + 2.13 \tag{1.92}$$

and also an equation to define the relative size of the zones of influence between two rough boundaries:

$$\sqrt{\frac{H_1}{H_2}} = \frac{1.86 \log\left(\frac{H_2}{k_2}\right) + 2.13}{1.86 \log\left(\frac{H_1}{k_1}\right) + 2.13} \tag{1.93}$$

Recognizing that $H_1 + H_2 = H$, the following equations are presented to further define the size of the zones of influence:

$$2\eta \log \frac{1-2\eta}{1+2\eta} = \left(1 - \sqrt{1-4\eta^2}\right)\left[\log(1-4\eta 2) + 1.69 - \log\left(\frac{k_r}{H}\frac{k_s}{H}\right)\right] + 2\eta \log\left(\frac{k_r}{k_s}\right) \tag{1.94}$$

$$(1 - 2\eta)^{5/8} - \frac{(1 + 2\eta)^{1/2}}{R_H^{\ 1/8}}\left[1.06 \log(1+2\eta) - 1.06 \log\left(\frac{k_r}{H}\right) + 0.90\right] = 0 \tag{1.95}$$

$$\text{where} \quad \eta = \frac{H_r}{H} - 0.5 \tag{1.96}$$

$$\text{and } R_H = \frac{2VH}{\nu} \tag{1.97}$$

Equation (1.94) is applicable to cases where two hydraulically rough boundaries of unequal roughness exist, with the subscripts r and s denoting the rougher and smoother of the two, respectively, while equation (1.95) applies to instances where one boundary is rough and the other is smooth. This work was primarily intended to aid in the analysis of ice jams [Tatinclaux and Gogus, 1983].

1.2.8 Chee (1985)

Chee, in 1985, published a paper on the topic of floating boundary river mechanics. For steady, uniform flow he reduced the Reynolds form of the Navier-Stokes equations to:

$$\frac{\partial}{\partial y}\left(\mu \frac{\partial \bar{u}}{\partial y} - \rho\, \overline{u'\, v'}\right) = -\, \rho\, g\, S_0 \tag{1.98}$$

Here m is the viscosity of the fluid, while S_0 represents the bed slope. The analysis then produced relations for average velocity and composite roughness, beginning with the following relations:

$$\tau_{ti} = \rho\; g\; S_0\, (H_i - y_i) \tag{1.99}$$

$$\tau_{ti} = \rho\; \kappa\; y_i^2 \left(\frac{du_i}{dy_i}\right)^2 \tag{1.101}$$

$$\varepsilon_i = \frac{y_i}{H_i} \tag{1.102}$$

which combine to produce:

$$\frac{du_i}{d\varepsilon_i} = \frac{u_{*i}}{\kappa} \frac{(1 - \varepsilon_i)^{1/2}}{\varepsilon_i} \tag{1.103}$$

$$\text{where} \qquad u_{*i} = \sqrt{g\, H_i\, S_0} \tag{1.104}$$

where the wide channel approximation is used to justify the use of $H_i = R_i$. This equation is then integrated to get:

$$(V_2 - V_1) = \frac{2}{3\kappa}(u_{*2} - u_{*1}) \tag{1.105}$$

Now, making use of the continuity equation to combine the two sections, the following is arrived at:

$$V = \frac{1}{2}(V_1 + V_2) - \frac{1}{3\kappa}(u_{*2} - u_{*1})\left(\frac{A_2 - A_1}{A}\right) \tag{1.106}$$

Applying the Manning, momentum and boundary shear equations, respectively:

$$V_i = \frac{1}{n_i} R_i^{2/3} S_0^{1/2} \tag{1.107}$$

$$\rho\, g\, A\, L\, S_0 = \tau_1\, P_1\, L + \tau_2\, P_2\, L \tag{1.108}$$

$$\tau_i = \rho\, g\, R_i\, S_0 \tag{1.109}$$

The following equation results:

$$\kappa \frac{R^{1/6}}{n_2\, g^{1/2}} = \frac{\left(\lambda^{1/2} - 1\right)}{1 - \left(\frac{n_2}{n_1}\right)\lambda^{2/3}}\left(a + (1 - a)\lambda\right)^{1/6} \tag{1.110}$$

$$\text{where } a = \frac{P_2}{P} \tag{1.111}$$

$$\text{and} \quad \lambda = \frac{R_2}{R_1} \tag{1.112}$$

An expression for composite roughness can also be derived from this:

$$\frac{n_2}{n} = \frac{\left[a + (1 - a)\frac{n_2}{n_1}\lambda^{5/3}\right]}{\left[a + (1 - a)\lambda\right]^{5/3}} \tag{1.113}$$

Again, this analysis makes use of the Prandtl mixing length theory as a basis for its development, casting doubt on its validity [Chee, 1985]. The results of further analysis applied to sections of irregular roughness were published a year later, with the technique being based on the previous paper [Chee and Ray, 1986].

1.2.9 Hendriksen and Davar (1986)

This paper presented the results of a field study which analyzed velocity profiles according to a binary law of velocity distribution which maintained a logarithmic profile near boundaries but became parabolic farther away. Difficulties in obtaining velocity profiles in very shallow or slow channels were noted [Hendriksen and Davar, 1986].

1.2.10 Wuebben (1986)

In this investigation the case of a mobile boundary flow under an ice cover was examined. This laboratory study noted the familiar effects of an ice cover: an increased water depth combined with decreased bed shear and flow velocity. However, it also noted a reduction in sediment transport, bed roughness and bedform height, as well as an increase in bedform wavelength, that could not be studied in previous fixed bed investigations. It was seen that the addition of an ice cover resulted in changes in bed and energy slopes of a system, but this was qualified with the remark that it was not as likely to take place in nature as the scale of sediment transport required is so much larger. It was also noted that an increase in ice cover roughness results in an increase in bed roughness for the same stream power. Perhaps most importantly, though, it was stated that "data did not support the hypothesis that the flow below a defined plane of zero shear could be treated as an independent system", further supporting the findings of Hanjalic and Launder (1972) and Lau (1982) [Wuebben, 1986].

1.2.11 Gerard and Beltaos (1987)

In 1987, Gerard discussed an earlier paper by Beltaos in which it was stated that the use of the Sabaneev equations for ice covered flow were "justified by a lack of more reliable information" [Beltaos, 1983]. In Beltaos' reply to the discussion, it is noted that the generally accepted equation for rough turbulent flow:

$$\frac{u}{u_*} = 2.5 \ln \frac{y}{k_s} + 8.5 \qquad (1.114)$$

is not valid for values of R/k below approximately 0.6 [Bayazit, 1976]. It is stated that the first constant drops to 1.25 for an R/k value of 0.4 and to 0.63 for a value of 0.2, under open channel flow conditions. This effect is something that must be considered in any analysis of closed channel flows [Gerard and Beltaos, 1987].

1.2.12 Summary

Research performed in the second generation of the study of ice covered flows clarified certain aspects of the physics of these flows and in doing so invalidated many of the analyses of the first generation. Earlier research considered two independent zones of influence, often assuming that average velocities in the two zones were equal and that the plane of maximum velocity was coincident with that of zero shear stress. Later research has shown that though this may be valid for equal roughnesses of bed and cover, differences in these roughnesses causes the average velocity to be higher in the smoother boundary zone and the plane of zero shear stress to be closer than the plane of maximum velocity to the smooth boundary. Moreover, the very assumption of two independent zones may not be valid, as many studies, both experimental and computational, have exhibited significant interaction between the zones.

The second phase of study has also generated equations, backed up with experimental data, which may be used with greater confidence than earlier ones. Those of Tatinclaux and Gogus stand out above the rest.

Further questions concerning more complex aspects of the ice covered flow phenomenon have also been raised. Areas of the problem to be investigated further include the effect of very high relative roughnesses of flows, the effect of covered flows on bed shear which is related to sediment load and its influence on von Karman's constant, and the behavior of secondary flows in ice covered channels.

1.3 Goals of This Study

This study was undertaken with the aim of verifying previous work and gaining a familiarity with the principles governing the ice covered flow phenomenon. Use was made of measurement techniques and analysis procedures commonly used in open channel flow and fluid mechanics research. Some, such as the use of the Preston tube to measure boundary shear and velocities, were, to the writer's knowledge, unique in ice covered flow research.

Direct and derived measurements of flow depths, velocity profiles, boundary shear stresses and boundary roughnesses were taken to aid in the analysis. In most cases a number of techniques were used to determine the value of certain parameters, such as boundary shear and roughness, to ensure confidence in the results. The data acquired allowed inferences to be made concerning boundary shear distribution, effective roughnesses and energy dissipation.

Flow measurements were also used to determine the validity of analytical methods which have traditionally been used to describe ice covered flows. Other relations determined by later researchers were also examined by applying experimental data to them.

2.0 Experimental Apparatus and Procedure

A series of experiments were performed in a flume located in the T. Blench Hydraulics Laboratory at the University of Alberta to investigate the phenomenon of flow in a wide, ice covered channel. The ice cover, as well as the rough bed, was simulated by 3M brand Nomad® cushion plus floor matting, which is shown in Plate 2.1. This material, approximately one centimetre thick, features one smooth side and one rough side which is composed of matted fibers. Additionally, it floats with approximately nine-tenths of its thickness submerged, ideally simulating a rough ice cover.

Plate 2.1 - 3M Nomad® cushion plus floor matting used to simulate ice cover and bed roughness.

2.1 Experimental Apparatus

A flume 18 m long, 1.22 m wide and 0.65 m deep was used to perform these experiments. The flume is pictured on Plate 2.2 and Figure 2.1. A head tank, 2.44 m long and 1.44 m wide, was located at its upstream end. Located inside was a weir of masonry bricks, intended to damp the extreme turbulence resulting from the inflow of water from the supply line. Downstream of this, a full depth of 10 cm diameter pipes, approximately 1 m long, were packed to straighten the flow. At the upstream and downstream ends of the pipe array, a synthetic hairlike material was put in place to further reduce turbulence.

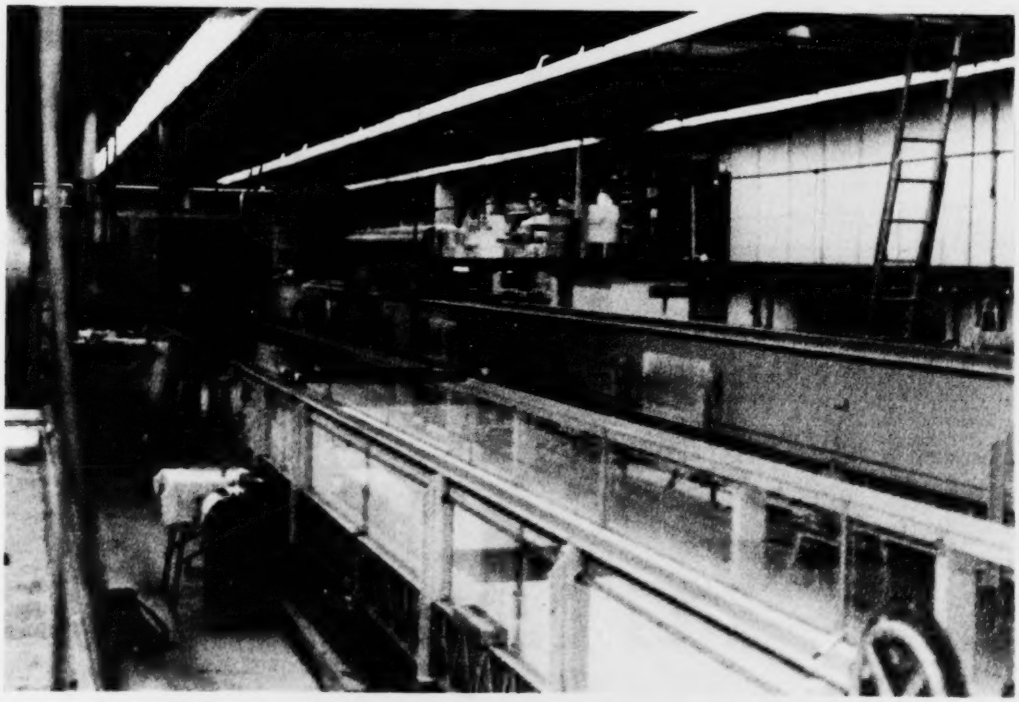

Plate 2.2 - Experimental flume in T. Blench Hydraulics Laboratory at the University of Alberta

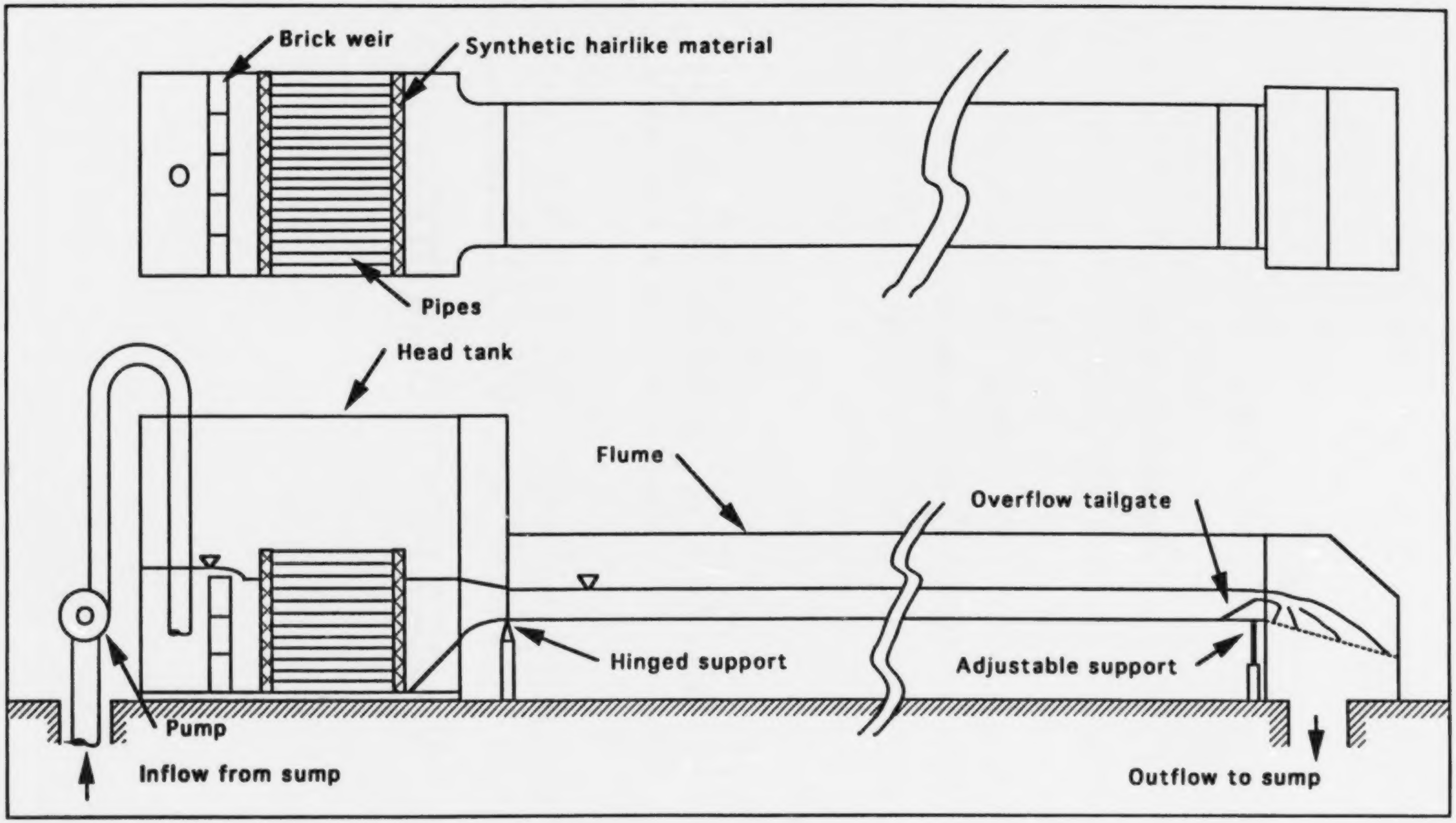
Brick weir
Synthetic hairlike material
Pipes
Head tank
Flume
Overflow tailgate
Hinged support
Adjustable support
Pump
Inflow from sump
Outflow to sump

Figure 2.1 - Experimental flume (not to scale)

The flume had an adjustable bed slope and a hinged overflow gate at the downstream end. Water was drawn from a sump under the laboratory floor by a Fairbanks-Morse 6310 two stage propeller pump and sent through a 20 cm diameter pipe to the head tank. After leaving the flume, it was returned to the sump. A maximum discharge of 80 L/s was attainable with this system. Water levels in the flume were then controlled through the variation of discharge, bed slope and tailgate elevation.

The flume had a hydraulically smooth aluminum bed along its length. This surface was used as a smooth bed in all runs where it was required. The smooth side of the six metre long Nomad® cover was used to simulate a smooth cover. Both rough boundaries were modelled using the rough side of the Nomad® matting. When using it as a bed material the generous application of a silicone adhesive ensured that it remained attached to the bed and did not bubble up to present a bedform roughness.

2.2 Experimental Procedure

For each run, direct measurements were made of discharge, flow depth, velocity profiles and longitudinal bed and surface profiles. From these, other parameters such as average velocities, boundary shear velocities and hydraulic roughnesses were calculated.

Twenty-four runs were performed, encompassing all combinations of rough and smooth bed; rough, smooth and no ice; and nominal discharges of 10, 20, 40 and 70 L/s. The nomenclature used to describe these runs will be of the form A/B/C where A is S or R, representing smooth or rough bed, B is S, R, or O, representing smooth or rough cover or open channel flow, respectively, and C is the nominal discharge in litres per second. All smooth bed runs were done at a bed slope of 0.00094 m/m and all rough bed runs at a slope of 0.00303 m/m.

To check that flows were fully turbulent, to ensure the applicability of turbulent flow equations, the Reynolds number for each run was calculated. This value was determined using the following equation:

$$R_e = \frac{4VR}{\nu} \tag{2.1}$$

The flow was accepted as fully turbulent if the Reynolds number exceeded 5000 [Miller, 1989].

An attempt was made to set the flows at normal depth by varying the tailgate elevation until a constant depth was measured along the length of the roughness. This method was deemed necessary because no value for the hydraulic roughness of the mat or flume bed was yet known. The relatively short length of the artificial roughness, as well as the fact that the flow was developing along its length, made this technique crude at best.

The test section was 5.5 m from the leading edge of the cover and 0.5 m from its end. It was hoped that this would ensure a fully developed flow. A check on this was done using the smooth bed and rough cover at a discharge of 70 L/s. Velocity profiles were taken at the test section and at a section 1.0 m upstream. They were taken at lateral intervals of 5 cm, to ensure more accuracy than the usual 15 cm, and compared. If no significant difference was noted, as this run would be one of those expected to have the longest development length, it would be reasonable to accept all runs as fully developed.

2.2.1 Discharge Measurement

Discharge through the flume was measured using a Foxboro 1808 magnetic flow meter installed on the 20 cm supply line. This sent a signal to a Foxboro E96R VA magnetic flow transmitter and the discharge was read on a Fluke 8000A digital multimeter to which it was connected. As well, velocity profiles were integrated over the depth of the channel to yield a value for discharge through the central portion of the channel.

2.2.2 Velocity Profile Measurement

The streamwise velocity was measured using a 3 mm diameter United Censor Preston tube. Small rectangular holes, 1.0 cm long in the streamwise direction and 0.5 cm wide, were cut in the cover to allow placement of the Preston tube. The tube was connected with plastic tubing to a Validyne model DP45-16 pressure transducer which produced an electrical output which varied linearly with velocity head. This was sent through a Validyne model CD379-1-2 meter to a Houston Instruments Omniscribe model B5237-5 stripchart recorder on which the turbulent fluctuations with time could be seen. The measurement apparatus is pictured on Plate 2.3. Readings were typically taken for one to two minutes so that a reasonable value of time-averaged velocity could be estimated. A velocity profile would be made up of anywhere from 15 to 40 measurements, depending on the depth of flow. Readings would be concentrated near the boundaries, where velocity gradients are higher, and decreased to a maximum one centimeter spacing further away. A typical section of recorder output is pictured on Plate 2.4.

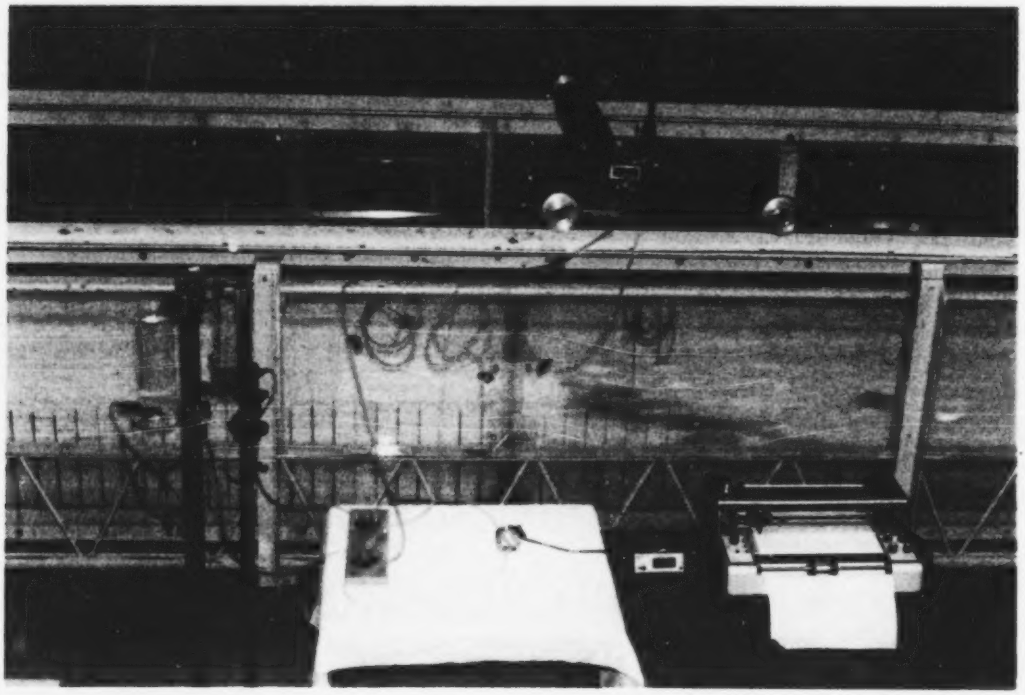

Plate 2.3 - Velocity measurement apparatus

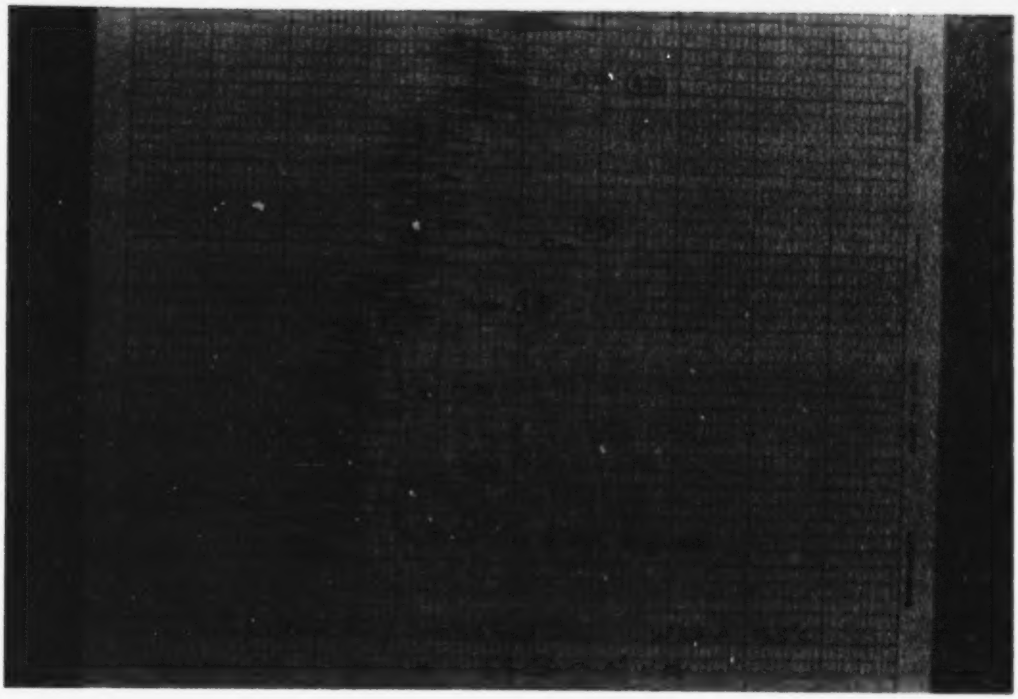

Plate 2.4 - Typical chart recorder output

In order to accurately simulate flow in a wide (width >> depth) channel, aspect ratios of the flow were kept high to ensure the effects of sidewall friction were minimized. It should be noted that the addition of a surface cover on a rectangular channel effectively doubles the aspect ratio, further reducing the influence of the sidewall. Velocity profiles were taken at five lateral stations at the test section, on the centerline of the channel as well as 15 and 30 centimetres to either side of it. Thus, only the central portion of the channel was considered. These five profiles were then averaged to produce an average velocity profile for each run. Due to sidewall friction, slightly more than 50% of the flow occurs in the central half of the flume. Therefore, to determine a more accurate measurement of discharge, the average velocity profile was integrated across its depth to produce an average velocity, which was expected to be slightly higher than that measured by the magnetic flow meter.

2.2.3 Flume Surveys

Slopes of the flume bed and water surface (piezometric head line) were determined by surveying the reach extending four metres upstream of the test section. Five measurements were made at each section, directly as well as 15 and 30 centimetres to the left and right of the centreline. A slight rightward tilt in the flume was noted, so average elevations at each section were used for both the bed and water surface profiles. Measurements were made to an accuracy of 0.1 mm using a Geotec AL-23 level and a metal rod on a rail-mounted traverse. The rod had a pointed conical tip to aid in determining the location of the water surface. These measurements also allowed the depth of flow to be determined.

2.2.4 Boundary Shear Measurement

The measurement of boundary shear stress is important in any investigation of channel flow, but especially so in this experiment where there are cases of unequal boundary roughnesses. From the data collected there are two ways to determine the shear velocity at a boundary.

The first is through an analysis of the velocity profile. Proceeding from the Karman-Prandtl equation for rough turbulent flow, applied at two points in the 30% of the profile closest to the boundary, one may subtract one equation from the other and arrive at:

$$\frac{u_2 - u_1}{u_*} = 5.75\left(\log \frac{y_2}{k_s} - \log \frac{y_1}{k_s}\right) \tag{2.2}$$

Combining the logarithmic terms and rearranging, this becomes:

$$u_* = \frac{1}{5.75}\left(\frac{u_2 - u_1}{\log (y_2/y_1)}\right) \tag{2.3}$$

This derivation may likewise be applied to the corresponding equation for smooth turbulent flow to yield the same result.

An alternative method involves only one velocity measurement with the Preston tube placed on the boundary. A more detailed discussion of the development of this method is located in Appendix A. Here, three equations, applied to three ranges of flow, are presented. Use is made of several intermediate parameters to aid in clarity:

$$x^* = \log\left(\frac{u^2 D_p^2}{8 v^2}\right) \tag{2.4}$$

$$y^* = \log\left(\frac{u_*^2 D_p^2}{8v^2}\right) \tag{2.5}$$

$$D^+ = \frac{u_* D_p}{v} \tag{2.6}$$

Here D_p is the diameter of the Preston tube. The applicable equations, with their corresponding conditions, are:

a) $0 < y^* < 1.5$ and $D^+ < 11.2$

$$y^* = 0.037 + 0.5\,x^* \tag{2.7}$$

b) $1.5 < y^* < 3.5$ and $11.2 < D^+ < 110$

$$y^* = 0.8287 - 0.1381\,x^* + 0.1437\,x^{*2} - 0.0060\,x^{*3} \tag{2.8}$$

c) $3.5 < y^* < 5.3$ and $110 < D^+ < 1600$

$$x^* = y^* + 2.0 \log\left(1.95\,y^* + 4.10\right) \tag{2.9}$$

These equations are valid for smooth turbulent flows in pressure gradients ranging from mildly adverse to mildly favorable. Here no pressure gradient exists, so their use is valid.

For rough turbulent flows, it is preferable to use the velocity profile method detailed earlier, but an alternative technique based on a knowledge of the boundary roughness, virtual origin and the appropriate value of the parameter B in the following equation also exists:

$$\frac{u}{u_*} = 5.75 \log \left(\frac{D_p/2 + y_0}{k_s} \right) + B \qquad (2.10)$$

The origin of this method also detailed in Appendix A. Its accuracy is taken as being within 10% of the actual value.

2.2.5 Roughness Calculation

Given the previously obtained data, two methods exist to determine the boundary roughness. These are based on the measured velocity profile and bulk flow measurements.

The first method again involves an examination of the 30% of the velocity profile most proximate to the boundary. It is based on the equations for smooth or rough turbulent flow, which are, respectively:

$$\frac{u}{u_*} = 5.75 \log \frac{y u_*}{\nu} + 5.5 \qquad (2.11a)$$

$$\frac{u}{u_*} = 5.75 \log \frac{y}{k_s} + 8.5 \qquad (2.11b)$$

Bringing the constants into the logarithmic terms, and introducing the parameter k_v to represent viscous roughness, these equations become:

$$\frac{u}{u_*} = 5.75 \log \frac{30y}{k_v} \qquad (2.12a)$$

$$\frac{u}{u_*} = 5.75 \log \frac{30y}{k_s} \tag{2.12b}$$

$$\text{where } k_v = \frac{3.3\nu}{u_*} \tag{2.13}$$

If the velocity profile curves are non-dimensionalized by dividing velocity by shear velocity, it is apparent that at the point where the left hand side of either equation equals zero, the log term must also equal zero. Therefore, the argument of the log function must equal unity. Thus,

$$k_s, k_v = 30\ y \qquad \text{when} \qquad \frac{u}{u_*} = 0 \tag{2.14}$$

Alternatively, with accurate flow measurements, one may use the dimensionless Chezy equation to determine the roughness of the boundary:

$$V = C_* \cdot \sqrt{gRS_f} \tag{2.15}$$

where the radical term is equal to the shear velocity and the conveyance coefficient has been empirically defined as:

$$C_* = 2.5 \ln \frac{R}{k} + 6.2 \tag{2.16}$$

for channel-like flows (Gerard, 1988). Taking the constant into the logarithmic term and rearranging yields:

$$k = \frac{12R}{e^{C_*/2.5}} \tag{2.17}$$

where $$C_* = \frac{V}{u_*} \tag{2.18}$$

So, the boundary roughness may be determined from measurements of hydraulic radius, average flow velocity and boundary shear velocity. The latter may be determined from the methods previously presented or, for the case of fully developed flow at normal depth, by the use of the radical term from the dimensionless Chezy equation. In this experiment it was decided to use the former as the developing flow in the upstream reach, combined with the possible error included in survey measurements, combined to reduce confidence in the latter.

2.2.6 Summary of Experiments

In summary, a series of experiments was performed to investigate the phenomenon of ice covered flow. Initial open channel runs were followed by subsequent ones in a closed channel, with a synthetic cover to simulate ice. Measurements of velocity profiles, slopes and discharges allowed the computation of boundary shear stresses and roughnesses. All of this data, once acquired, would be analyzed to produce some insight into ice covered flows.

3.0 Analysis of Experimental Data

The experiments described took place over a period of four months in the summer and fall of 1991, with supplementary experiments performed in August of 1992. Except for some preliminary work, done to ensure that the data acquired was acceptable, all analysis was done after the completion of data collection. Turbulent fluctuations in the raw data were time-averaged by drawing a best-fit line through each reading. Data was then processed using various computer applications.

3.1 Verification of Fully Developed Flow

Given the experimental setup used, it was required that all covered flows be fully developed within 5.5 m of the leading edge of the cover, and all open channel flows within 10.0 m of the start of the flume. Two methods of determining whether flows were fully developed are described here.

A previous investigation into flow development lengths was done using the same flume as these experiments were performed in [Jasek, 1992]. This study determined reach lengths necessary for full flow development in the case of open channel flow with both smooth and rough boundaries. It was determined that in the case of smooth boundary flow, a distance of approximately 60 depths of flow is required for full flow development, while for a rough boundary with k_s = 30 mm a distance of half this will suffice. This experiment presented a slightly different situation in that it involved a covered flow and a considerable length of open channel flow upstream of the cover's leading edge. If the plane of zero shear between the bed and cover is taken as the division between the two zones of influence, then it was assumed that the thickness of the zone may be taken as equivalent to the flow depth in the open channel case. Based on a 5.5 m development length, the thickness of the zone of influence should then not exceed 0.090 m for the smooth boundary or 0.180 m for the rough. As seen in Table 3.1, all runs fell within limits for fully developed flow which are set forth here.

SMOOTH BOUNDARIES				ROUGH BOUNDARIES			
Run	Boundary	Depth (m)	Depths to Test Section	Run	Boundary	Depth (m)	Depths to Test Section
S/R/10	Bed	0.0197	279	R/R/10	Bed	0.0261	211
S/R/20	Bed	0.0313	176	R/R/20	Bed	0.0410	134
S/R/40	Bed	0.0409	134	R/R/40	Bed	0.0512	107
S/R/70	Bed	0.0492	112	R/R/70	Bed	0.0736	75
S/S/10	Bed	0.0323	170	R/S/10	Bed	0.0400	138
S/S/20	Bed	0.0383	144	R/S/20	Bed	0.0575	96
S/S/40	Bed	0.0525	105	R/S/40	Bed	0.0850	65
S/S/70	Bed	0.0764	72	R/S/70	Bed	0.1185	46
S/O/10	Bed	0.0537	186	R/O/10	Bed	0.0374	267
S/O/20	Bed	0.0682	147	R/O/20	Bed	0.0564	177
S/O/40	Bed	0.1274	78	R/O/40	Bed	0.0769	130
S/O/70	Bed	0.1713	58	R/O/70	Bed	0.0978	102
S/S/10	Cover	0.0332	166	S/R/10	Cover	0.0483	114
S/S/20	Cover	0.0367	150	S/R/20	Cover	0.0602	91
S/S/40	Cover	0.0505	109	S/R/40	Cover	0.0966	57
S/S/70	Cover	0.0761	72	S/R/70	Cover	0.1167	47
R/S/10	Cover	0.0104	529	R/R/10	Cover	0.0249	221
R/S/20	Cover	0.0180	306	R/R/20	Cover	0.0370	149
R/S/40	Cover	0.0258	213	R/R/40	Cover	0.0518	106
R/S/70	Cover	0.0329	167	R/R/70	Cover	0.0699	79
Flow development requires:			60	Flow development requires:			30

Figure 3.1 - Development Lengths to Test Section

As a further check on the flow development, one of the most critical runs (S/R/70) was performed more intensively than the rest to gauge whether full development had been achieved. In that run, 13 profiles were taken at each test section instead of the usual five. Two sections, the usual one, 5.5 m from the leading edge of the cover, and another 1.0 m upstream, were measured and compared. The average profile at each section is shown in Figure 3.1, and it is apparent from this that the flow was indeed fully developed. This further supports the conclusion that full flow development occurred in all runs.

3.2 Averaging of Velocity Profiles

For each run vertical velocity profiles were taken at five locations at each section. The initial run, done to establish that the flow was fully developed, revealed the existence of secondary flows. Thus, it was not sufficient to measure just one profile. Based on the results of this run, it was felt that an average of five profiles would yield an adequate two-dimensional representation of the flow.

Due to the fact that readings were not always taken at the same distance from the boundary for all profiles, some method of averaging had to be devised. The technique which was chosen involved having a data point on the average profile for every distance from the boundary that existed on any of the five profiles of which it was comprised. For instance, if one profile had measurements at 1.5, 2.0, 3.0 and 5.0 mm from the boundary, and another had them at 1.5, 2.0, 4.0 and 6.0 mm, the average profile

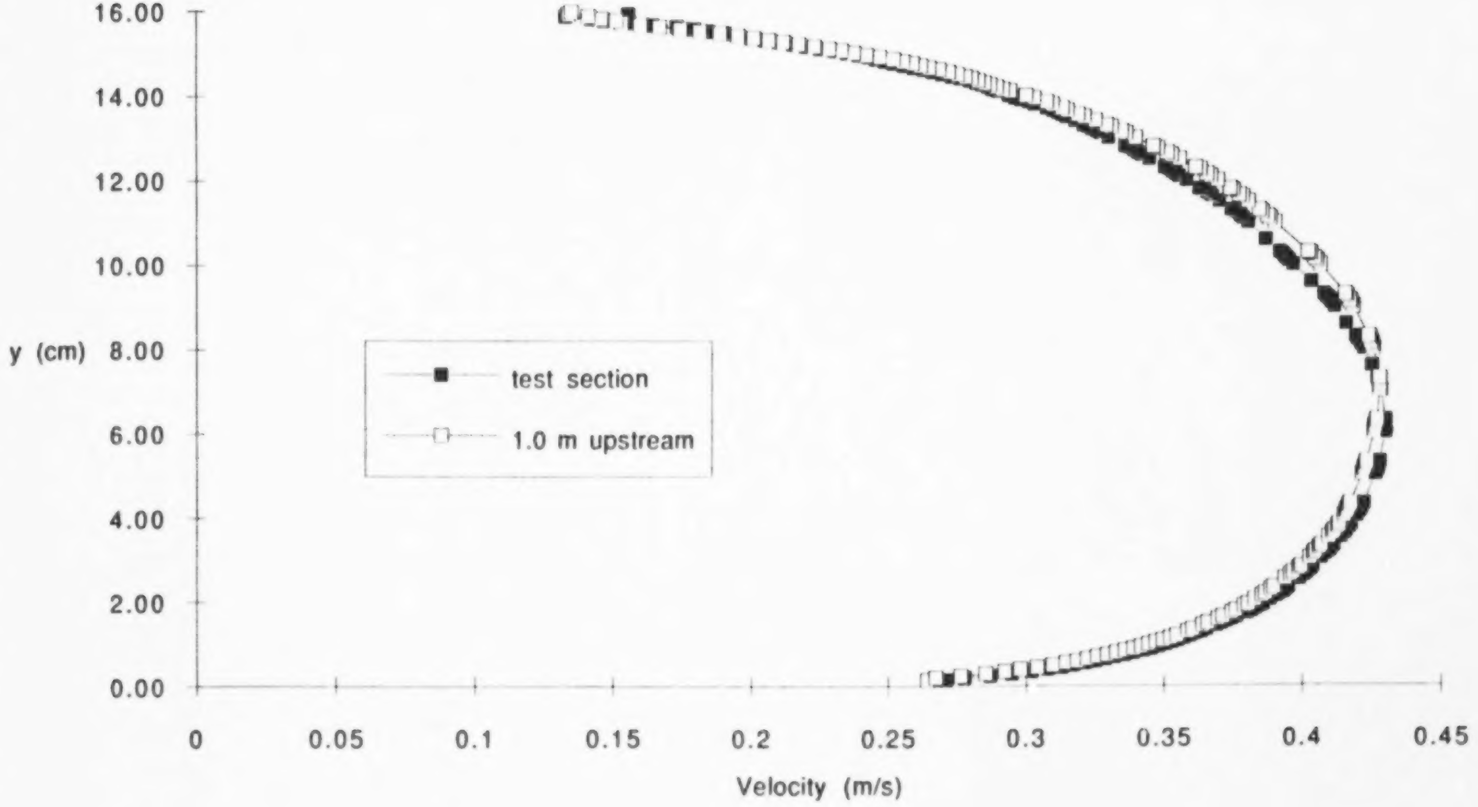

Figure 3.1 - Average velocity profiles for run S/R/70 at test section and 1.0 m upstream

would show data points at 1.5, 2.0, 3.0, 4.0, 5.0 and 6.0 mm. It is apparent then that the average profile may contain many times more data points than were taken for any single profile. In order to ensure a smooth average profile in which all five component profiles were weighted equally, intermediate data points which corresponded to distances from the boundary on the average profile were inserted, where required, into each individual profile. Velocity values for these data points were determined by linear interpolation with the actual data points above and below. This ensured that all of the component profiles were weighted equally on the composite profile.

Another problem encountered in averaging the profiles was a slight lateral tilt in the flume. This was only a matter of a few millimetres, but due to high velocity gradients near the boundary, it was necessary to match the top and bottom boundary elevations. The adjustment was done by determining the average depth of the five profiles and compressing or expanding component profiles as required to set them to this depth. The change was accomplished by inserting or removing a measure of depth, as required, into the central portion of the profile, where velocities were highest and velocity gradients were the smallest. This change in depth was in no case more than 3.0 millimetres. An example of a profile which exhibited this problem is shown in Figure 3.2, with the adjusted profile.

Average profiles, as well as the component profiles comprising them, are shown in Figures 3.3 to 3.8. Scatter in the component profiles, which in general appears to be greater for larger discharges, confirms the existence of secondary flows.

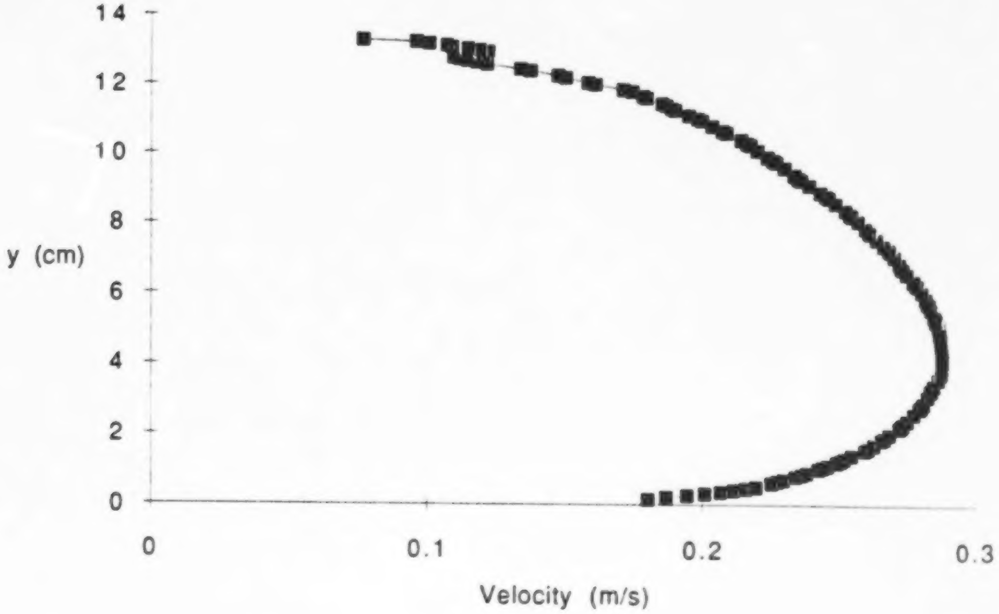

Figure 3.2(a) - Average velocity profile for run S/R/40 before adjustment

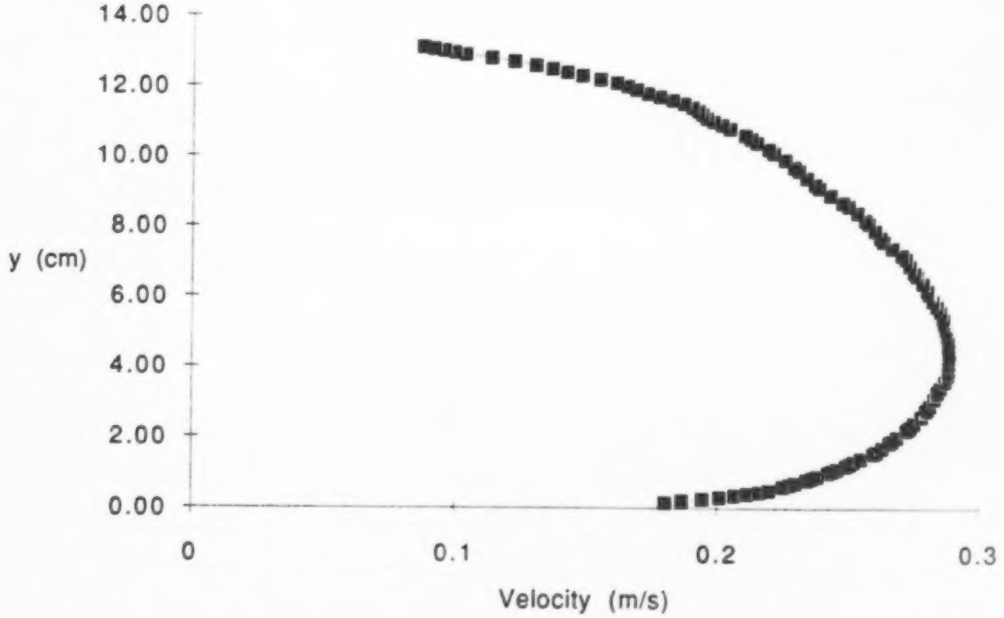

Figure 3.2(b) - Average velocity profile for run S/R/40 after adjustment

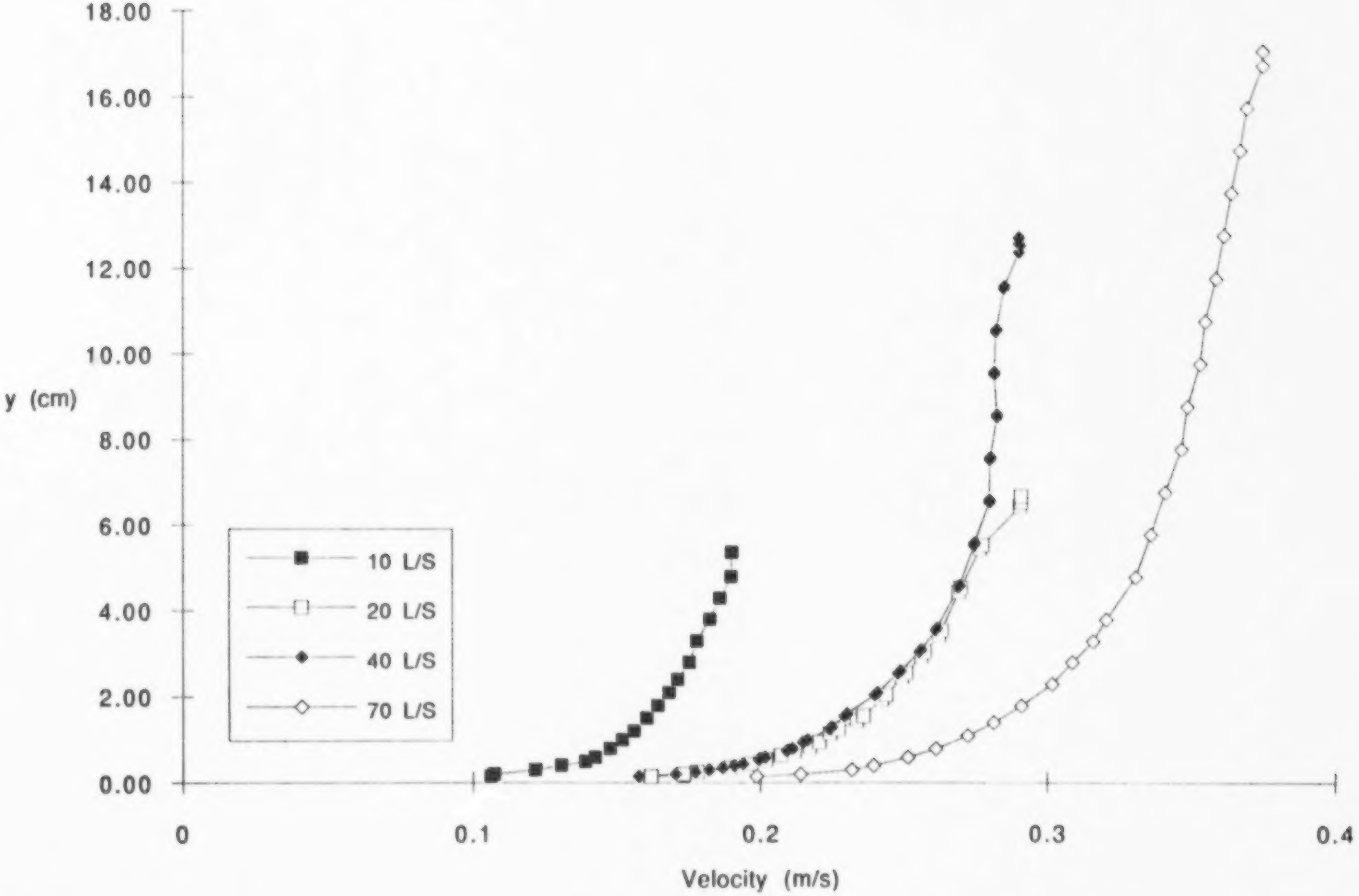

Figure 3.3(a) - Averaged velocity profiles for runs S/O/10, 20, 40 and 70

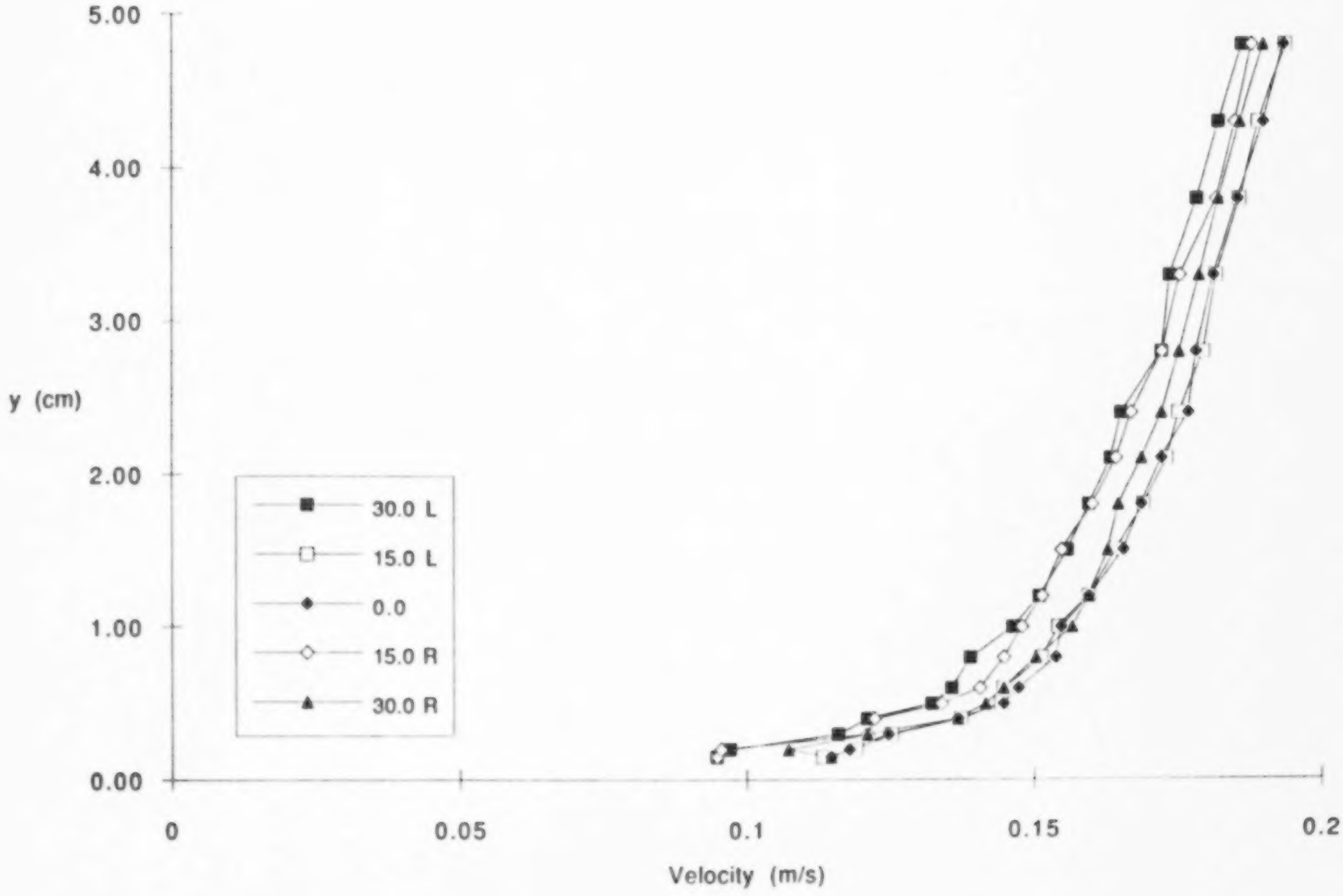

Figure 3.3(b) - Component velocity profiles for run S/O/10

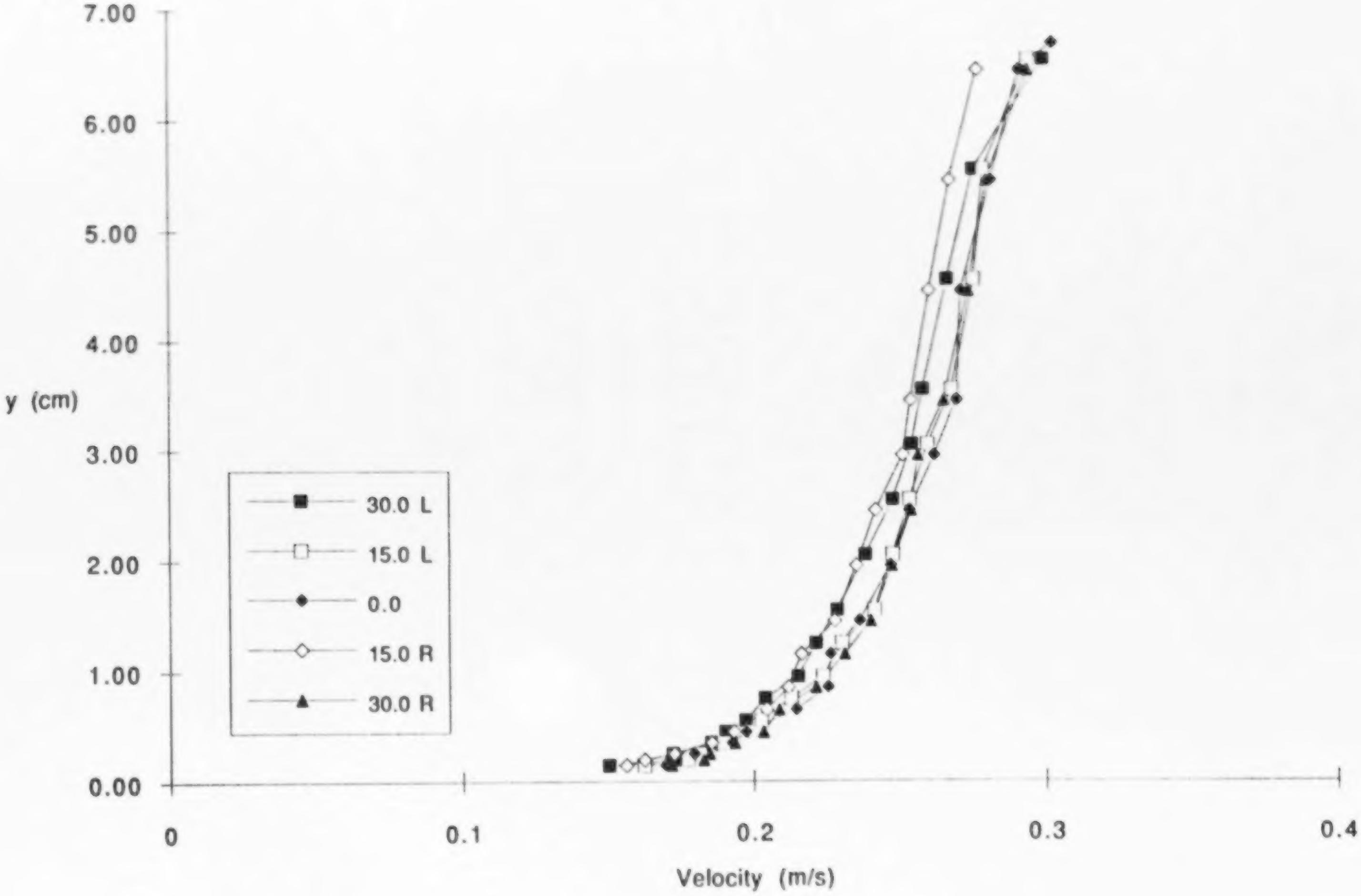

Figure 3.3(c) - Component velocity profiles for run S/O/20

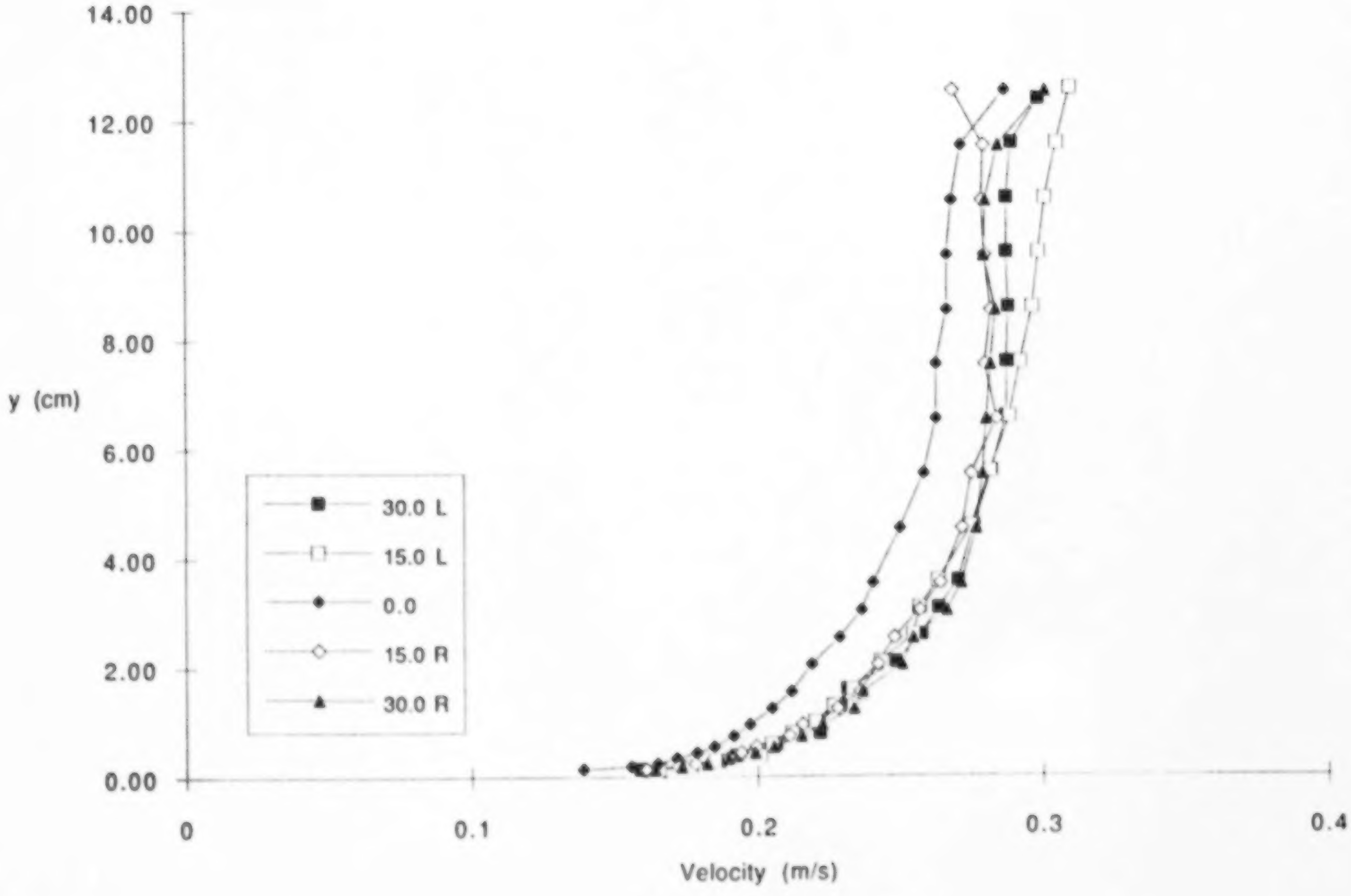

Figure 3.3(d) - Component velocity profiles for run S/O/40

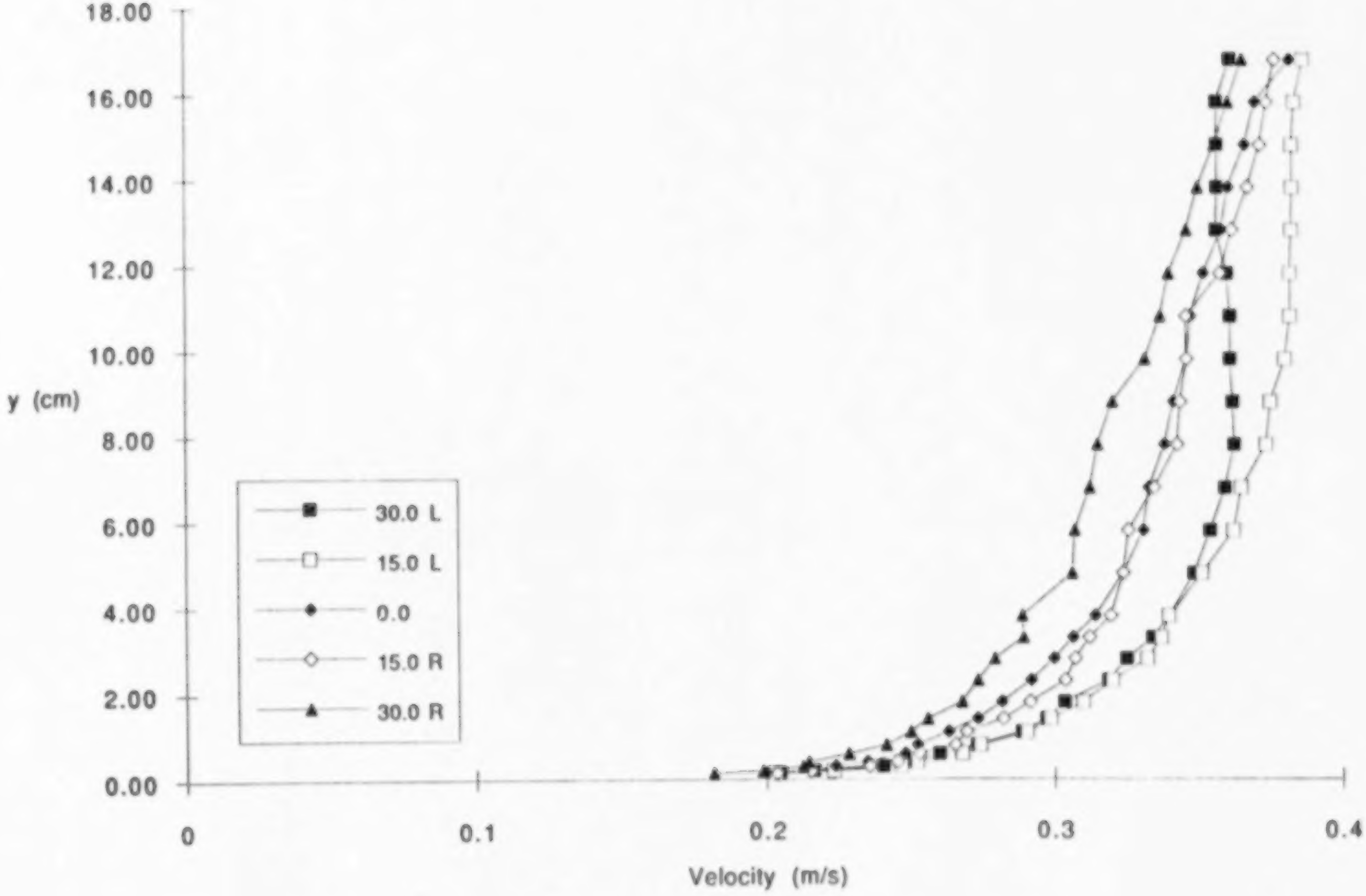

Figure 3.3(e) - Component velocity profiles for run S/O/70

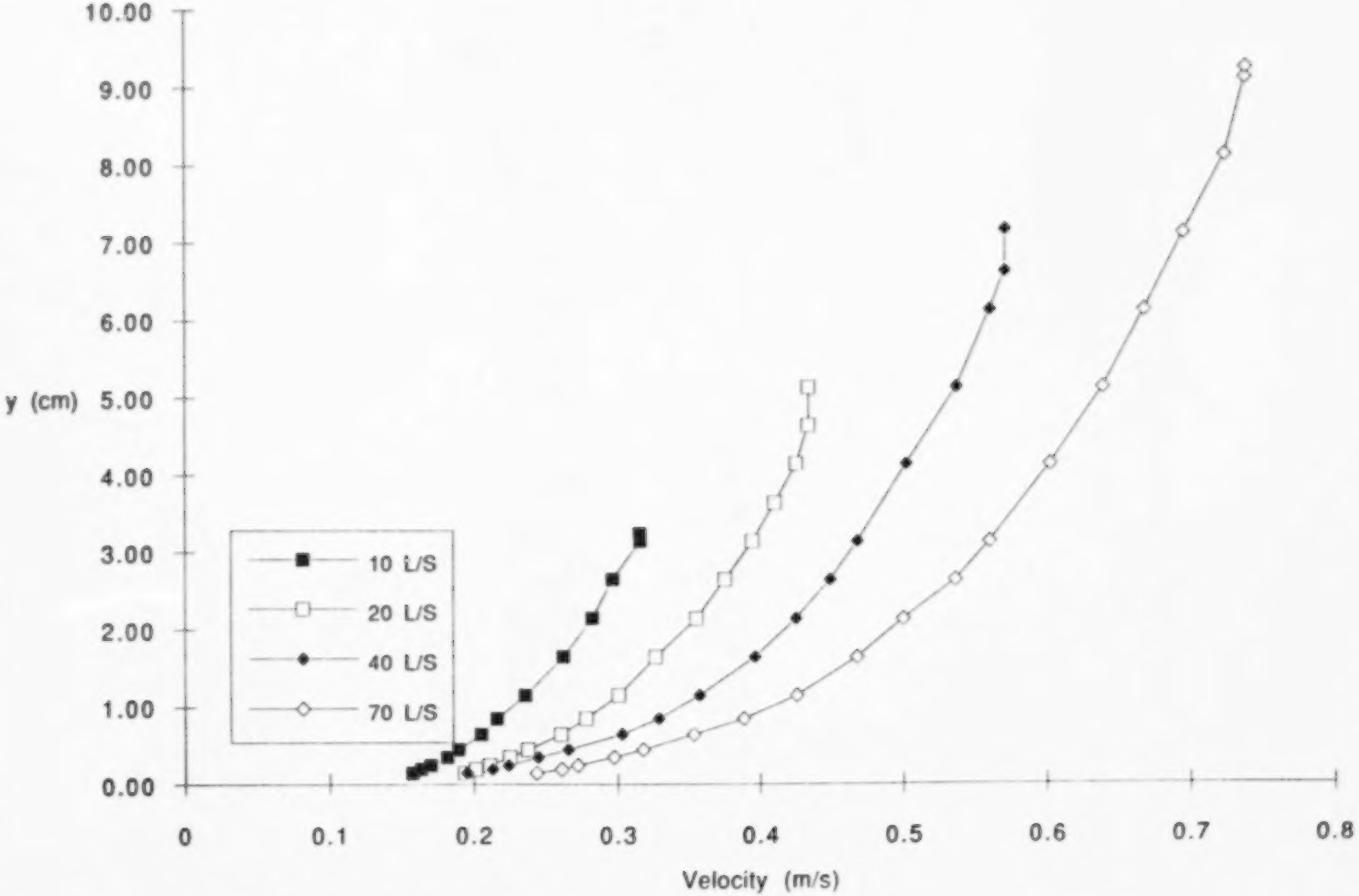

Figure 3.4(a) - Averaged velocity profiles for runs R/O/10, 20, 40 and 70

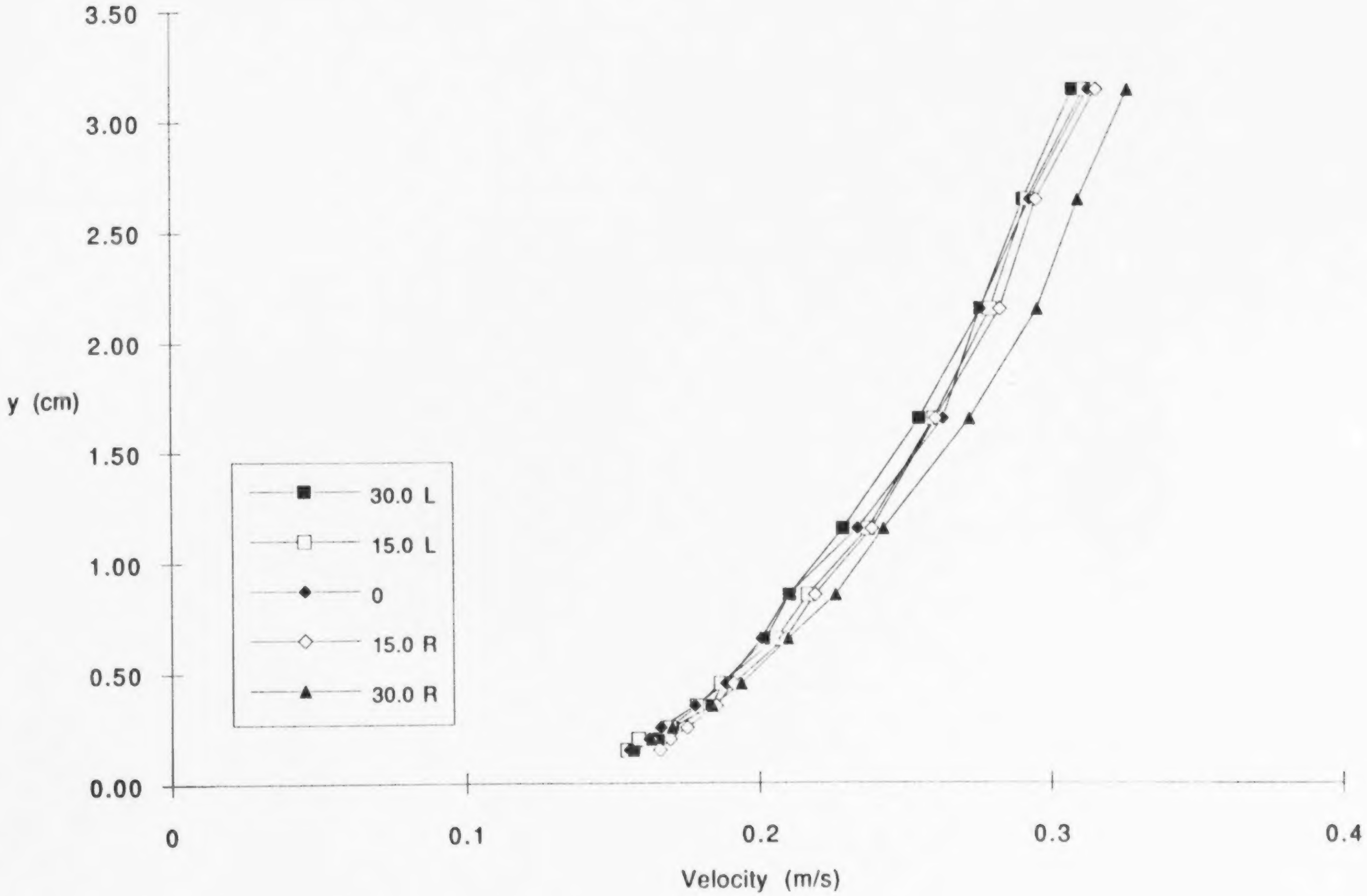

Figure 3.4(b) - Component velocity profiles for run R/O/10

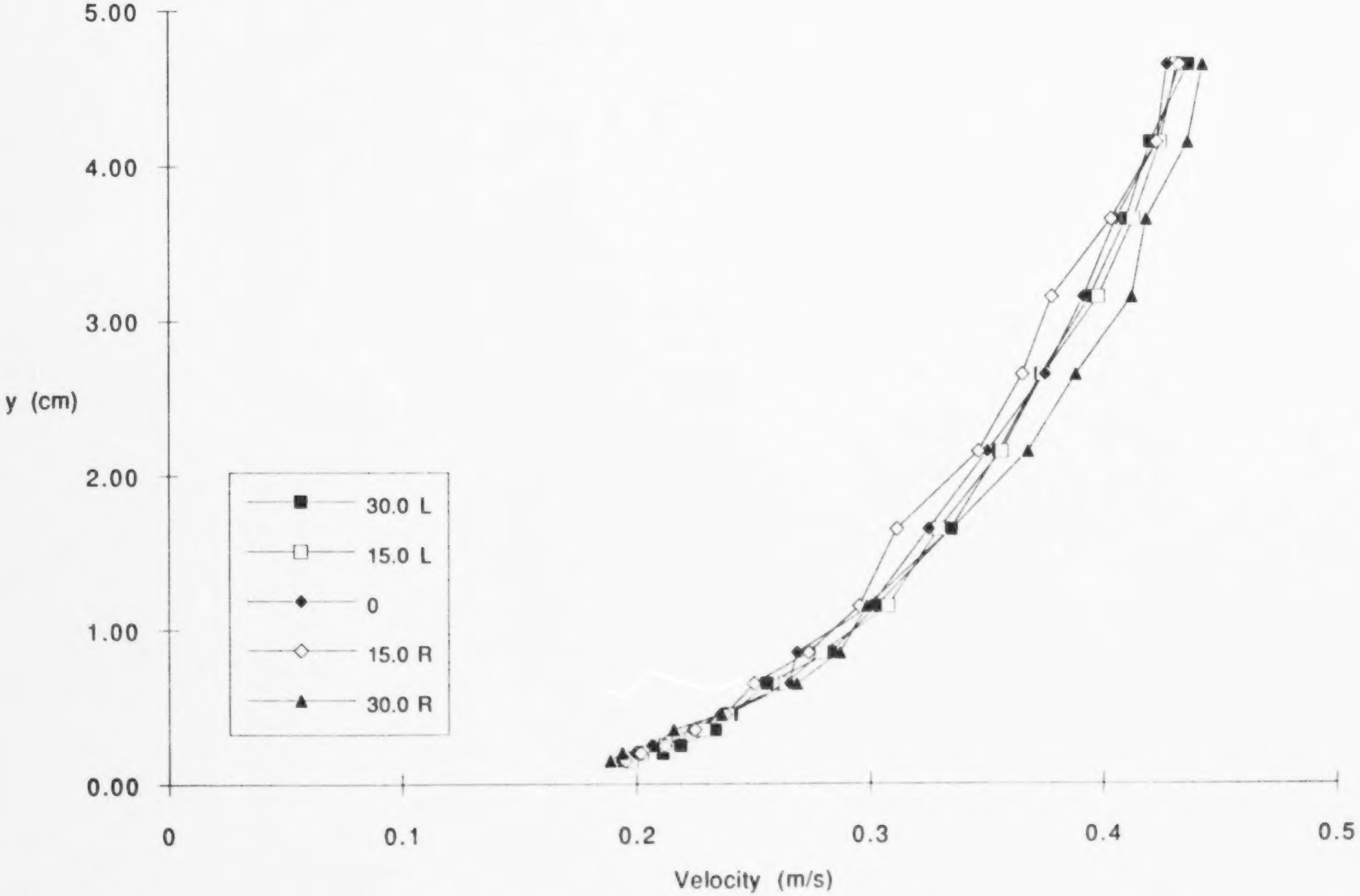

Figure 3.4(c) - Component velocity profiles for run R/O/20

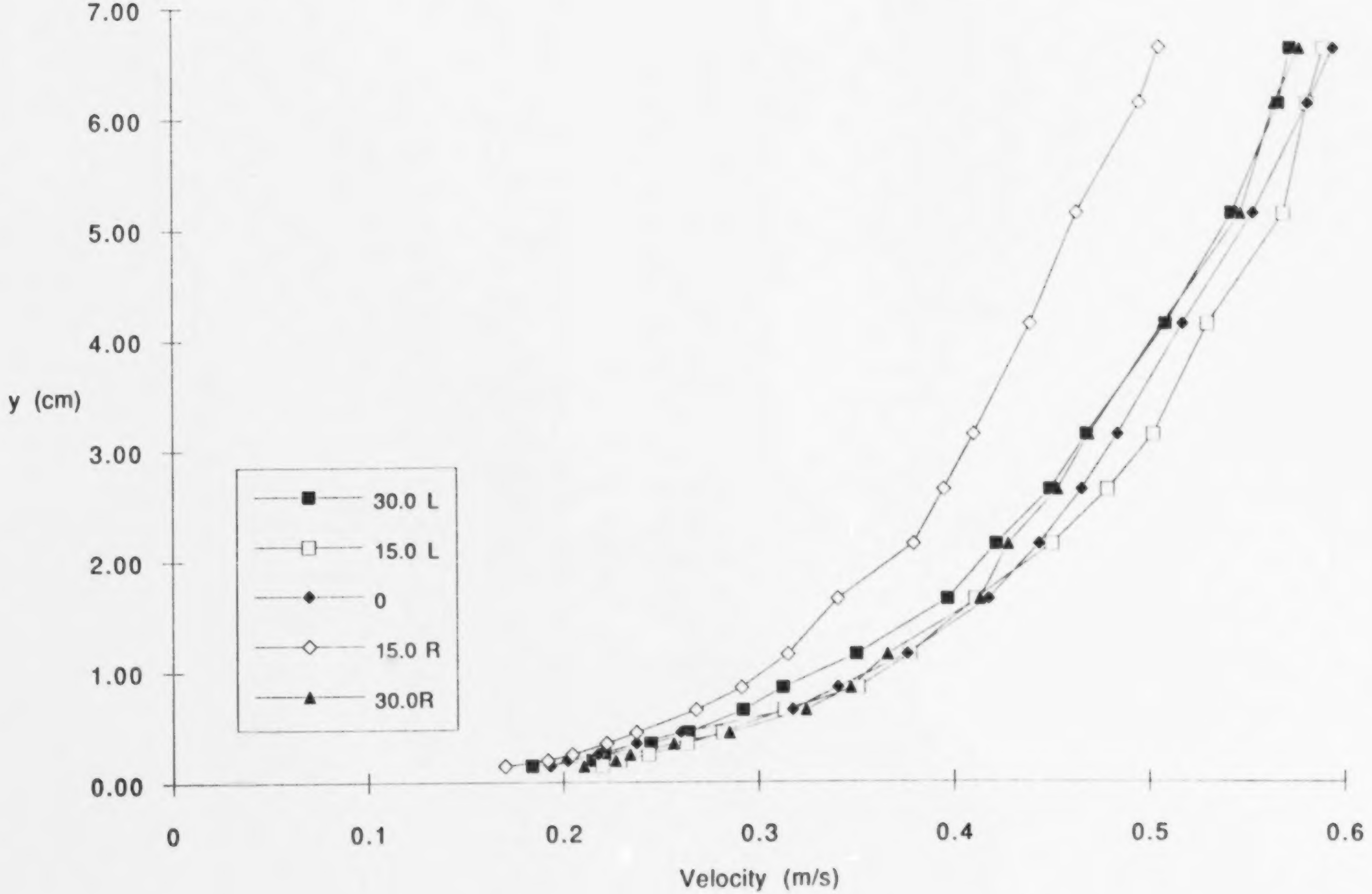

Figure 3.4(d) - Component velocity profiles for run R/O/40

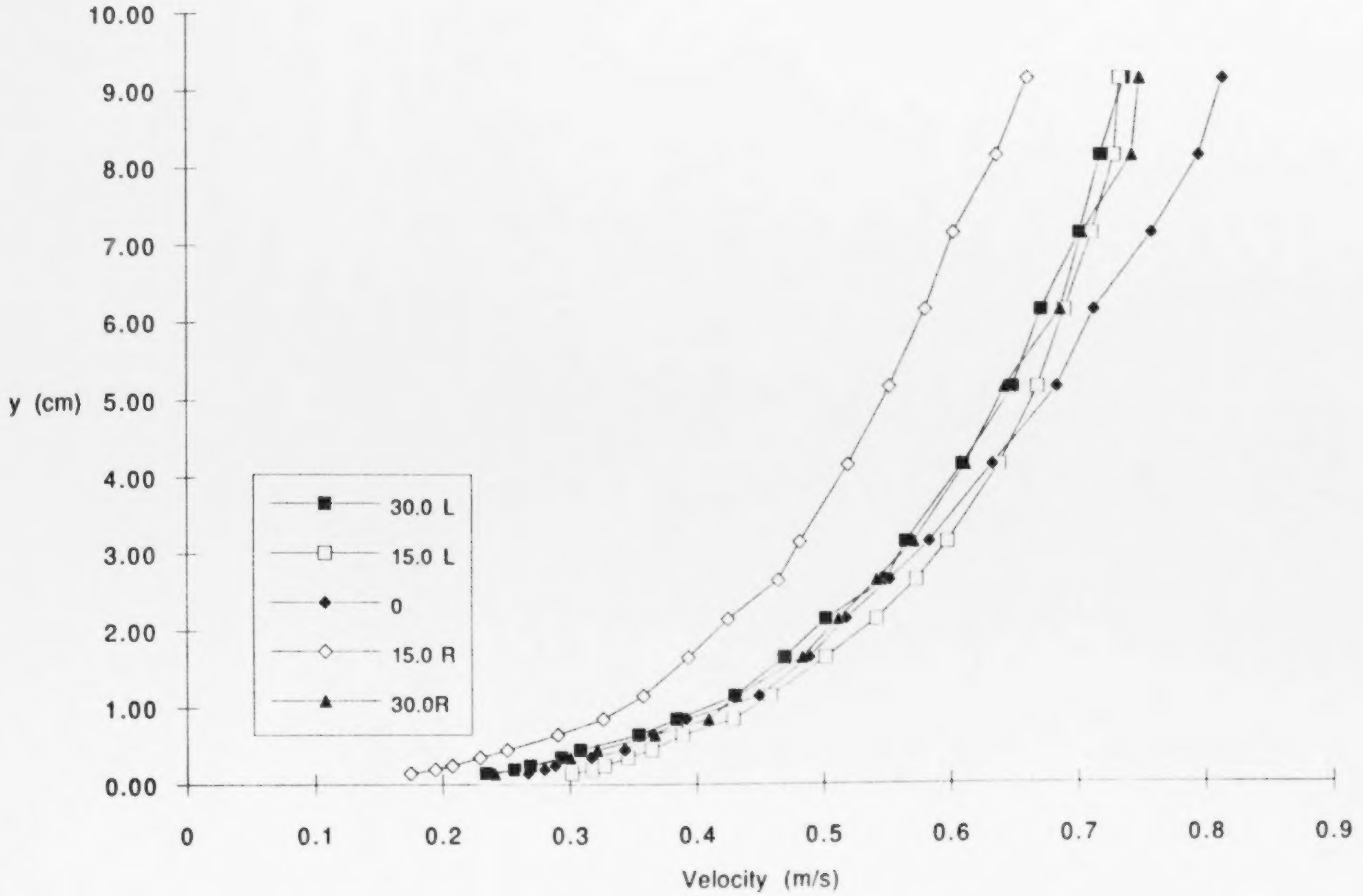

Figure 3.4(e) - Component velocity profiles for run R/O/70

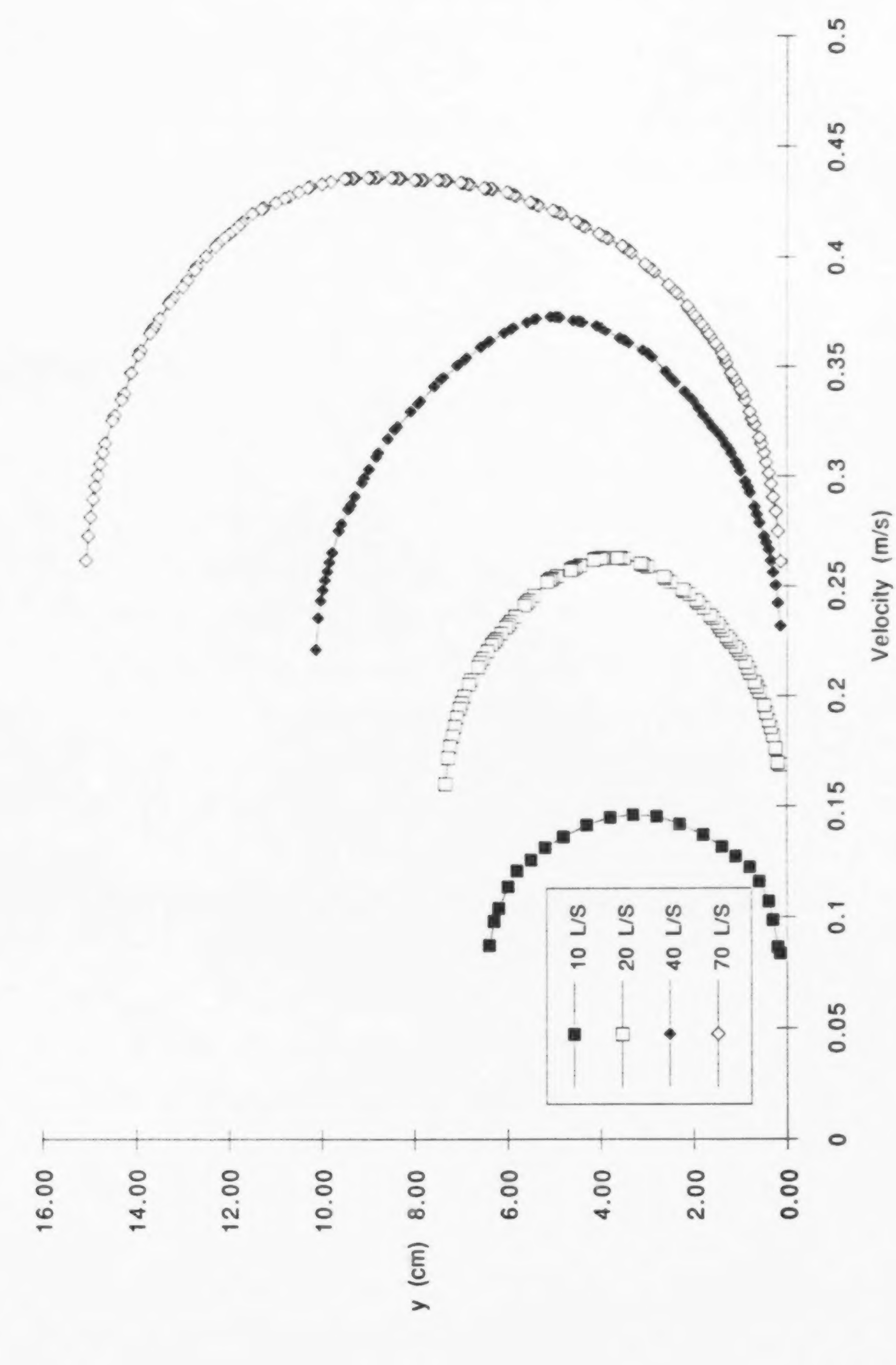

Figure 3.5(a) - Averaged velocity profiles for runs S/S/10, 20, 40, and 70

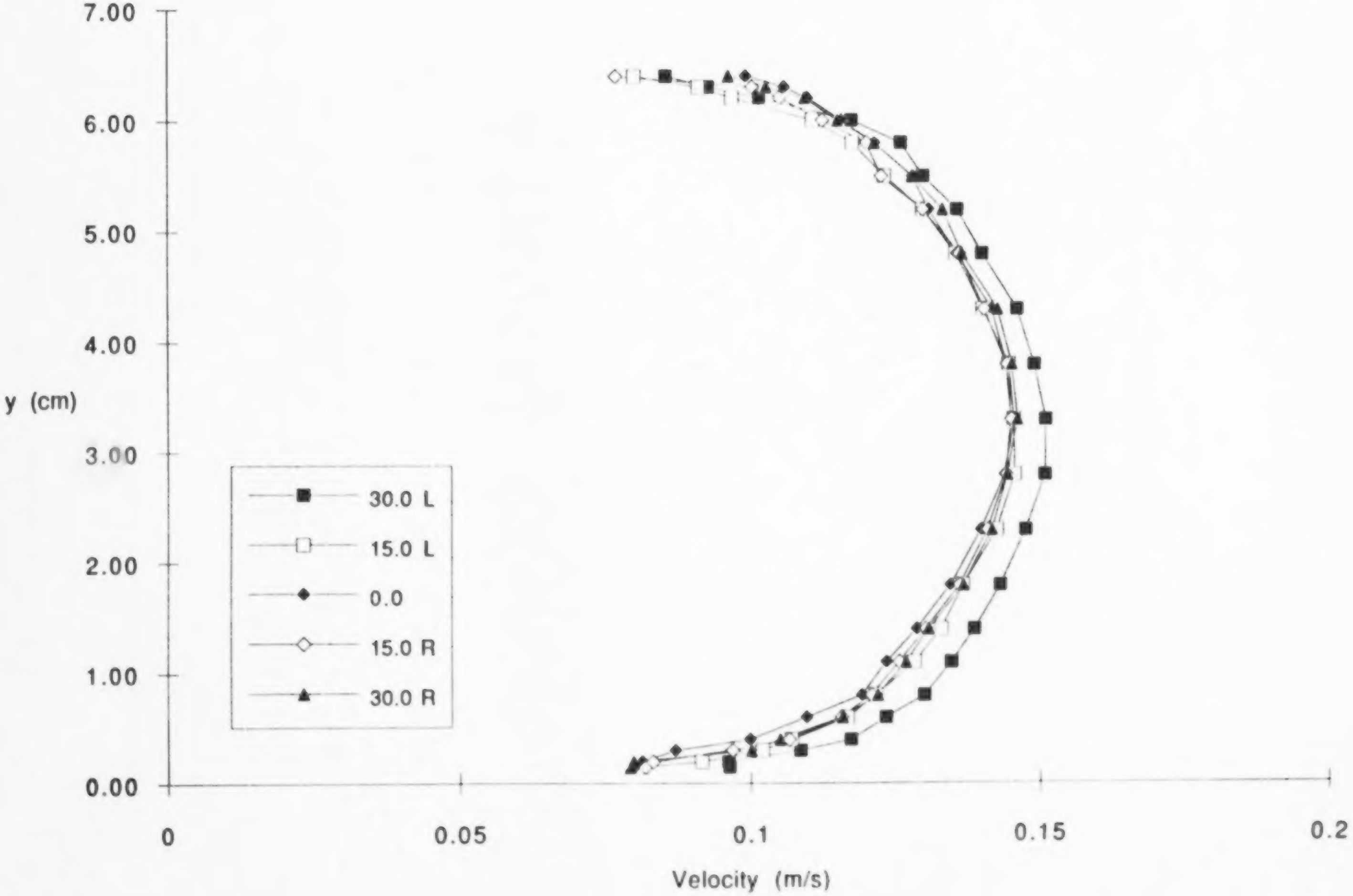

Figure 3.5(b) - Component velocity profiles for run S/S/10

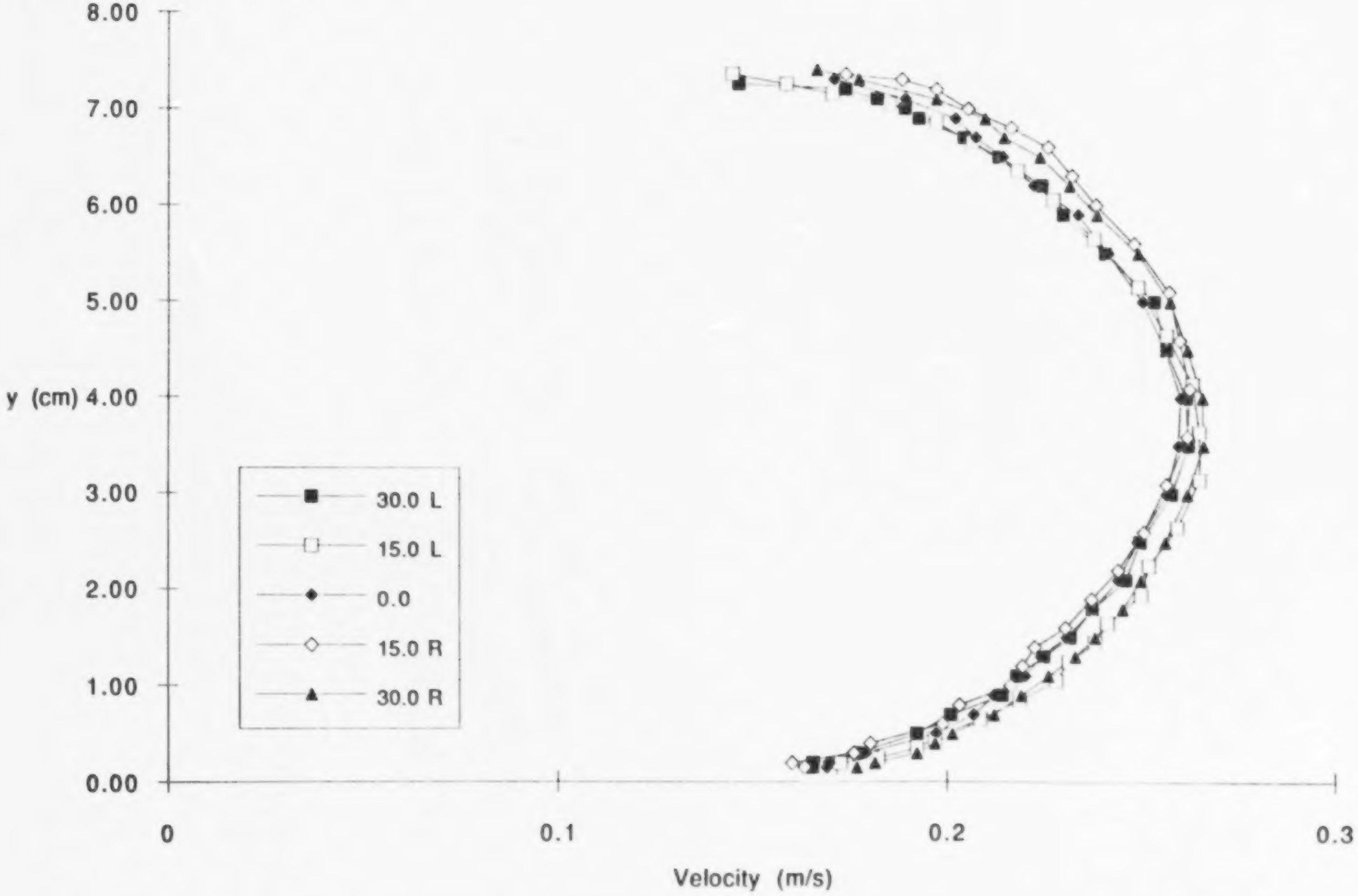

Figure 3.5(c) - Component velocity profiles for run S/S/20

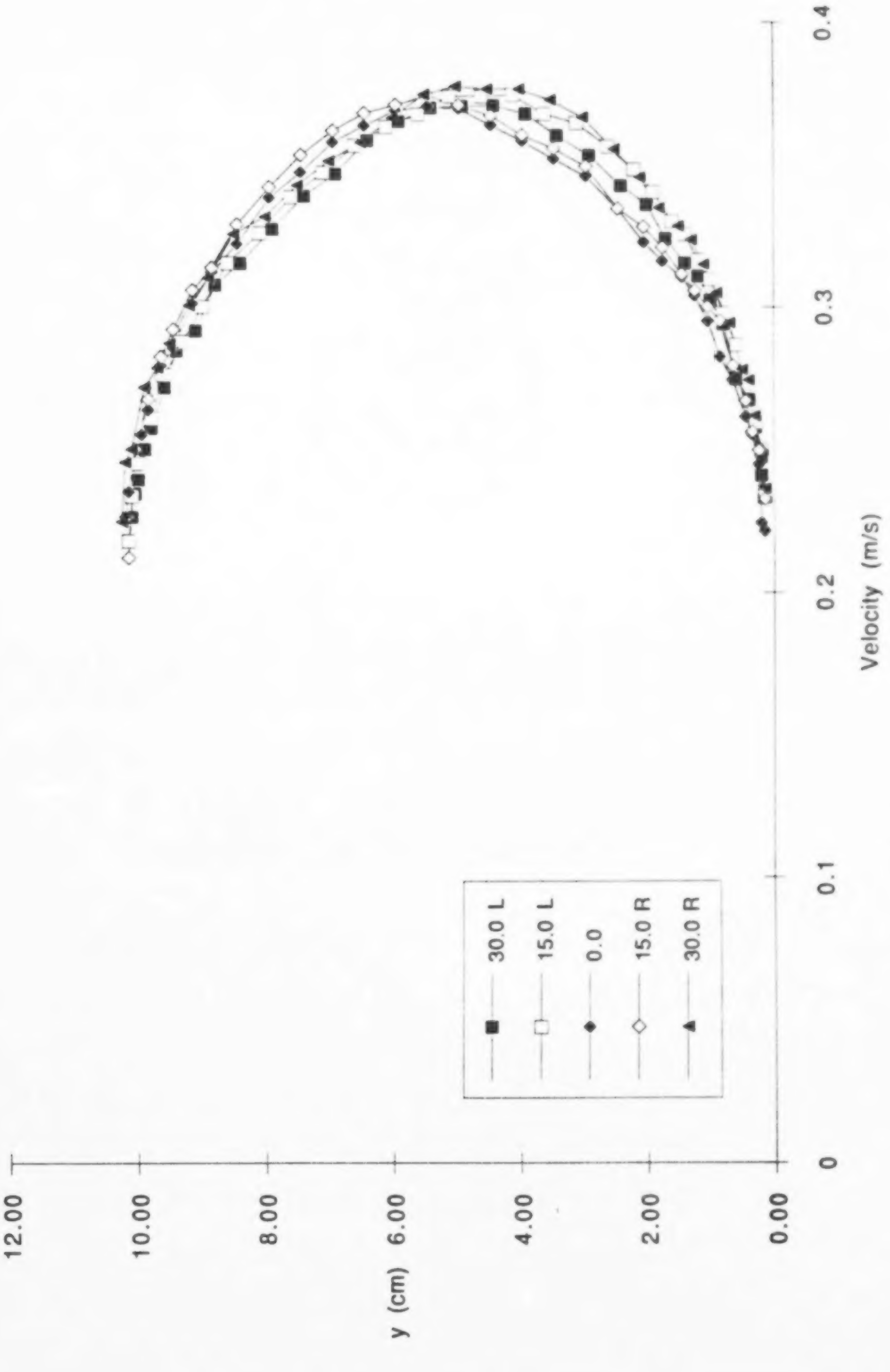

Figure 3.5(d) - Component velocity profiles for run S/S/40

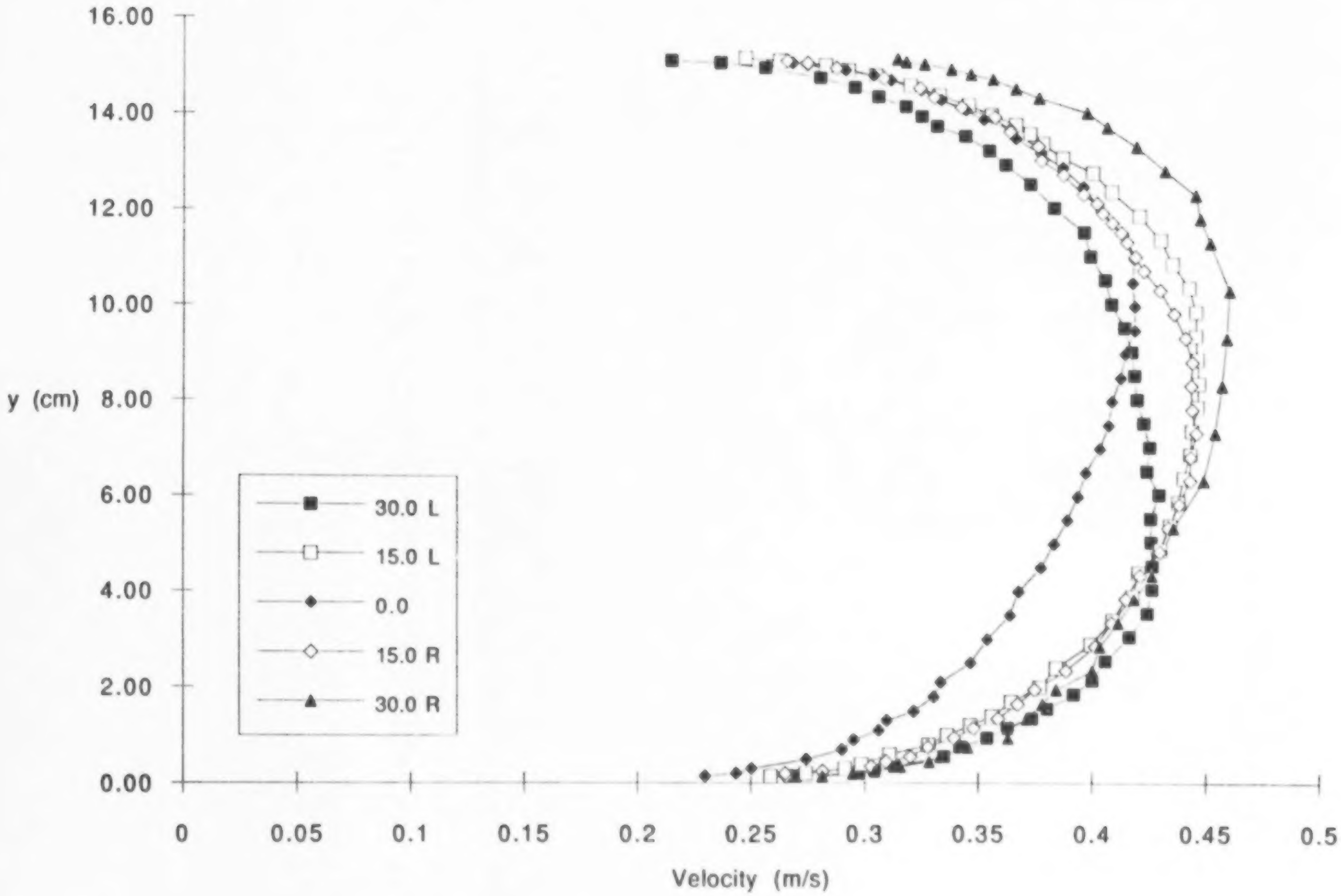

Figure 3.5(e) - Component velocity profiles for run S/S/70

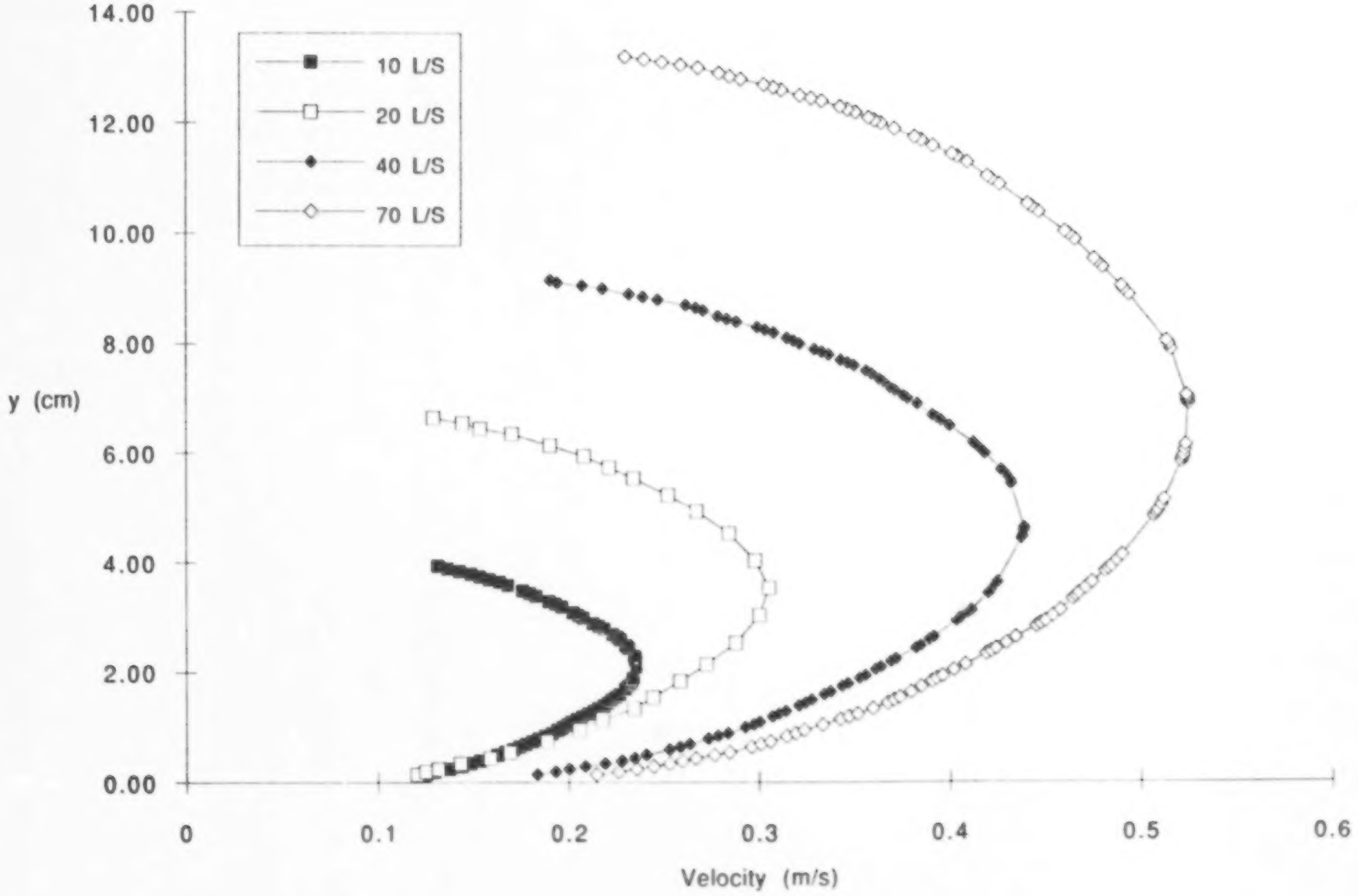

Figure 3.6(a) - Averaged velocity profiles for runs R/R/10, 20, 40 and 70

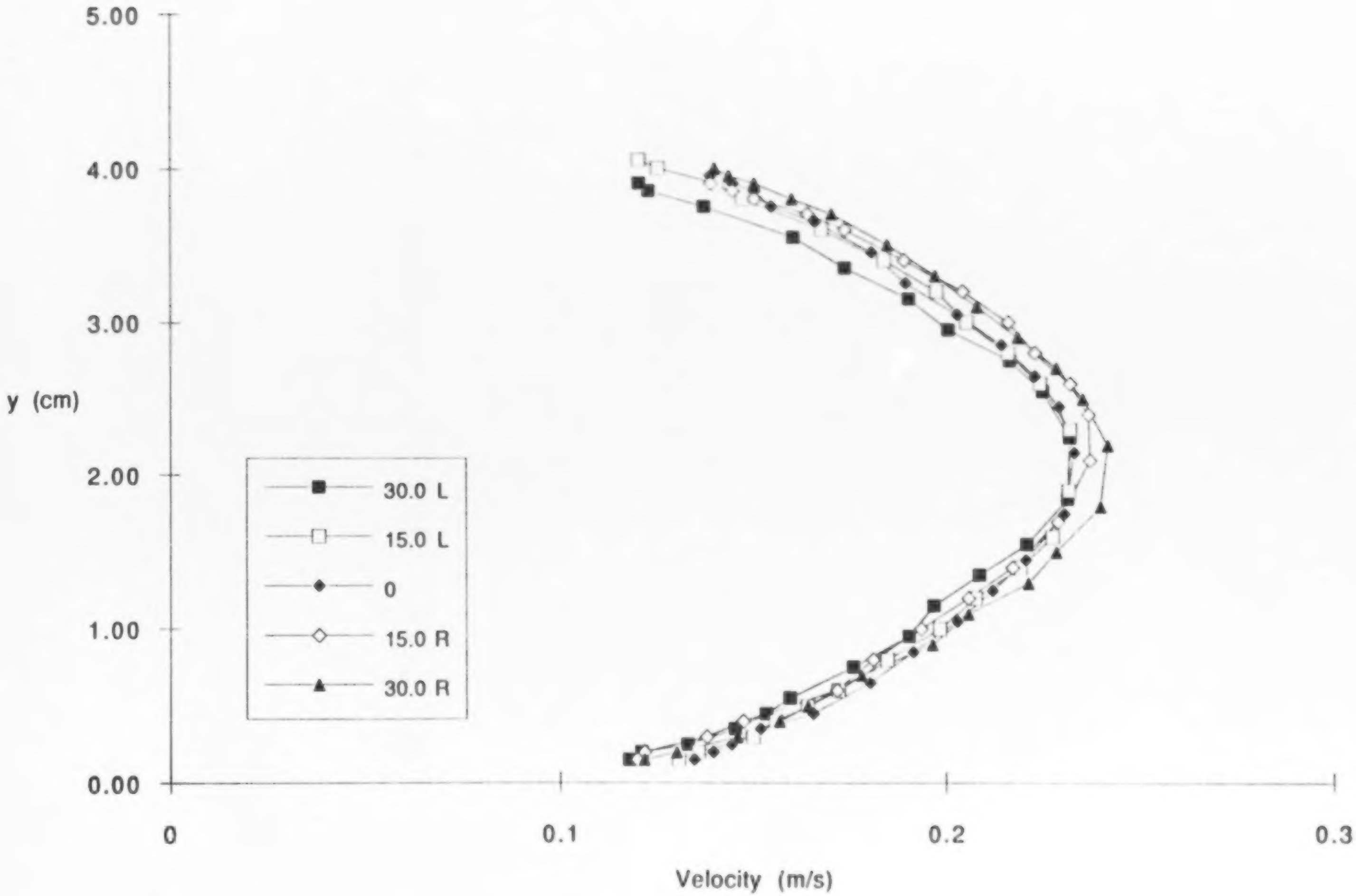

Figure 3.6(b) - Component velocity profiles for run R/R/10

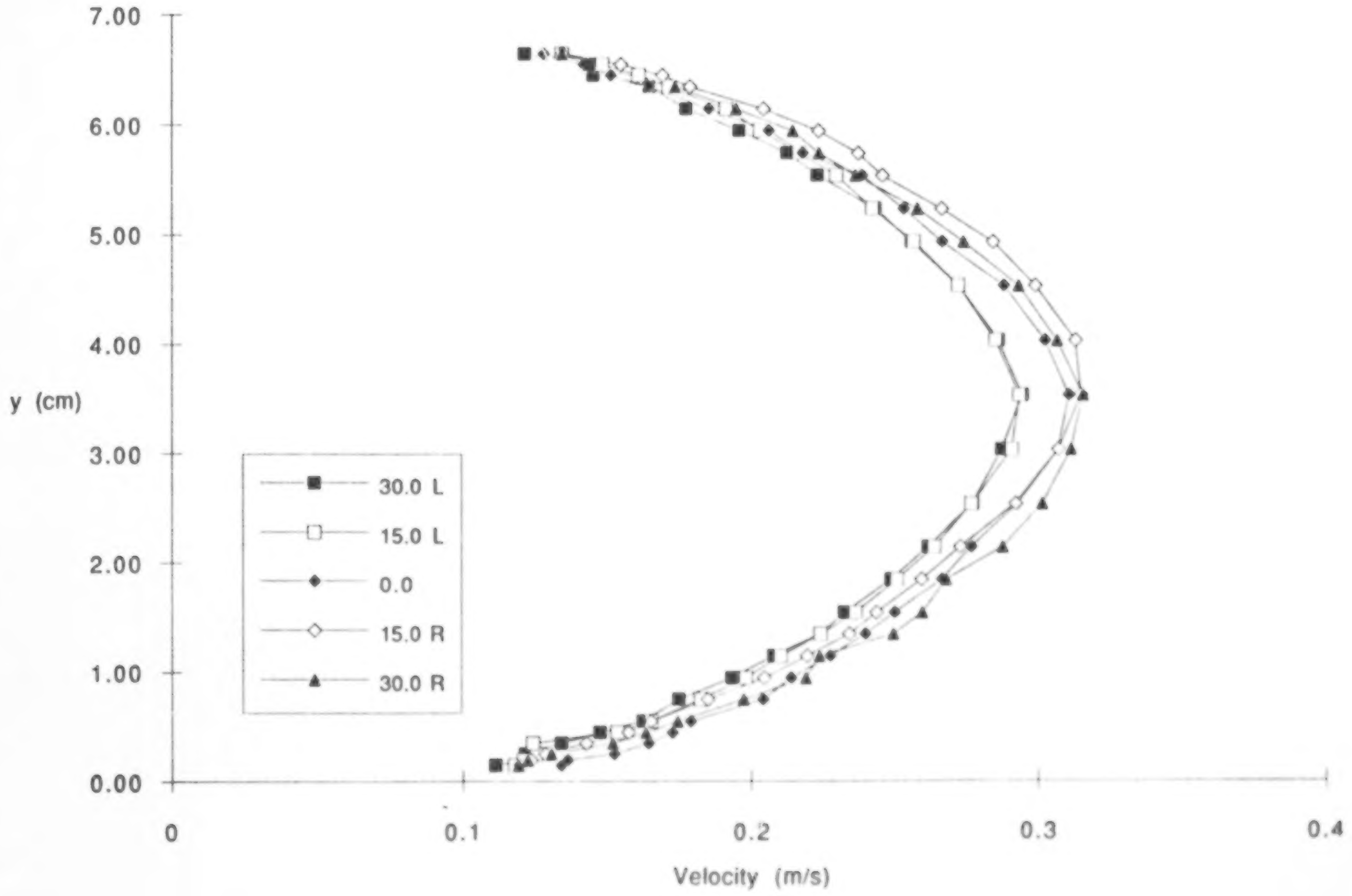

Figure 3.6(c) - Component velocity profiles for run R/R/20

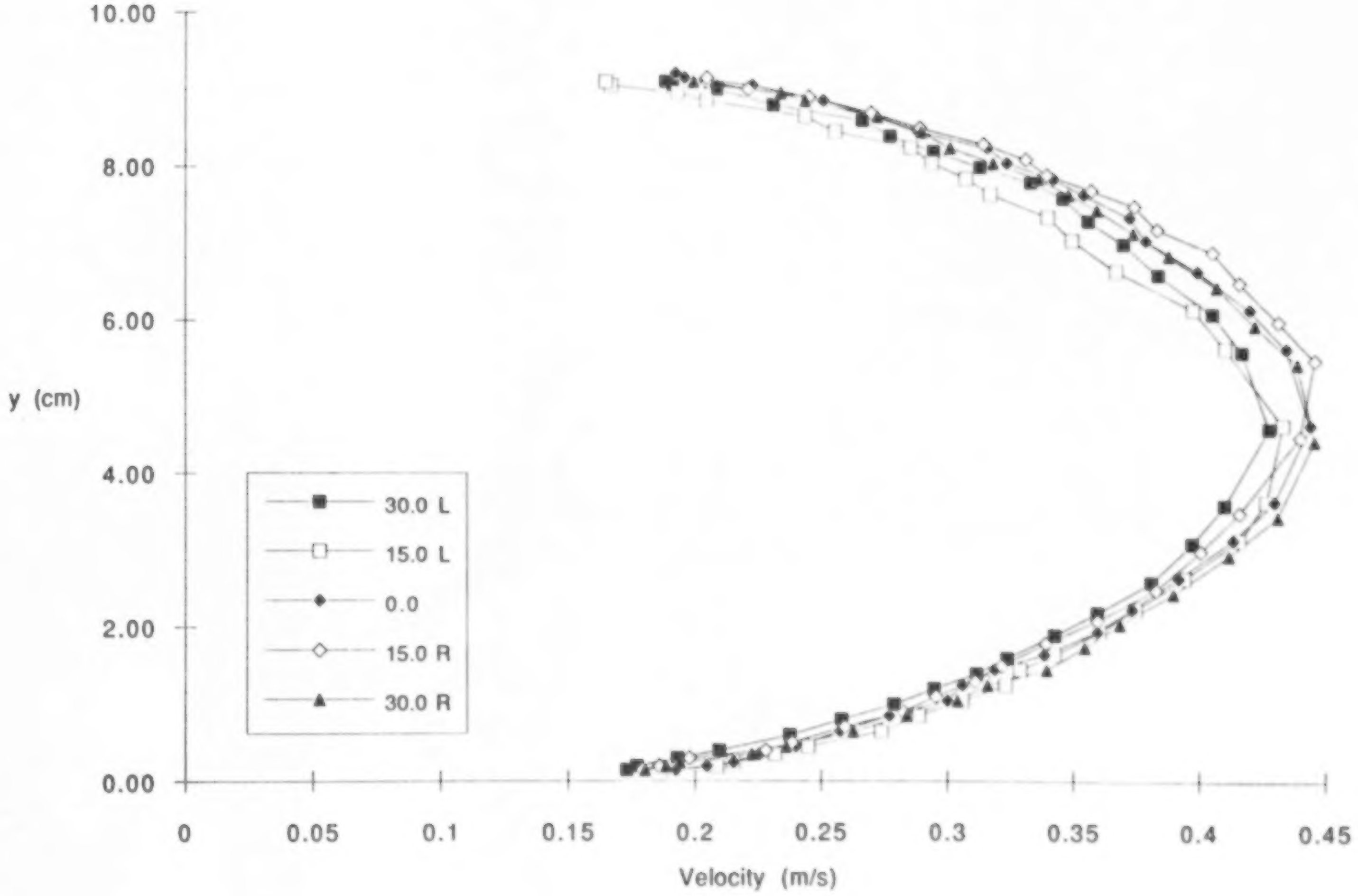

Figure 3.6(d) - Component velocity profiles for run R/R/40

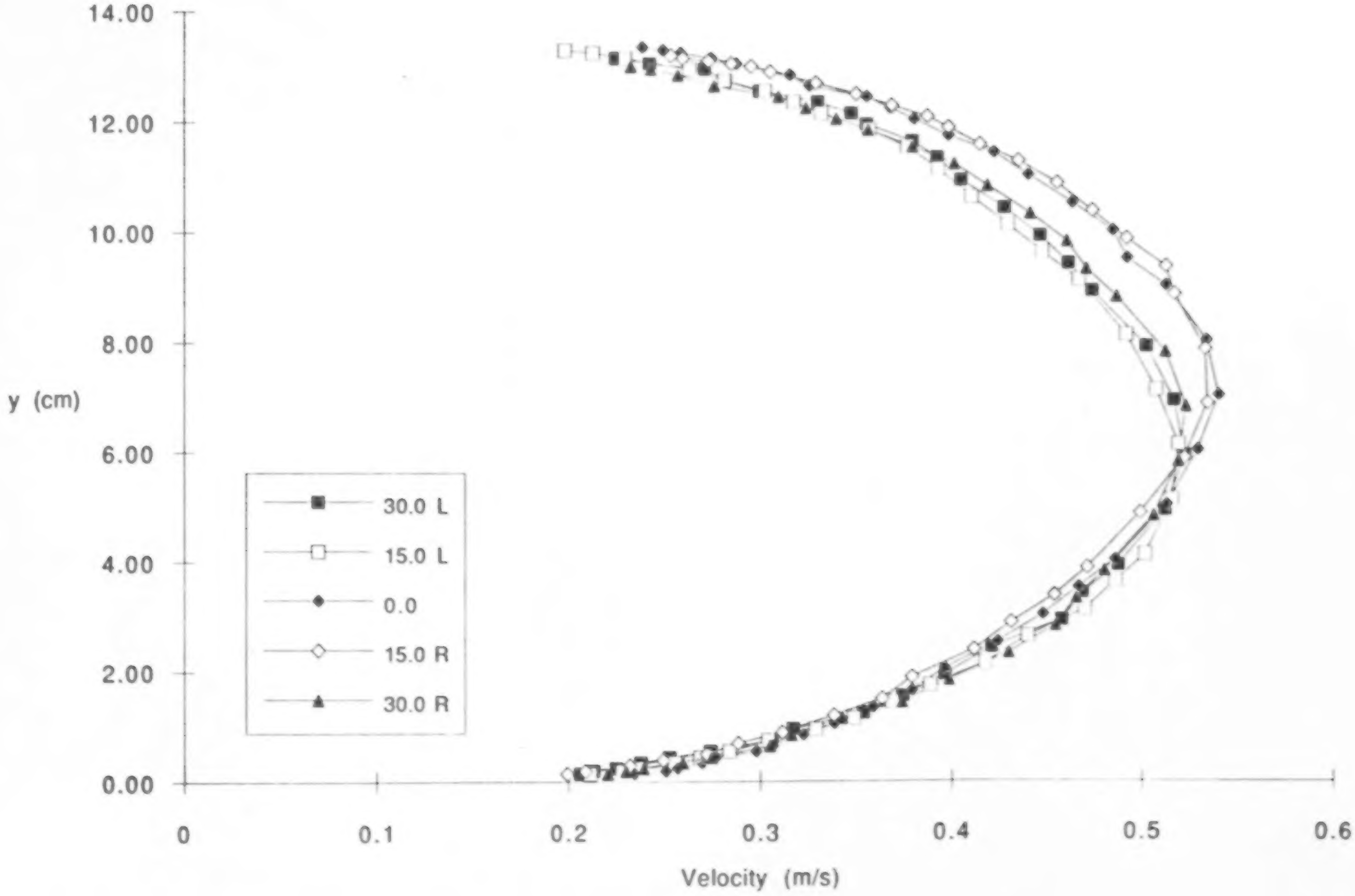

Figure 3.6(e) - Component velocity profiles for run R/R/70

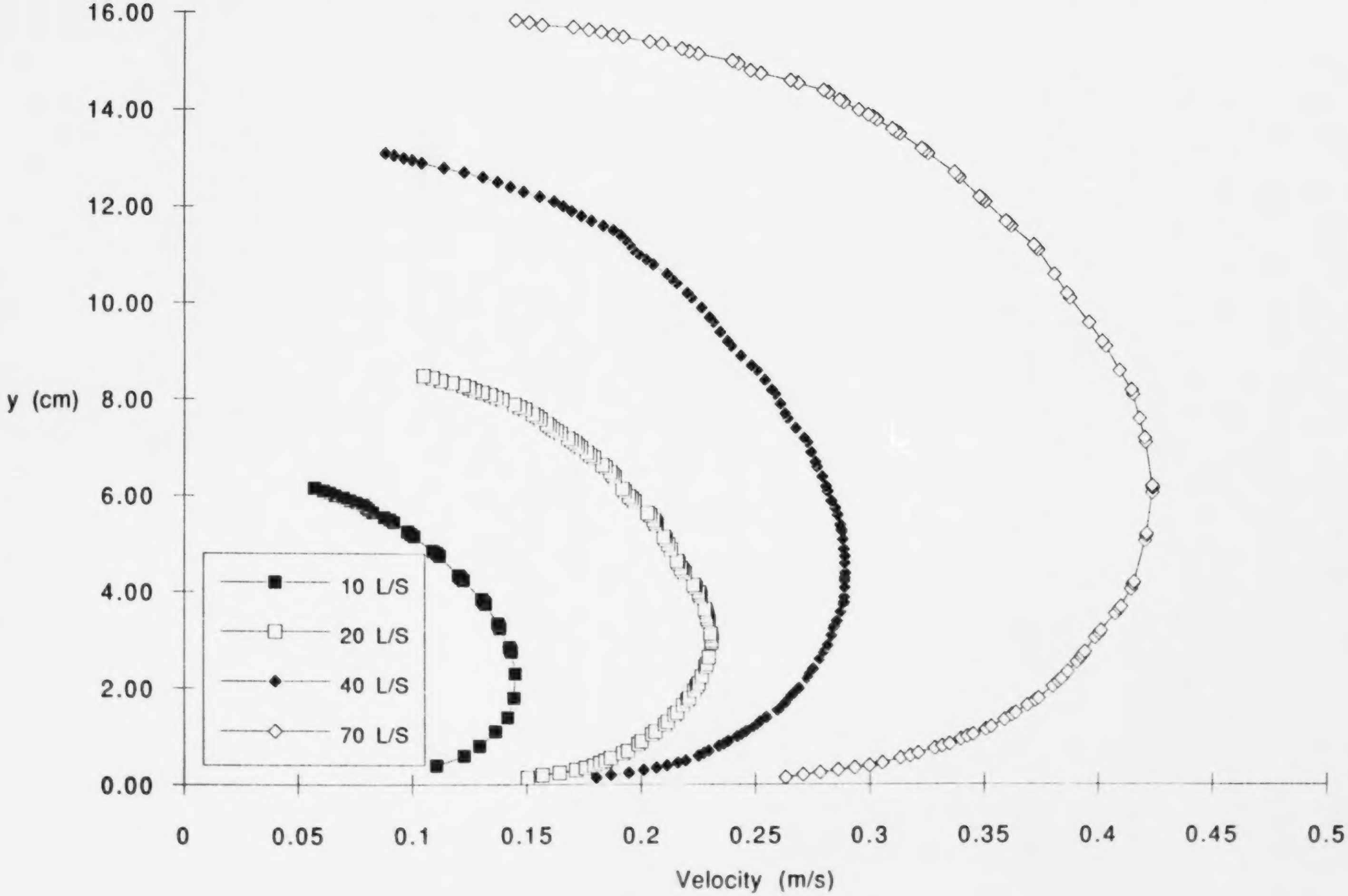

Figure 3.7(a) - Averaged velocity profiles for runs S/R/10, 20, 40 and 70

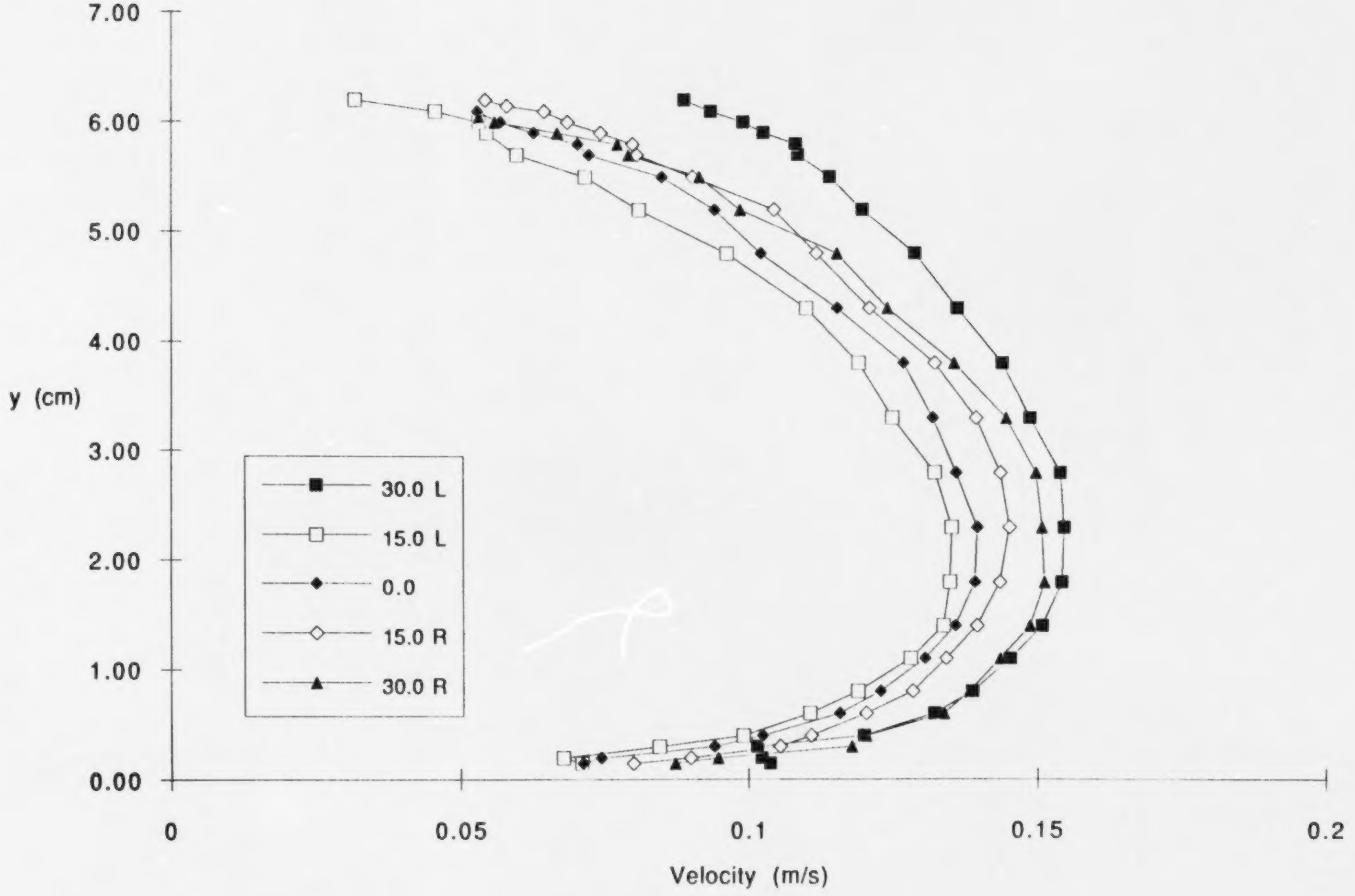

Figure 3.7(b) - Component velocity profiles for run S/R/10

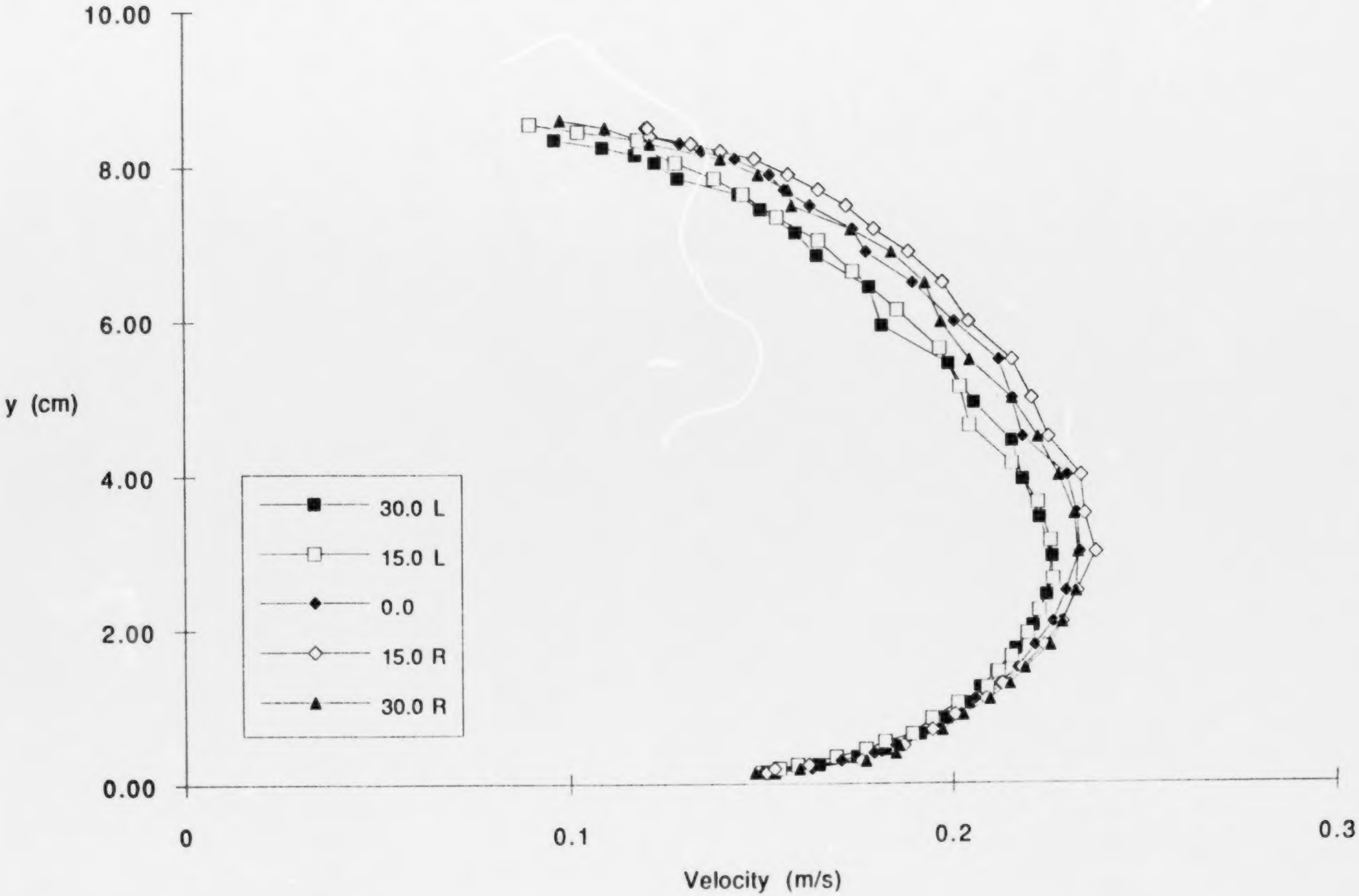

Figure 3.7(c) - Component velocity profiles for run S/R/20

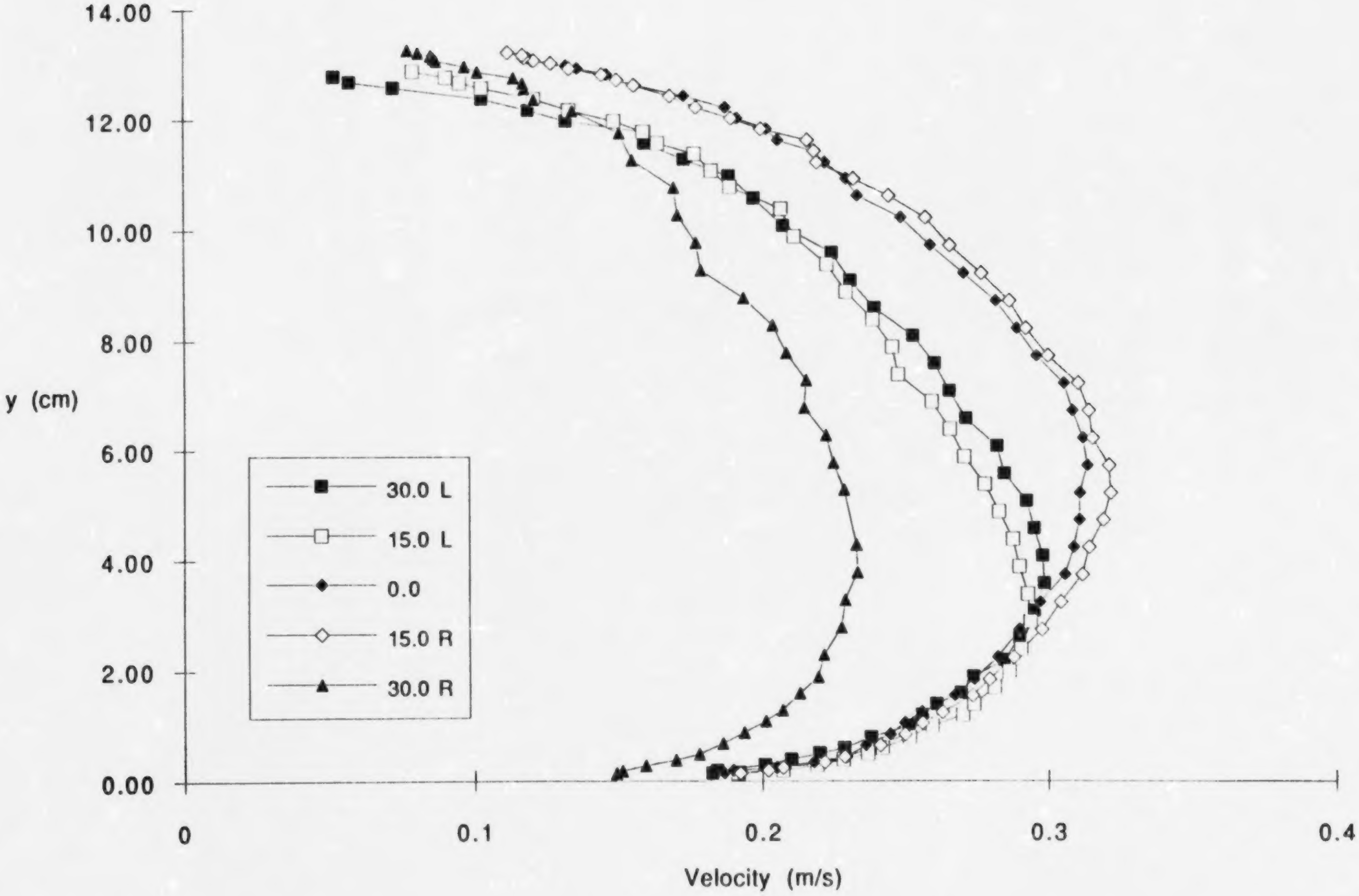

Figure 3.7(d) - Component velocity profiles for run S/R/40

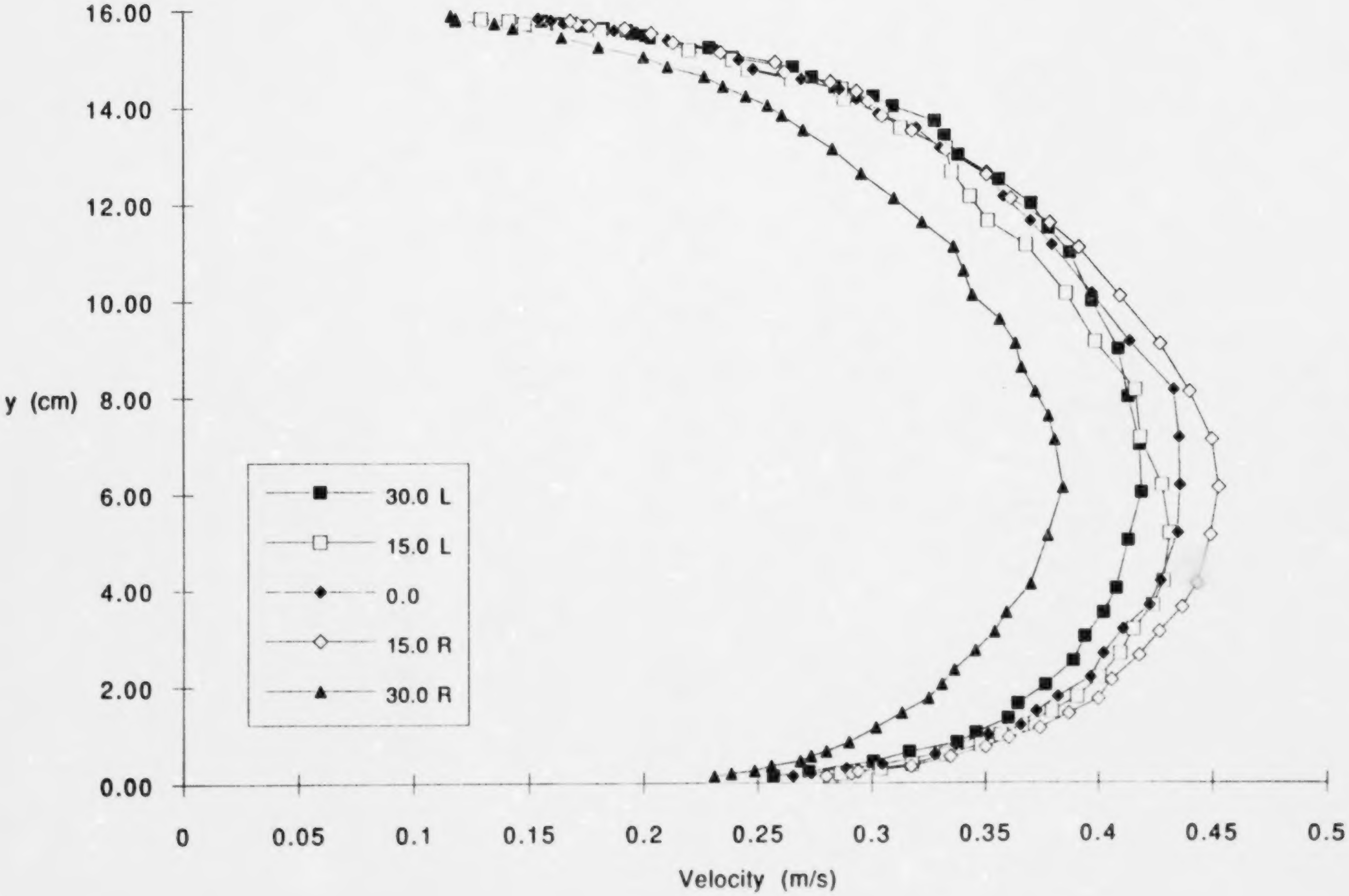

Figure 3.7(e) - Component profiles for run S/R/70

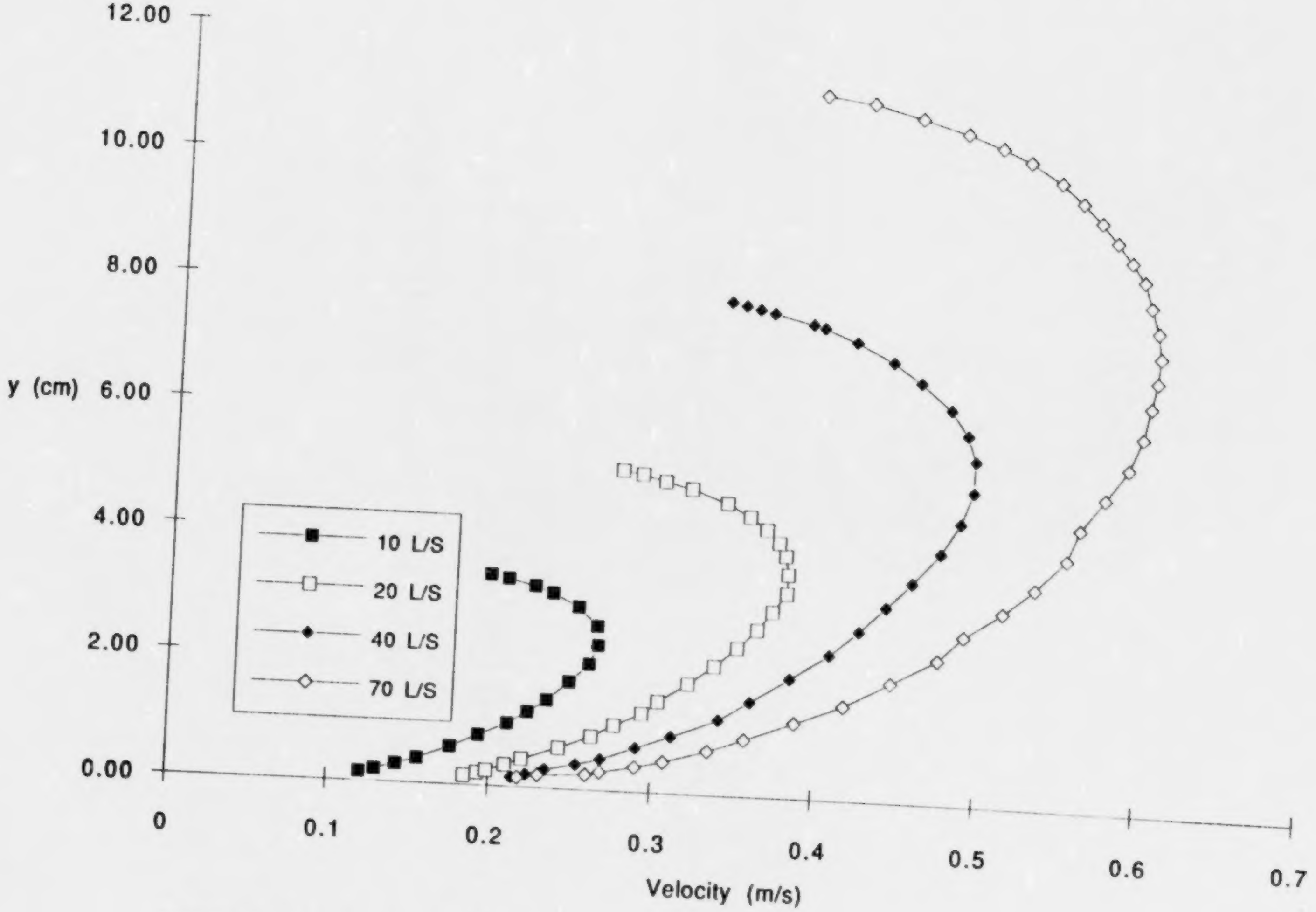

Figure 3.8(a) - Averaged velocity profiles for runs R/S/10, 20, 40 and 70

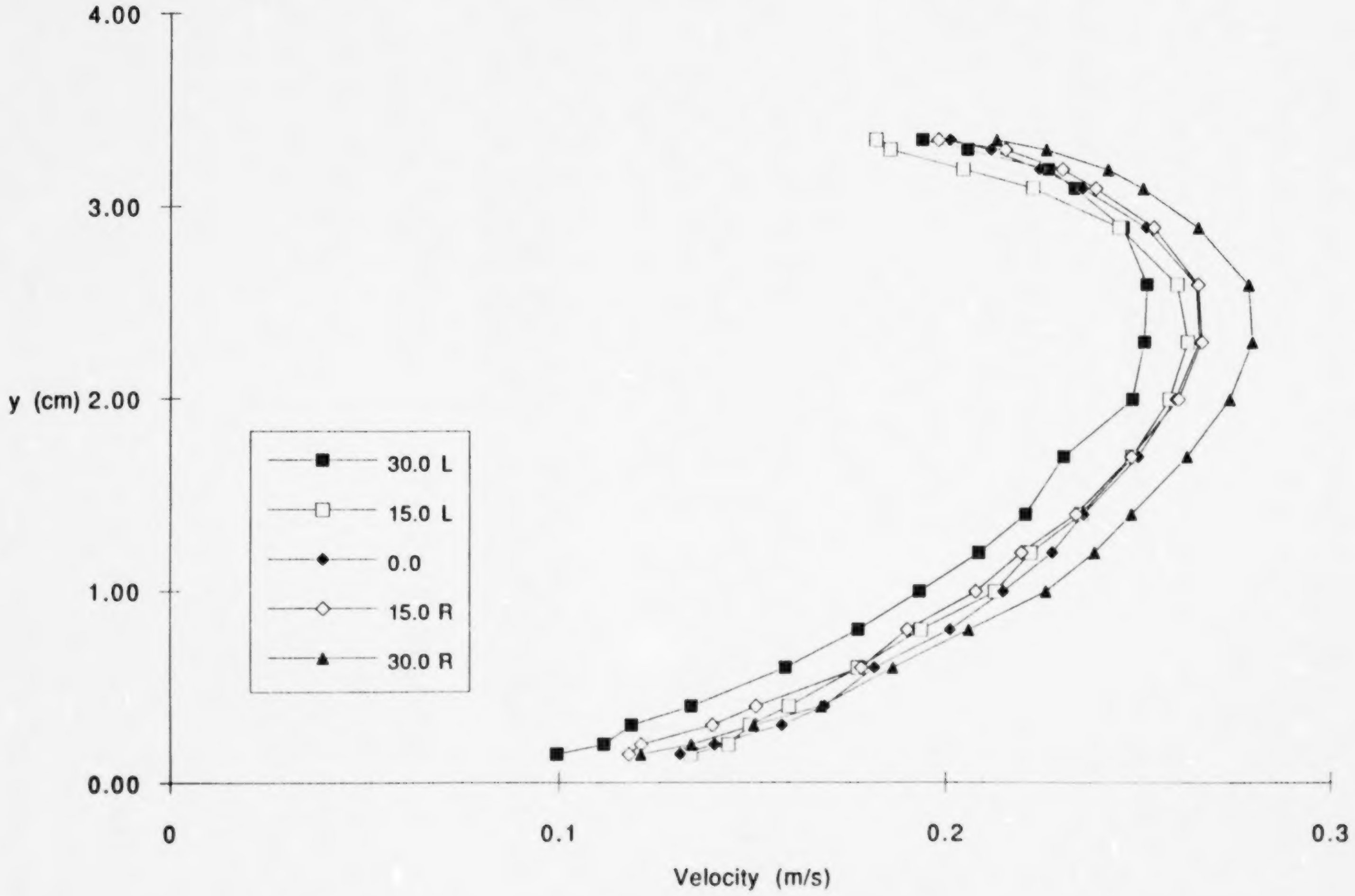

Figure 3.8(b) - Component velocity profiles for run R/S/10

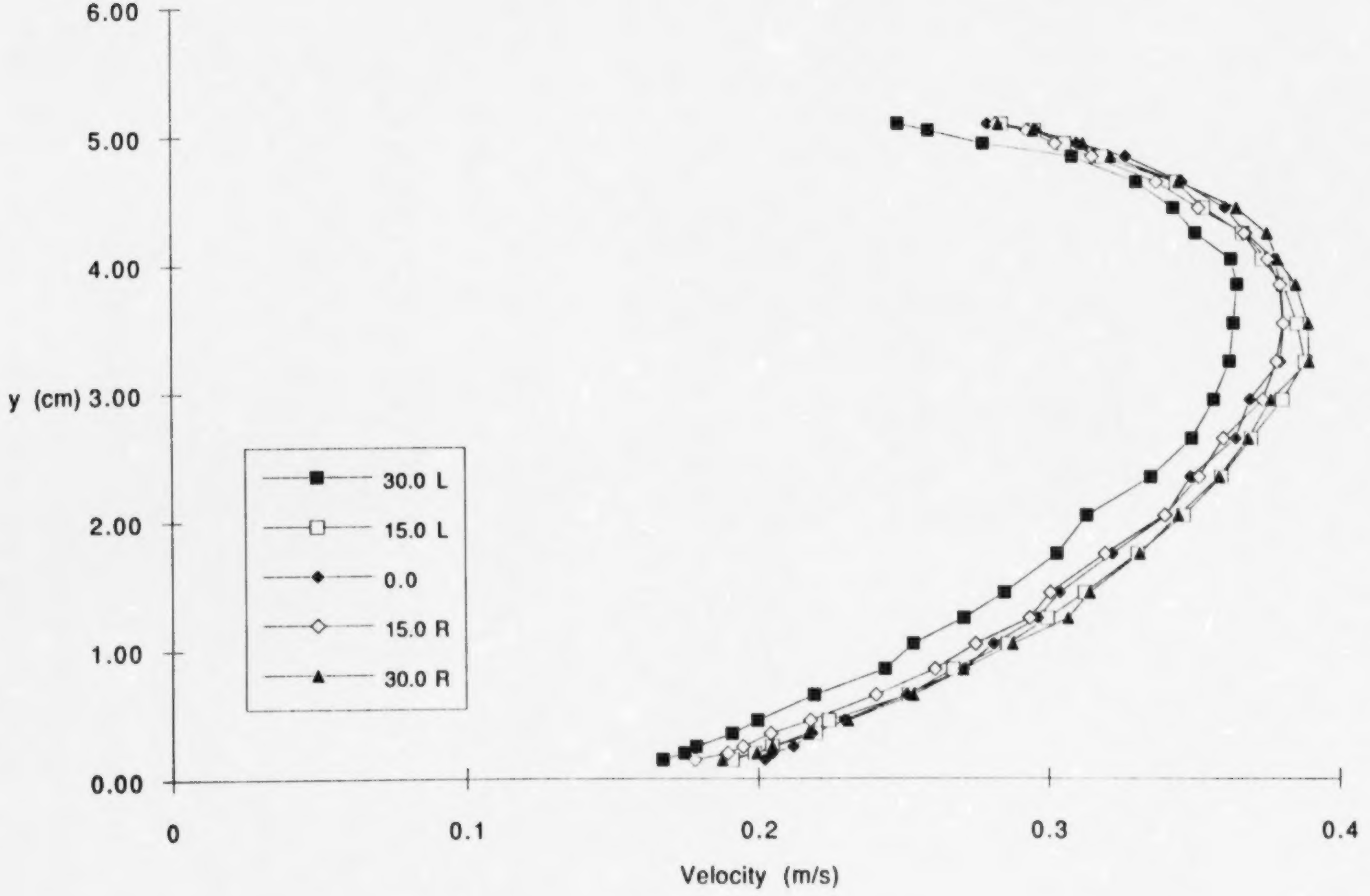

Figure 3.8(c) - Component velocity profiles for run R/S/20

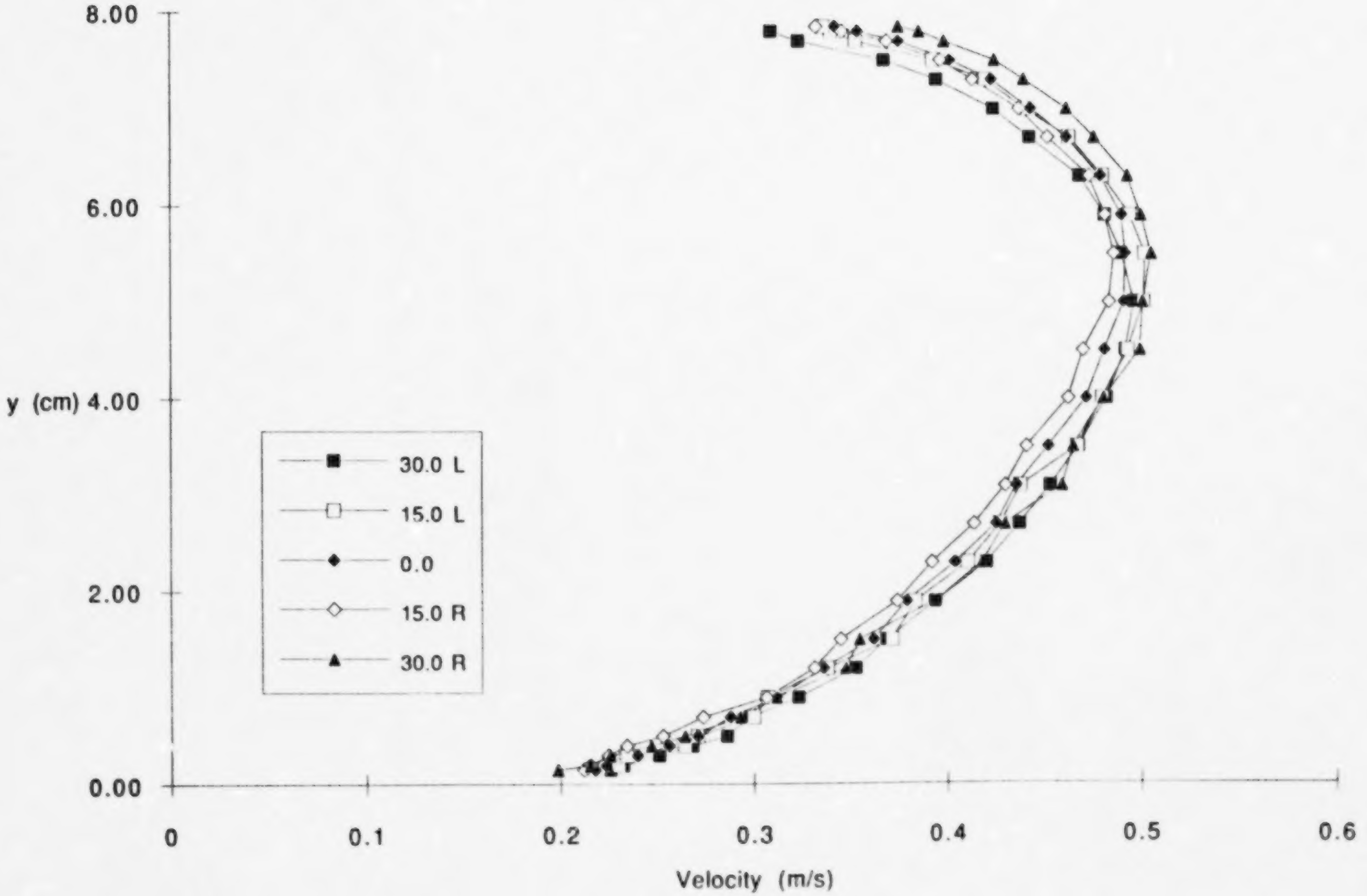

Figure 3.8(d) - Component velocity profiles for run R/S/40

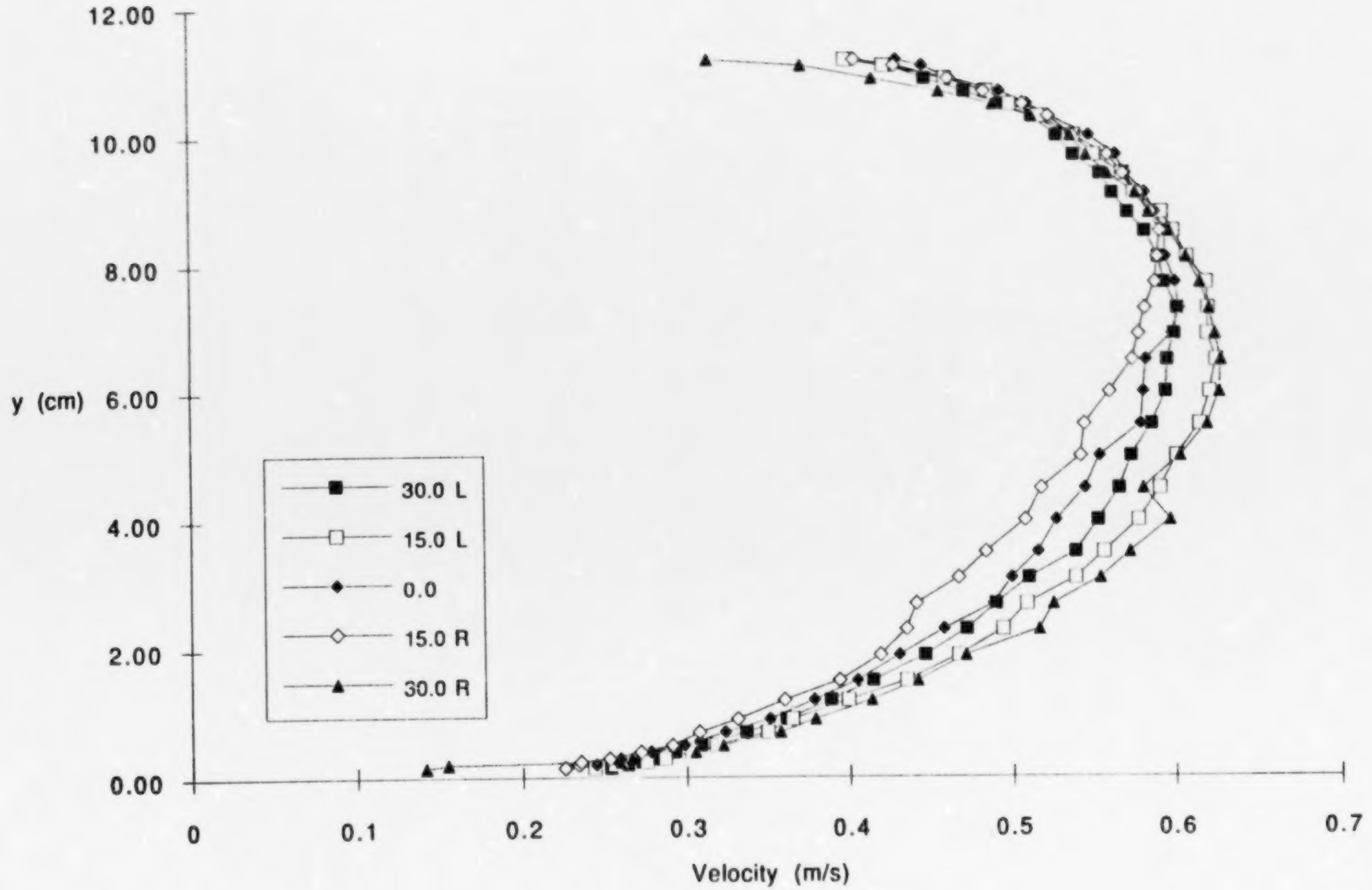

Figure 3.8(e) - Component velocity profiles for run R/S/70

3.3 Location of Virtual Origin

The lower portion of each velocity profile was expected to adopt a logarithmic velocity distribution, and this turned out to be so. The origin of the velocity profile, where the velocity goes to zero, is at the actual boundary surface for the smooth boundary. For the rough boundary, however, it lies somewhat below the top of the roughness. Previous studies have determined this to be anywhere from 0.15D to 0.30D below the surface of a hemispherical roughness of diameter D [Bayazit, 1976] and 60% of the depth below the surface of a mat roughness [Jasek, 1992].

The location of the virtual origin was determined by two methods, both of which involved using a semi-logarithmic plot of the velocity profile. Initially, velocity was plotted against the distance the center of the Preston tube was above the boundary. A least squares regression analysis was done on this line. Then the same profile was plotted again, adding 0.5 mm to each distance measurement. This was repeated at the same increment until a maximal regression coefficient was obtained. The value added to this profile was then the depth of the virtual origin below the surface. Use of this technique yielded varying values of virtual origin depth, with the smooth boundary having an average value of 0.7 mm and standard deviation of 0.9 mm, while the rough boundary had an average value of 5.3 mm and standard deviation of 0.9 mm.

The main problem with the previous procedure is that the regression coefficients were very similar for quite a range of virtual origin depths. In many cases, the choice of depth depended on the fourth decimal place of the regression coefficient. Obviously, to have more confidence in the results, some other criterion had to be considered. Instead of considering the regression coefficient, then, it was recognized that if the velocity profile was to follow the Karman-Prandtl equations for turbulent flow (2.11a,b), the slope of the non-dimensionalized profile was required to be 5.75 on a semi-logarithmic plot. Basically, the same procedure as before was followed, but this time the distance was incremented until the required slope was achieved. This yielded much more consistent values for depth of virtual origin, with the smooth boundary yielding an average value of 0.0 mm with a standard deviation of 0.3 mm, and the rough boundary an average value of 5.0 mm with a standard deviation of zero. Thus, both techniques yield similar values for depth of virtual origin. The latter, which is accepted with greater confidence, provides the expected value for the smooth boundary and a reasonable, consistent value for the rough boundary. A demonstration of the determination of the depth of virtual origin is shown on Figure 3.9.

3.4 Average Velocities

Average velocities for each zone of influence were determined through numerical integration by use of the trapezoidal rule [Davis, 1981]. The plane of zero shear stress was taken to be the division between the two zones of influence. Assuming a linear distribution of shear stress, the zero shear plane is defined by dividing the depth of flow into two portions according to the ratio of boundary shears.

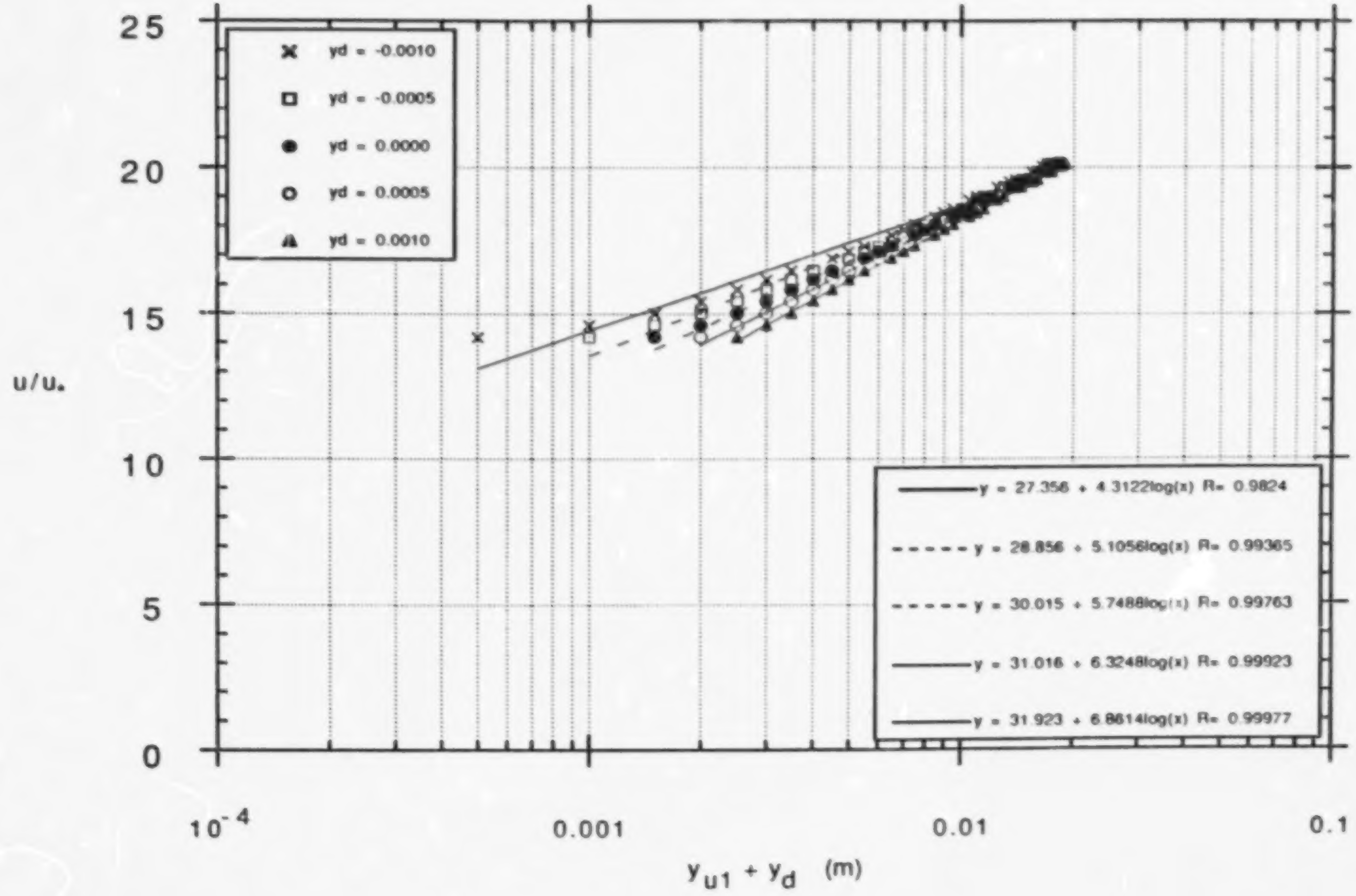

Figure 3.9 - Determination of depth of virtual origin

It should be noted that in this calculation, as in others, distances are measured to the virtual origin.

The calculated average velocities are shown in Table 3.2. It is seen that the average ratio of zone velocities for similar boundaries is 1.00 with a standard deviation of 0.03, while for dissimilar boundaries the ratio is 1.16 with a standard deviation of 0.06. In the latter instance, the smooth boundary zone displayed a higher average velocity and was associated with a thinner zone of influence.

	Average Velocity in Zone (m/s)			
Run	Bed Influenced	Cover Influenced	Ratio	Notes
S/S/10	0.118	0.126	1.075	
S/S/20	0.230	0.229	0.995	Cover/Bed
S/S/40	0.332	0.323	0.973	Average Ratio
S/S/70	0.390	0.397	1.018	1.00
R/R/10	0.164	0.164	1.004	
R/R/20	0.216	0.214	0.988	Standard Deviation
R/R/40	0.326	0.319	0.979	0.03
R/R/70	0.412	0.407	0.988	
S/R/10	0.123	0.107	1.152	
S/R/20	0.204	0.176	1.161	Smooth/Rough
S/R/40	0.256	0.219	1.167	Average Ratio
S/R/70	0.371	0.344	1.079	1.16
R/S/10	0.184	0.224	1.219	
R/S/20	0.286	0.336	1.175	Standard Deviation
R/S/40	0.341	0.432	1.266	0.06
R/S/70	0.485	0.524	1.079	
S/O/10	0.166	-	-	
S/O/20	0.251	-	-	
S/O/40	0.264	-	-	
S/O/70	0.337	-	-	
R/O/10	0.225	-	-	
R/O/20	0.329	-	-	
R/O/40	0.434	-	-	
R/O/70	0.561	-	-	

Table 3.2 - Average Velocities and Ratios of Zones

3.5 Shear Stresses

Boundary shears, in the form of shear velocities, were determined by the two methods outlined in section 2.2.4. A very good agreement between the two techniques was apparent; the maximum difference between the two values computed for the same situation was 10%, with over half within 2%. In calculating shear velocities using the Preston tube technique, all of the smooth boundary runs fell within the limits which correspond to the second equation and all of the rough boundary runs met the criteria for fully rough flow. With the velocity profile technique, shear velocities were determined after the virtual origin had been adjusted to the appropriate value.

In computing the cover-to-bed or rough-to-smooth ratios of shear stresses, and in all subsequent calculations, the value of shear velocity determined by the Preston tube technique was used for all smooth boundaries. This technique seems quite rugged and ensuring that the tube was in direct contact with the smooth boundary was relatively simple. For the rough boundary, where this positioning was not as definite, the velocity profile technique was taken as yielding values to be held in greater confidence. It should be noted, though, that in most cases the values are so close as to render this decision inconsequential. Boundary shear velocities computed by both methods are shown in Table 3.3 for purposes of comparison. Ratios of cover-to-bed shears are provided for like boundary runs, and rough-to-smooth shear ratios are provided for runs involving dissimilar boundaries.

Run	Bed Shear Velocity (m/s)			Cover Shear Velocity (m/s)			Ratio Cover/Bed Rough/Smooth
	Preston	Profile	% Diff	Preston	Profile	% Diff	
S/S/10	0.0077	0.0077	1	0.0078	0.0081	3	1.03
S/S/20	0.0129	0.0131	1	0.0124	0.0122	2	0.96
S/S/40	0.0167	0.0168	1	0.0161	0.0162	1	0.96
S/S/70	0.0185	0.0186	1	0.0184	0.0186	1	1.00
R/R/10	0.0355	0.0355	0	0.0342	0.0340	1	0.96
R/R/20	0.0444	0.0435	2	0.0353	0.0392	10	0.90
R/R/40	0.0513	0.0516	1	0.0525	0.0522	0	1.01
R/R/70	0.0540	0.0545	1	0.0517	0.0518	0	0.95
S/R/10	0.0076	0.0076	0	0.0187	0.0188	1	2.48
S/R/20	0.0118	0.0113	5	0.0226	0.0228	1	1.92
S/R/40	0.0136	0.0135	1	0.0333	0.0321	4	2.36
S/R/70	0.0185	0.0186	0	0.0438	0.0441	1	2.38
R/S/10	0.0414	0.0417	1	0.0146	0.0159	8	2.85
R/S/20	0.0426	0.0423	1	0.0193	0.0186	4	2.19
R/S/40	0.0533	0.0528	1	0.0230	0.0221	4	2.30
R/S/70	0.0645	0.0677	5	0.0260	0.0269	3	2.60
S/O/10	0.0091	0.0090	1	-	-	-	-
S/O/20	0.0125	0.0127	1	-	-	-	-
S/O/40	0.0123	0.0124	1	-	-	-	-
S/O/70	0.0148	0.0147	0	-	-	-	-
R/O/10	0.0334	0.0331	0	-	-	-	-
R/O/20	0.0460	0.0449	4	-	-	-	-
R/O/40	0.0676	0.0641	6	-	-	-	-
R/O/70	0.0759	0.0729	2	-	-	-	-

Table 3.3 - Calculated boundary shears

The average ratio of cover to bed shear velocities for like boundaries was 0.97 with a standard deviation of 0.04. For unlike boundaries the average was 2.39 with a standard deviation of 0.28. Comparing the open channel bed shear velocities to those of the closed channels, it appears that there is not a great change in boundary shear due to the addition of the cover. The drop in bed shear due to the boundary shear that is taken by the cover seems to be offset to some extent by the increase in depth and drop in conveyance that result, as can be seen by taking a closer look at the problem. Using the Chezy equation (2.15), the conveyance coefficient equation (2.16) and the familiar wide channel assumption, the expression for unit discharge in an open channel may be equated with that for a closed channel with equal bed and cover roughnesses:

$$\left(2.5\ \ln \frac{H_1}{k_s} + 6.2\right)\sqrt{gH_1S_f}\,(H_1) = \left(2.5\ \ln \frac{H_2}{2k_s} + 6.2\right)\sqrt{gH_2S_f/2}\,(H_2) \qquad (3.1)$$

For typical values for H_1 and k_s of 0.10 m and 0.04 m, respectively, this equation may be solved iteratively to yield a value for H_2 of 0.136 m. This shows an increase in stage of 36% due to the introduction of a rough cover. This corresponds to a drop in average flow velocity to 74% of the open channel value. Noting that the conveyance coefficient also drops to 89% of its open channel value, it is apparent from equation (2.18) that the shear velocity will in this case drop to 83% of its original value, rather than simply being halved as might be expected.

Experimental values back up this analysis, as shown in Table 3.4. Here it is demonstrated that for a given bed slope and discharge, the bed shear tends to drop only slightly with the introduction of a cover. Depths for the S/O/40 and S/O/70 runs appear to be above normal, so the associated shear velocities should actually be higher, with cover to open bed shear ratios somewhere below unity.

Discharge (L/s)	Rough Bed Boundary Shear Velocity (m/s) Open Channel	Smooth Cover	Rough Cover
10	0.0331	0.0417	0.0355
20	0.0449	0.0423	0.0435
40	0.0641	0.0528	0.0516
70	0.0729	0.0677	0.0545
Average Ratio: Cover/Open		0.99	0.90
Discharge (L/s)	Smooth Bed Boundary Shear Velocity (m/s) Open Channel	Smooth Cover	Rough Cover
10	0.0091	0.0077	0.0076
20	0.0125	0.0129	0.0118
40	0.0123	0.0167	0.0136
70	0.0148	0.0185	0.0186
Average Ratio: Cover/Open		1.12	1.04

Table 3.4 - Effect of cover on bed shear

The calculation of the location of the theoretical point of zero shear involves assuming a linear distribution of shear stress across the depth of the flow. This is shown in Figure 3.10. As mentioned before, both experimental [Hanjalic and Launder, 1972] and computational [Lau, 1982] investigations point to flaws in this theory. However, its use is convenient in terms of simplifying the quantification of flow characteristics. If a linear distribution of shear is accepted, it may be shown that:

$$\frac{H_{bed}}{u_{*bed}} = \frac{H_{cover}}{u_{*cover}} \qquad (3.2)$$

where H_{bed} and H_{cover} represent the depth of the respective zones of influence. It can be shown then that:

$$H_{bed} = \left(\frac{u_{*bed}}{u_{*bed} + u_{*cover}}\right) H \qquad (3.3)$$

The depths calculated in this fashion are those previously noted in Table 3.1.

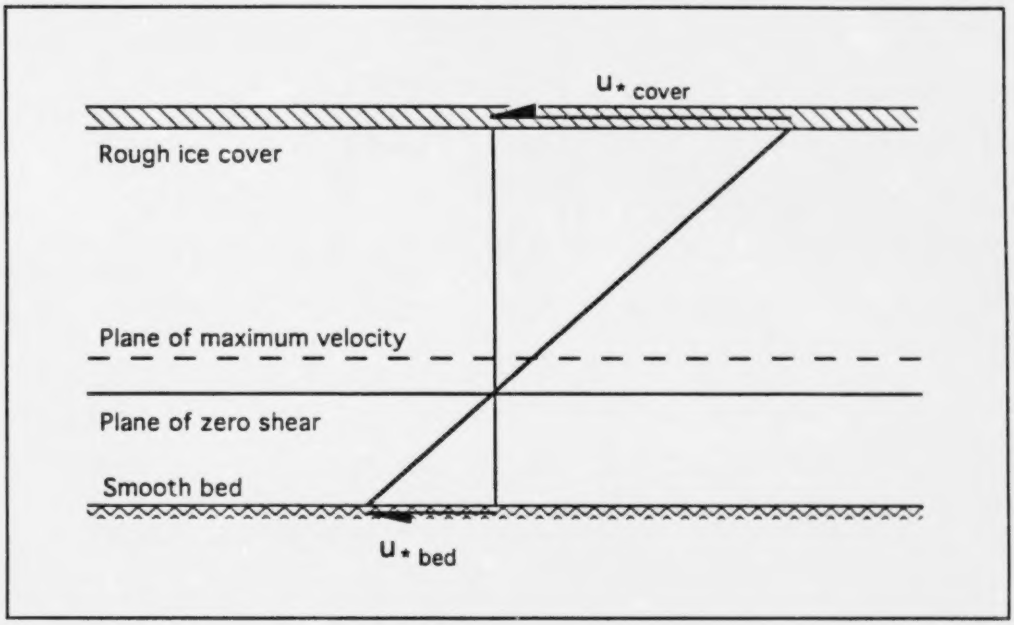
$u_{*\,cover}$
Rough ice cover
Plane of maximum velocity
Plane of zero shear
Smooth bed
$u_{*\,bed}$

Figure 3.10 - Distribution of shear stress across channel depth

3.6 Boundary Roughnesses

Boundary roughnesses were determined by the two methods previously outlined in section 2.2.5. For the smooth boundaries, in which viscous roughness varies inversely with shear velocity, the average difference between roughness values obtained by the profile and Chezy technique was 17%, with a standard deviation of 13%.

		Roughness					
Run	Boundary	Profile (m)	Chezy (m)	Diff %	Average (m)	Predicted Viscous (m)	Diff %
S/R/10	Bed	0.00025	0.00036	31	0.00031	0.00043	-30
S/R/20	Bed	0.00031	0.00037	16	0.00034	0.00028	22
S/R/40	Bed	0.00023	0.00027	15	0.00025	0.00024	3
S/R/70	Bed	0.00018	0.00020	10	0.00019	0.00018	7
S/S/10	Bed	0.00041	0.00083	51	0.00062	0.00043	45
S/S/20	Bed	0.00040	0.00037	-8	0.00039	0.00026	51
S/S/40	Bed	0.00023	0.00022	-5	0.00023	0.00020	14
S/S/70	Bed	0.00020	0.00020	0	0.00020	0.00018	12
S/O/10	Bed	0.00033	0.00041	20	0.00037	0.00036	2
S/O/20	Bed	0.00024	0.00026	8	0.00025	0.00026	-5
S/O/40	Bed	0.00025	0.00028	11	0.00027	0.00027	-1
S/O/70	Bed	0.00018	0.00022	18	0.00020	0.00022	-11
S/S/10	Cover	0.00058	0.00063	8	0.00061	0.00042	43
S/S/20	Cover	0.00023	0.00027	15	0.00025	0.00027	-6
S/S/40	Cover	0.00023	0.00019	-21	0.00021	0.00020	2
S/S/70	Cover	0.00016	0.00016	0	0.00016	0.00018	-11
R/S/10	Cover	0.00031	0.00027	-15	0.00029	0.00023	28
R/S/20	Cover	0.00013	0.00021	38	0.00017	0.00017	-1
R/S/40	Cover	0.00011	0.00017	35	0.00014	0.00014	-2
R/S/70	Cover	0.00015	0.00013	-15	0.00014	0.00013	10
Average percent difference:				17			15
Standard deviation:				13			15

Table 3.5 - Calculated smooth boundary viscous roughnesses

Here values of viscous roughness could also be determined based on the shear velocity and kinematic viscosity of water as in equation (2.13). A close agreement between the average measured roughness and the calculated viscous roughness is seen, with an average difference of 15% and a standard deviation of 15%.

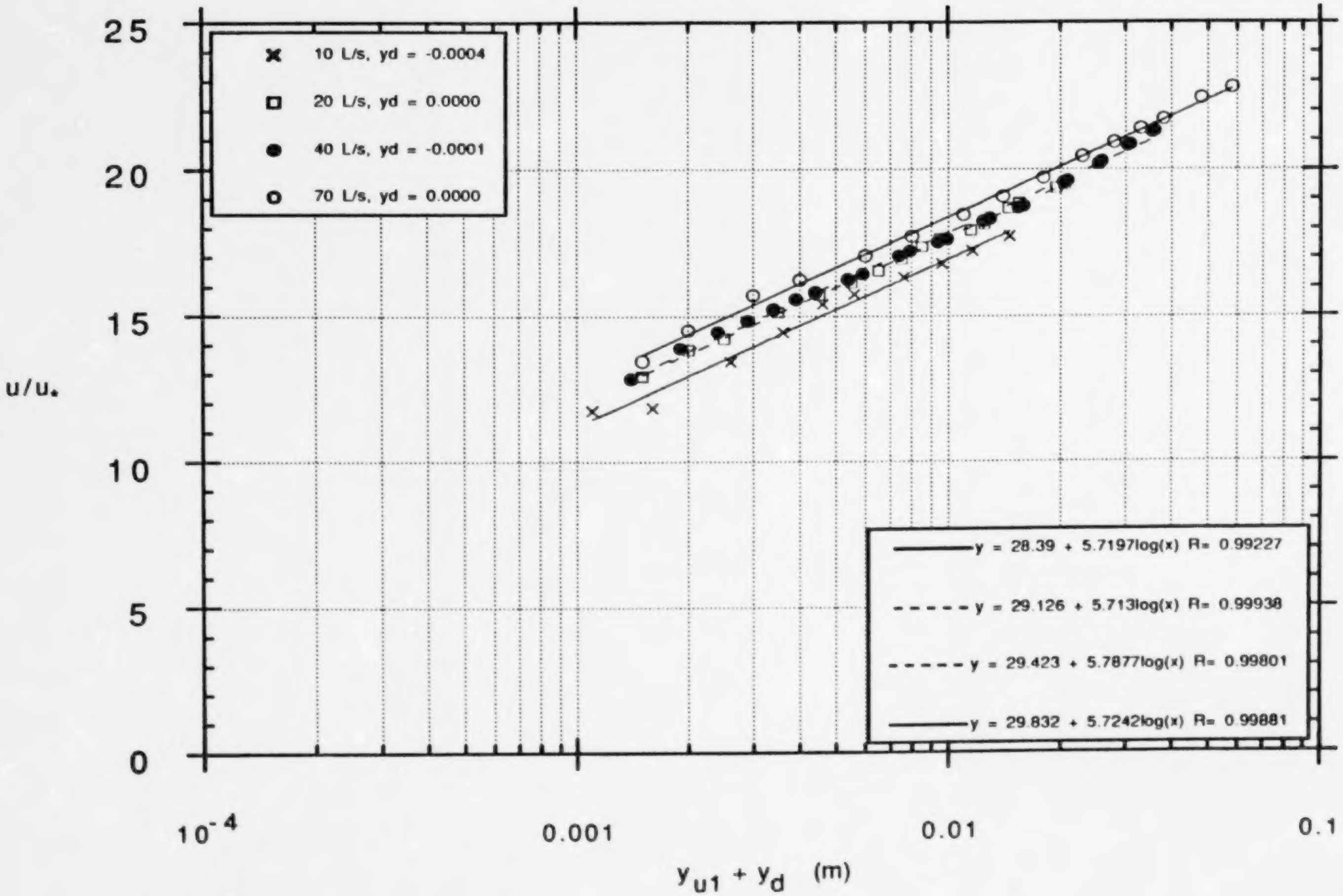

Figure 3.11(a) - Semi-logarithmic velocity profiles for S/O/bed runs

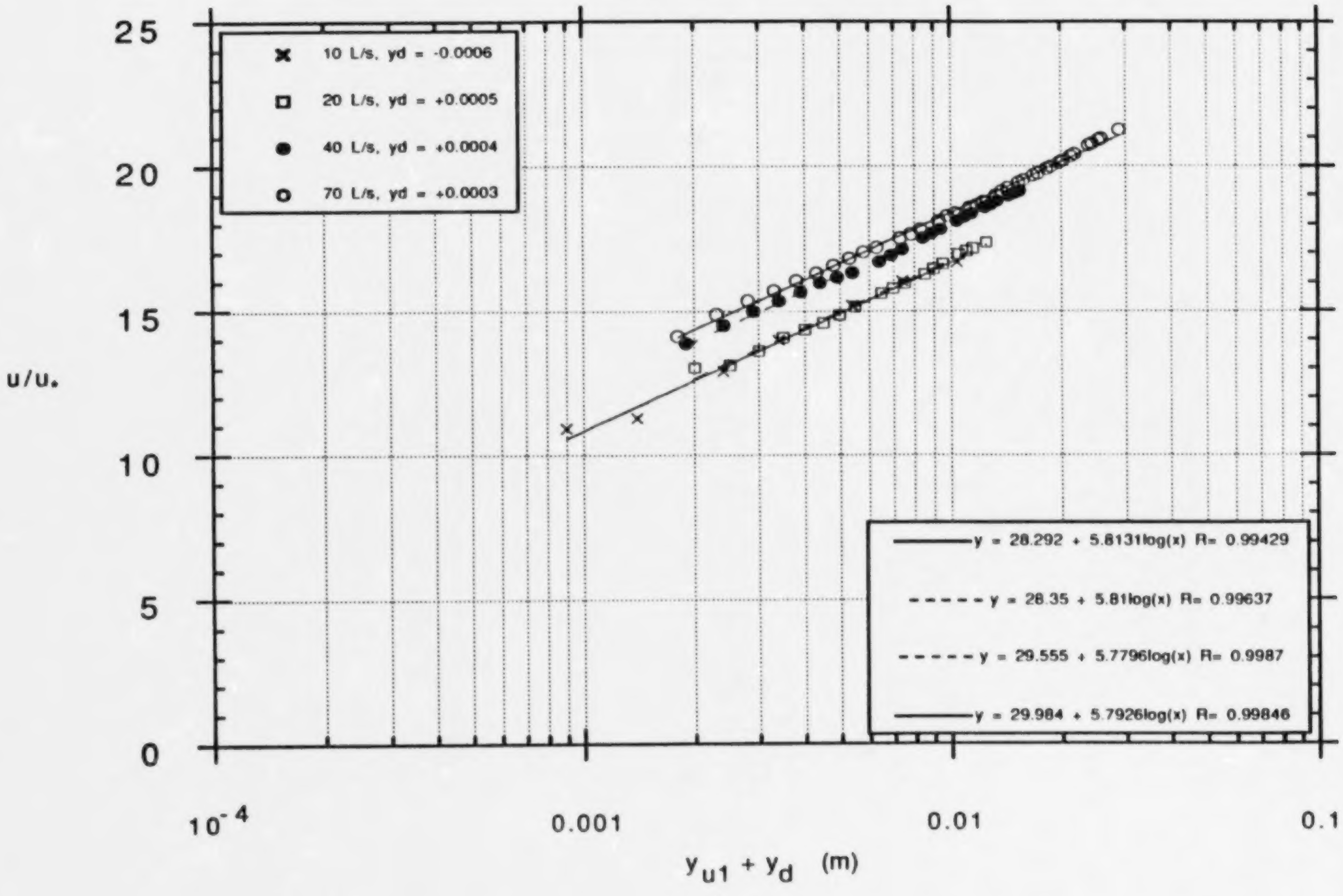

Figure 3.11(b) - Semi-logarithmic velocity profiles for S/S/bed runs

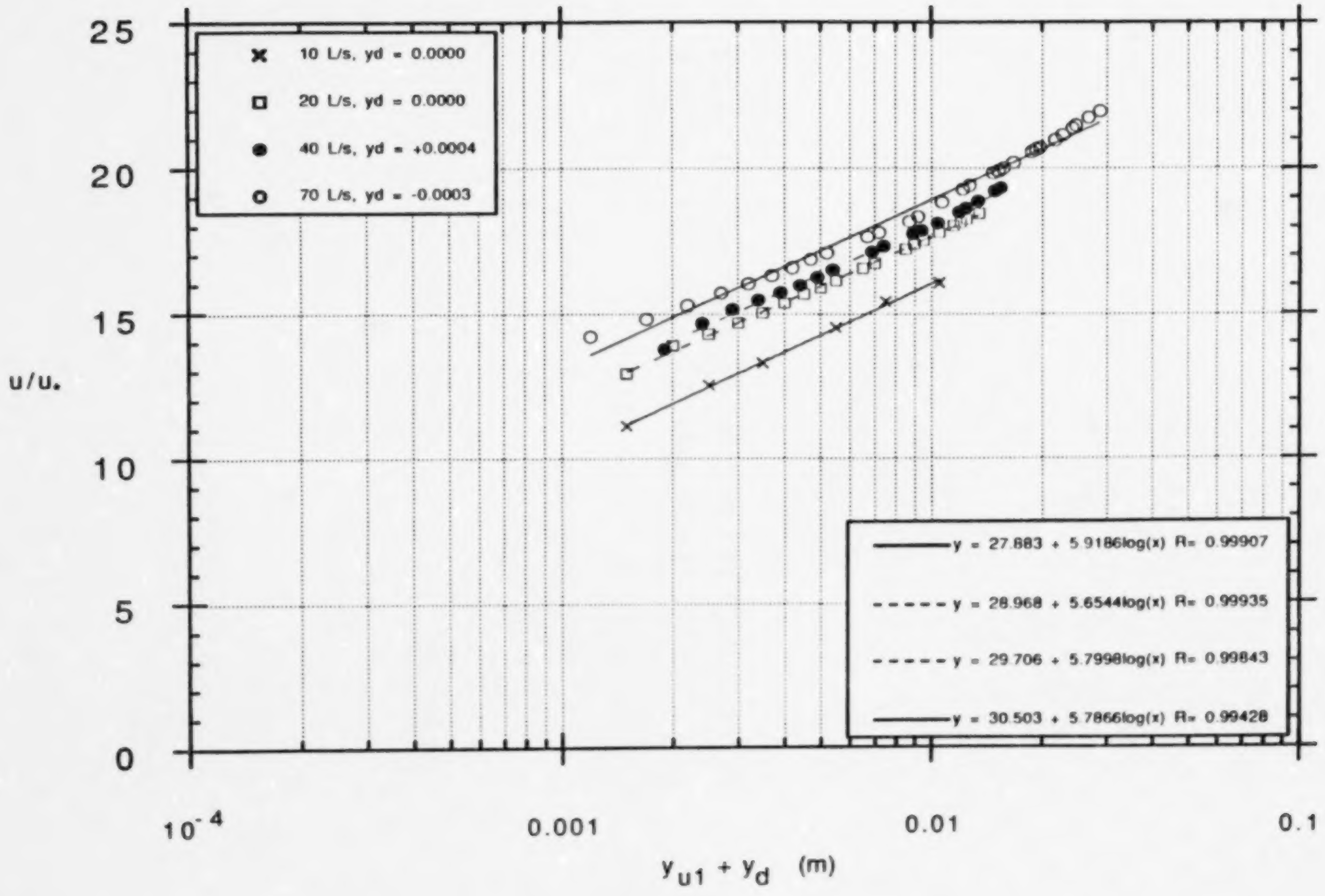

Figure 3.11(c) - Semi-logarithmic velocity profiles for S/S/cover runs

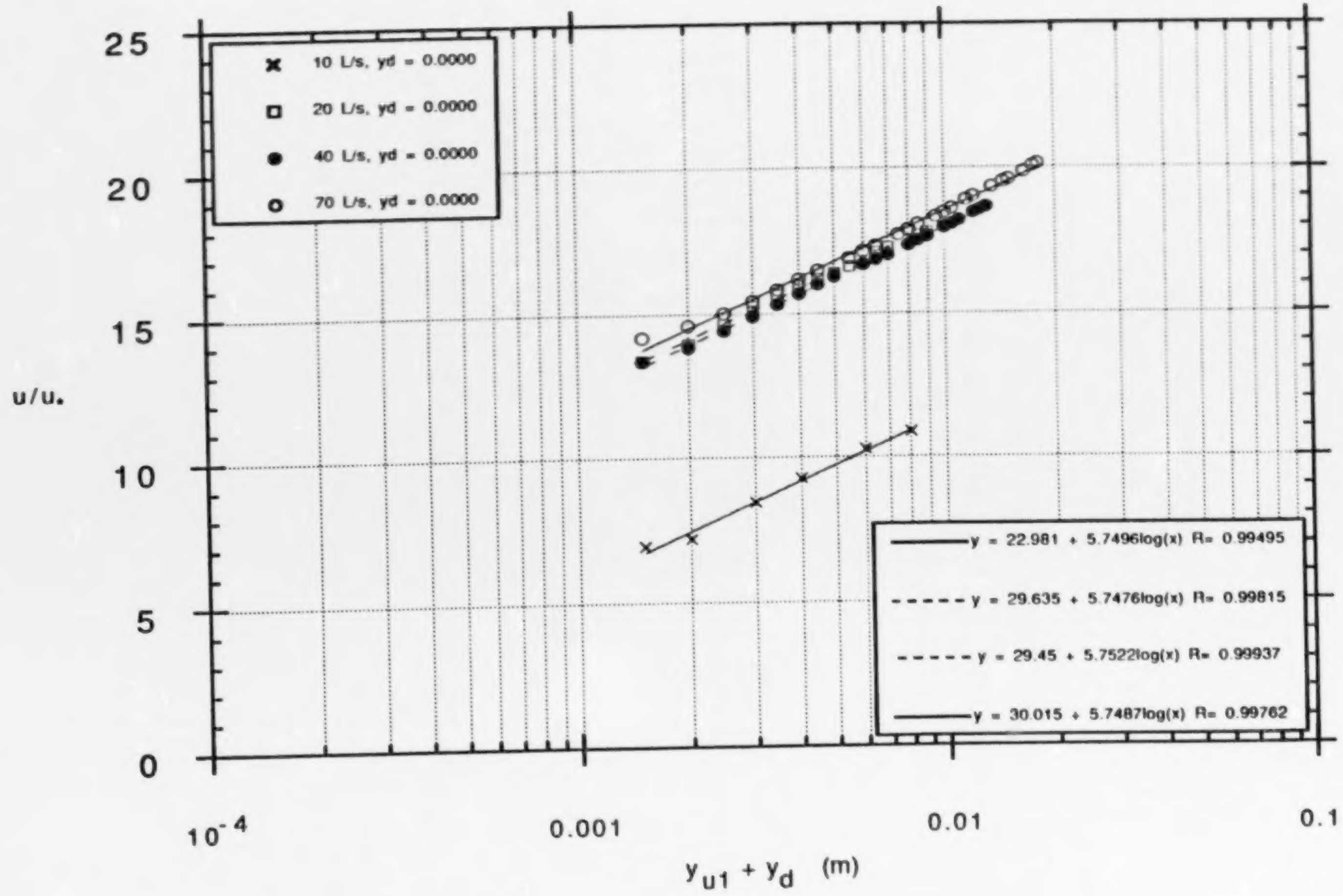

Figure 3.11(d) - Semi-logarithmic velocity profiles for S/R/bed runs

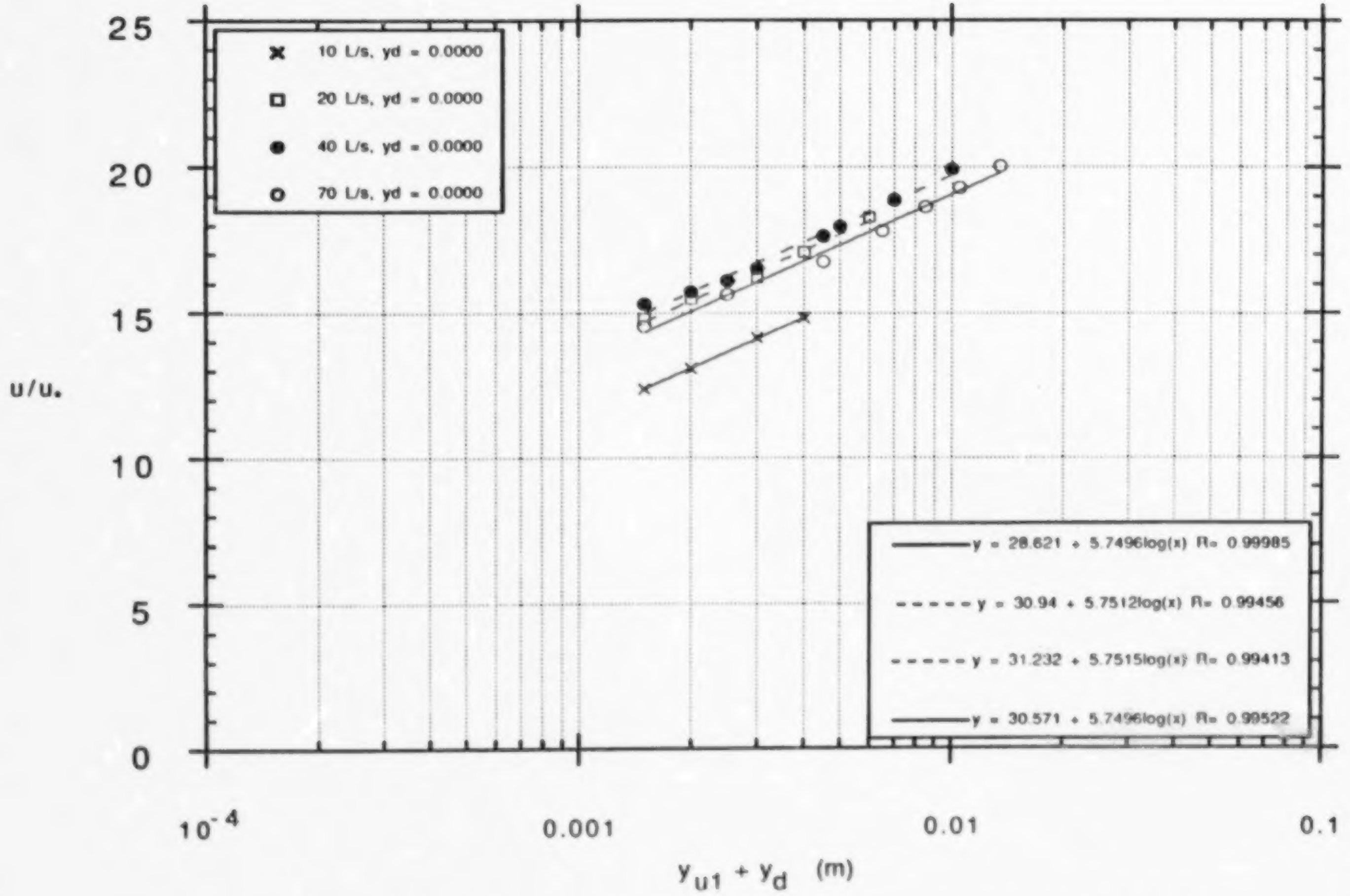

Figure 3.11(e) - Semi-logarithmic velocity profiles for R/S/cover runs

For the rough boundary, the average difference between roughness values obtained by the profile and Chezy technique was 7%, with a standard deviation of 7%.

		Roughness				
Run	Boundary	Profile (m)	Chezy (m)	Diff %	Average (m)	Ratio R/k
R/R/10	Bed	0.0478	0.0493	3	0.0486	0.54
R/R/20	Bed	0.0663	0.0674	2	0.0669	0.85
R/R/40	Bed	0.0469	0.0494	5	0.0481	1.06
R/R/70	Bed	0.0400	0.0430	7	0.0415	1.52
R/S/10	Bed	0.0606	0.0612	1	0.0609	0.83
R/S/20	Bed	0.0343	0.0319	-8	0.0331	1.19
R/S/40	Bed	0.0392	0.0537	27	0.0465	1.76
R/S/70	Bed	0.0505	0.0584	13	0.0544	2.45
R/O/10	Bed	0.0287	0.0295	3	0.0291	0.70
R/O/20	Bed	0.0343	0.0362	5	0.0353	1.20
R/O/40	Bed	0.0547	0.0614	11	0.0581	2.44
R/O/70	Bed	0.0498	0.0540	8	0.0519	3.68
S/R/10	Cover	0.0576	0.0590	2	0.0583	1.00
S/R/20	Cover	0.0303	0.0327	7	0.0315	1.24
S/R/40	Cover	0.0678	0.0758	11	0.0718	2.00
S/R/70	Cover	0.0524	0.0621	16	0.0572	2.41
R/R/10	Cover	0.0417	0.0431	3	0.0424	0.51
R/R/20	Cover	0.0453	0.0501	9	0.0477	0.76
R/R/40	Cover	0.0459	0.0542	15	0.0500	1.07
R/R/70	Cover	0.0332	0.0361	8	0.0346	1.44
		Average:		7	0.0484	
		Standard deviation:		7	0.0119	

Table 3.6 - Calculated rough boundary sand grain roughnesses

It is noted that equal measured values of roughness would have resulted in the collapse of all data onto one line. An average value of k_s = 0.048 m, with a standard deviation of 0.012 m was calculated. In examining the effect of low R/k values on the flow in the channel, as discussed in section 1.2.11, no significant effect

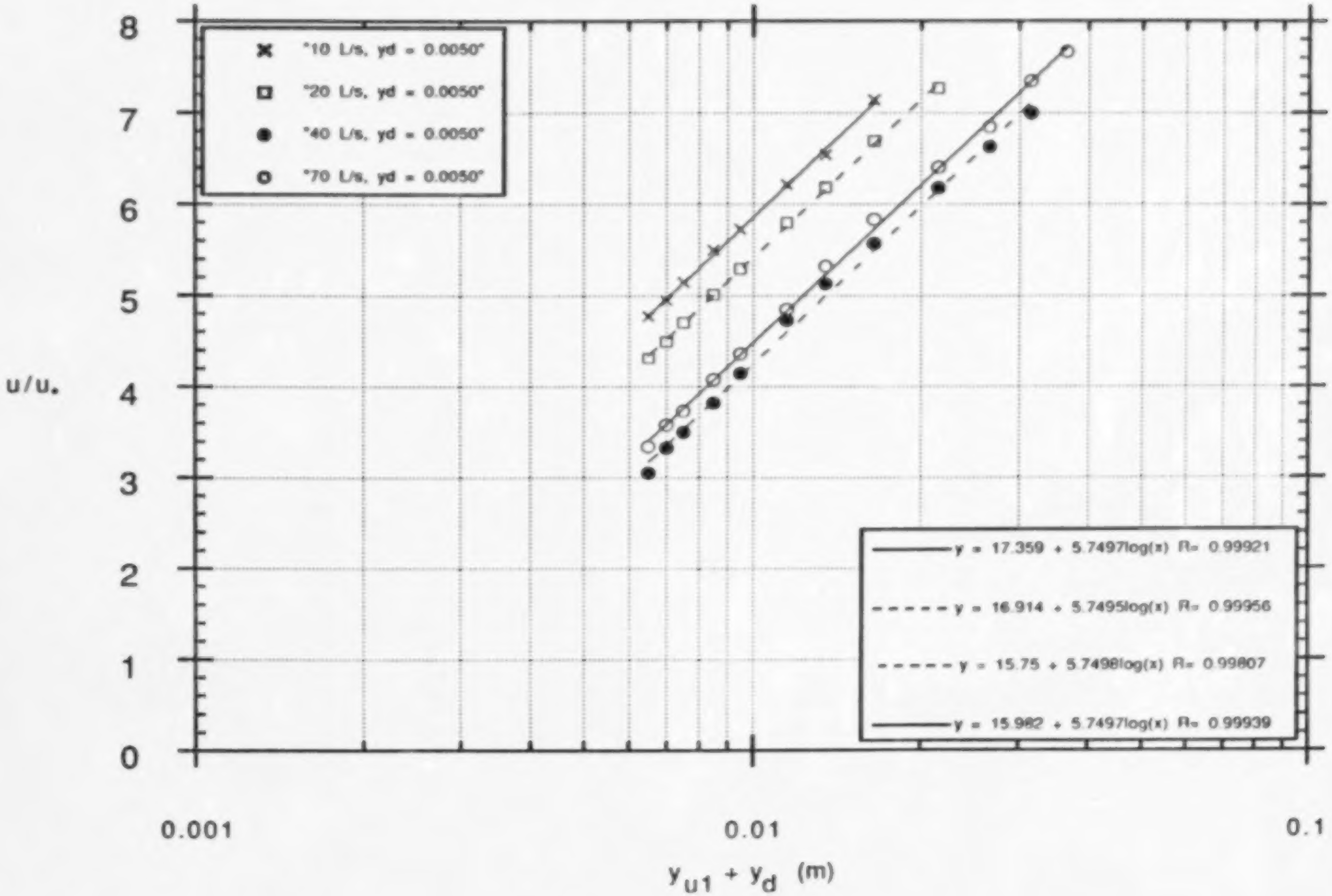

Figure 3.12(a) - Semi-logarithmic velocity profiles for R/O/bed runs

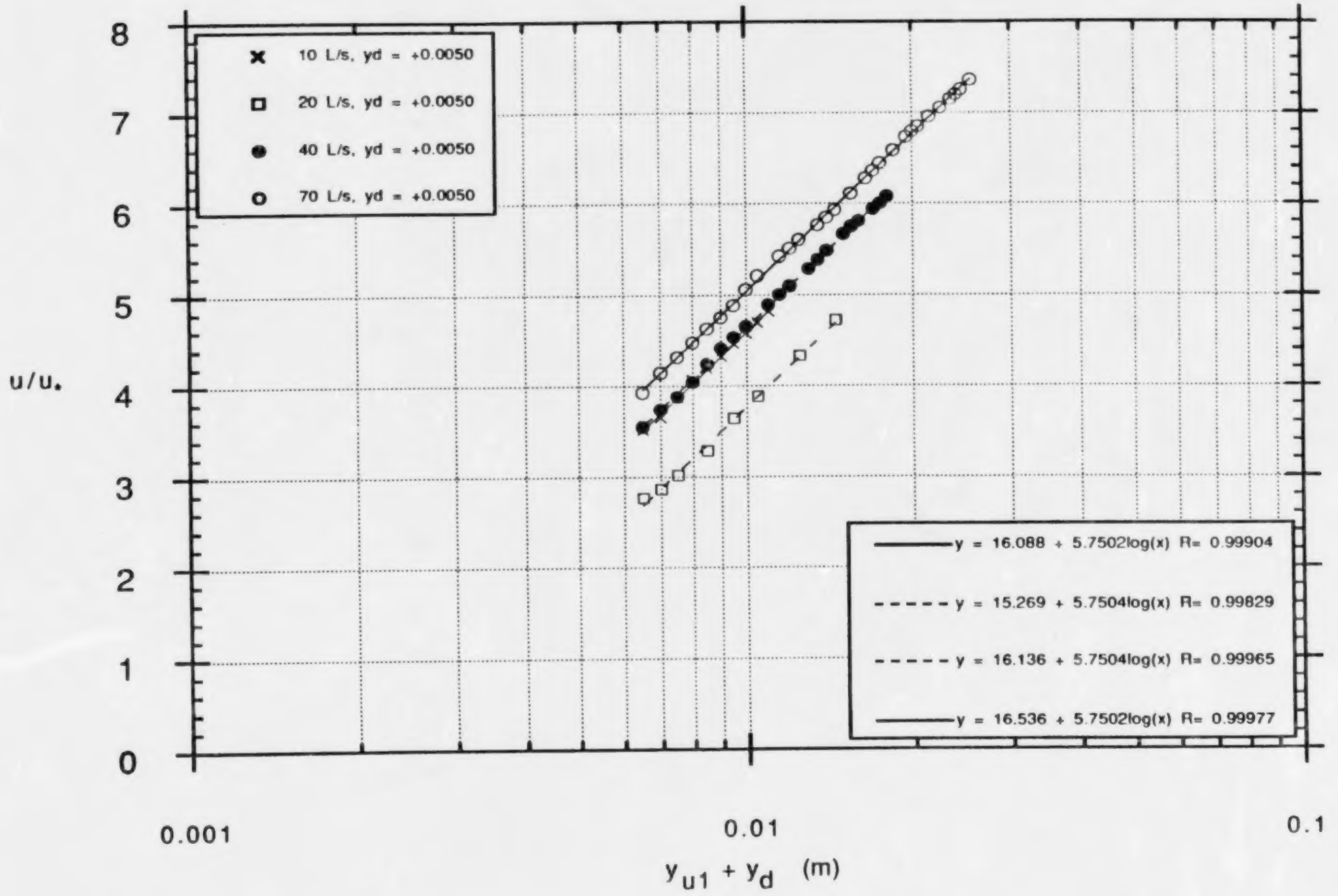

Figure 3.12(b) - Semi-logarithmic velocity profiles for R/R/bed runs

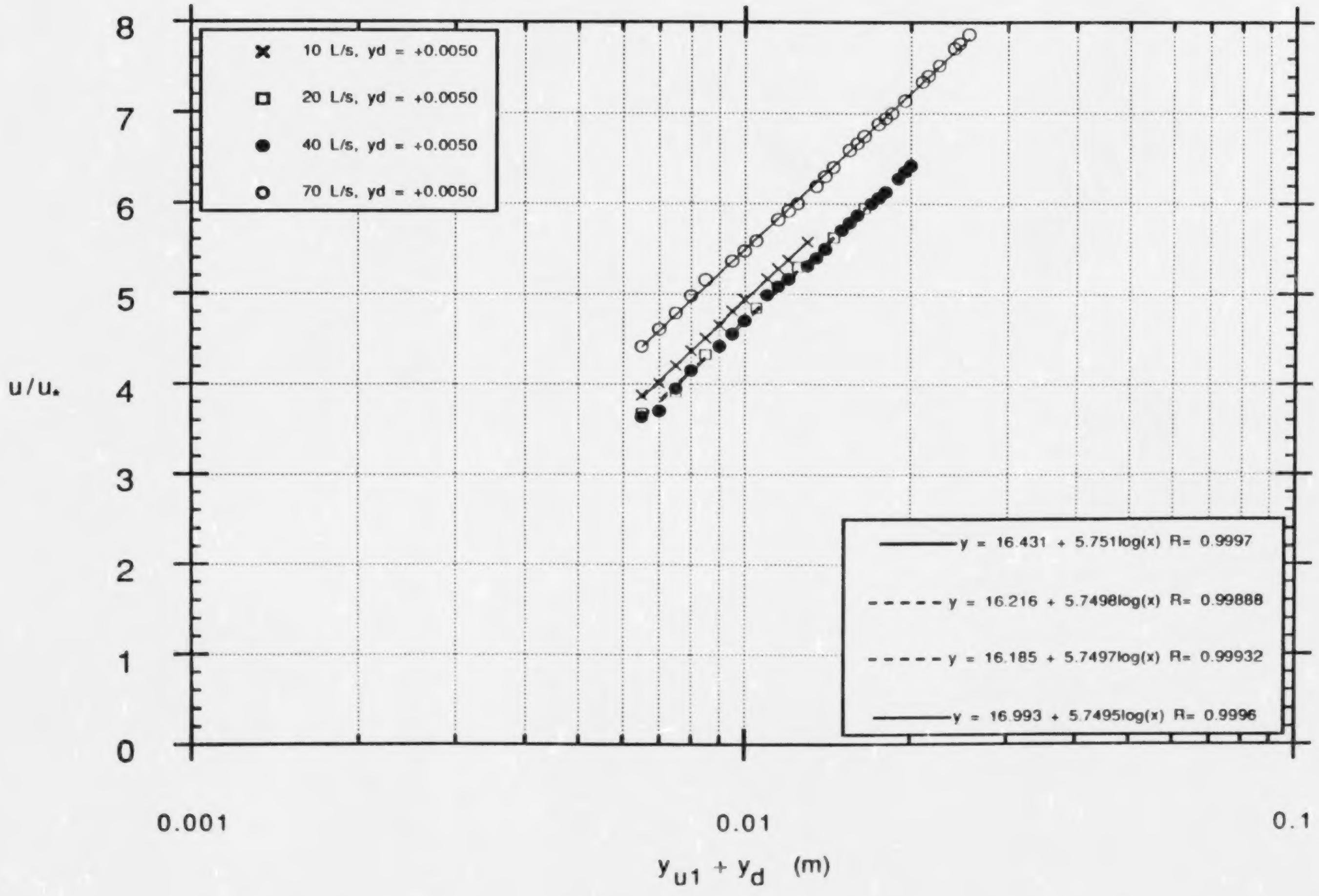

Figure 3.12(c) - Semi-logarithmic velocity profiles for S/R/cover runs

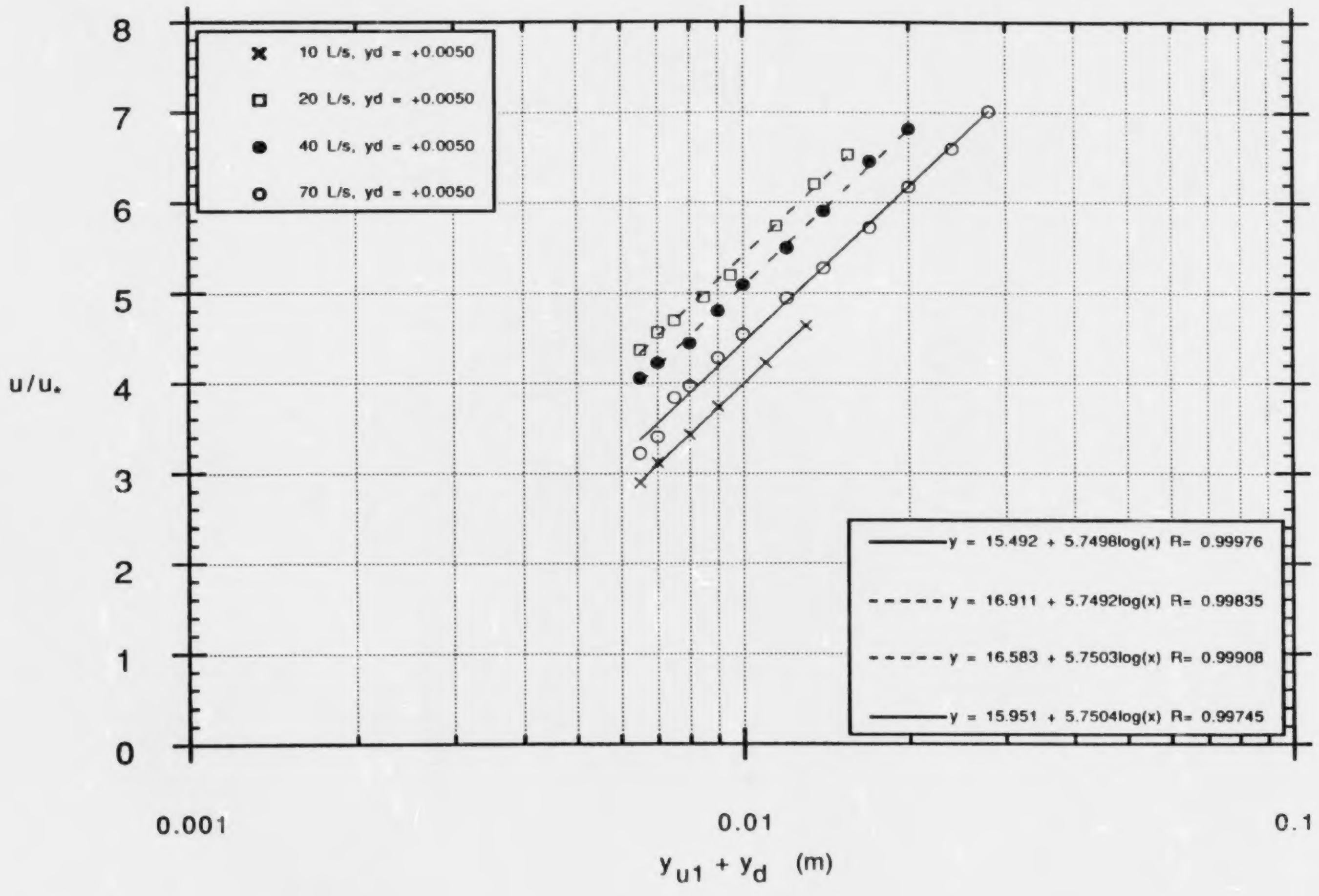

Figure 3.12(d) - Semi-logarithmic velocity profiles for S/R/cover runs

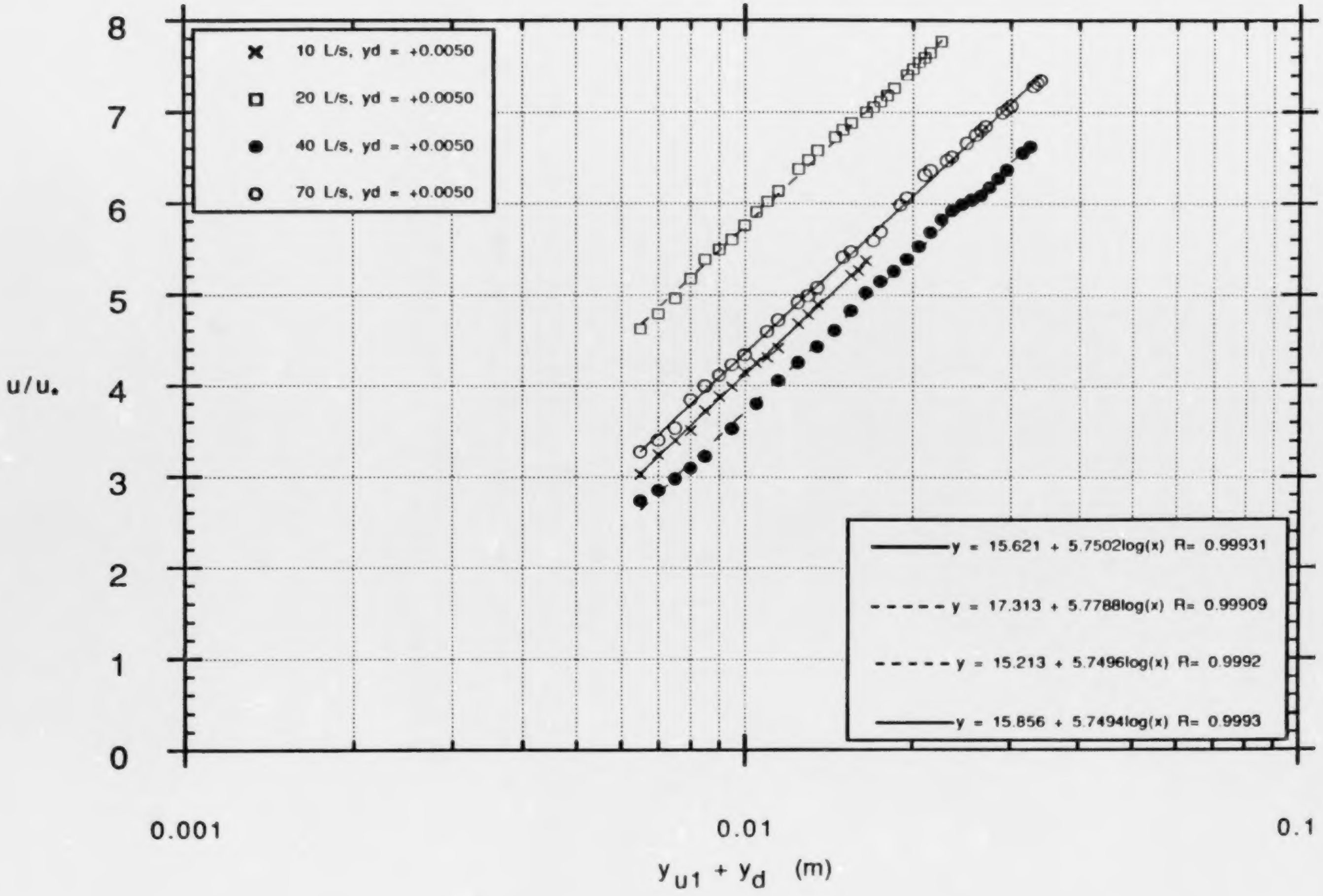

Figure 3.12(e) - Semi-logarithmic velocity profiles for S/R/cover runs

was seen. Only two values of R/k below the threshold value of 0.6 were seen here, though, and the scatter exhibited by the overall results precludes making any judgements concerning this phenomenon. The distribution of roughnesses with R/k ratio is shown on Figure 3.13.

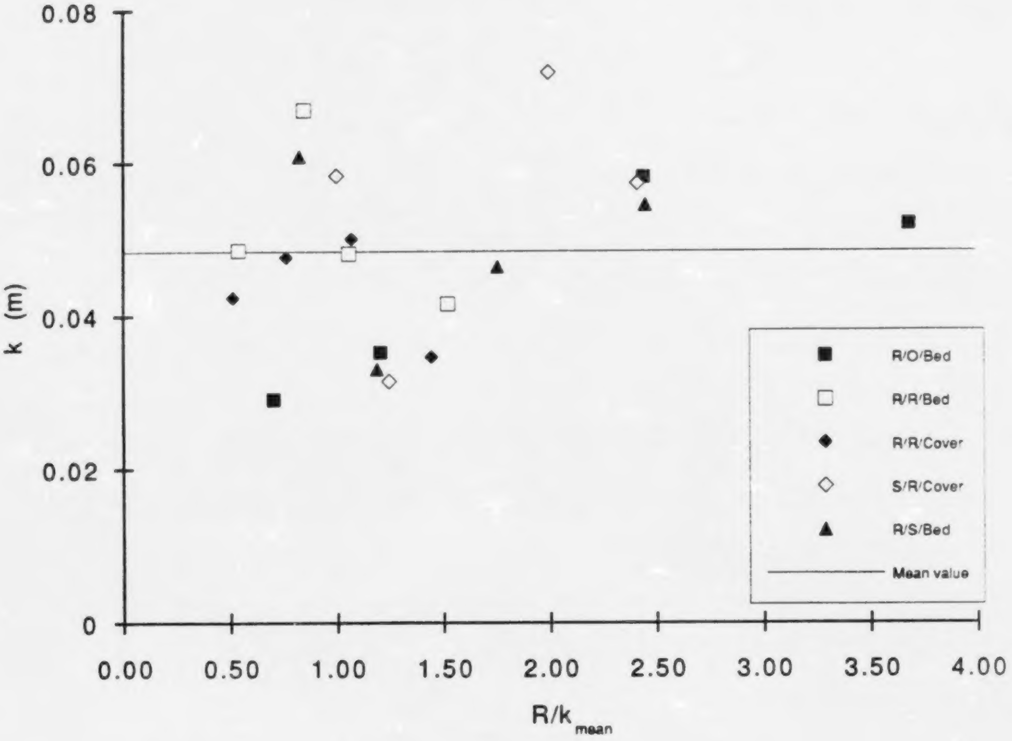

Figure 3.13 - Variation of measured roughness with R/k_{mean}

3.7 Summary of Results

In all, 24 separate runs were performed using all combinations of smooth boundary, rough boundary and open channel flows, with four different discharges. Flows were shown to be fully developed by an initial comparison of velocity profiles at two longitudinal stations, as well as by criteria set forth in a previous investigation (Jasek, 1992).

Five velocity profiles, evenly spaced laterally across the central portion of the test section, were taken for each run. These were then averaged, an action necessitated by both a slight lateral tilt in the flume and by the existence of secondary flows. Qualitative observations indicate that multiple secondary flow cells were set up across the channel, with their shape roughly circular, scaling on the depth of flow. Their intensity tended to increase with increasing discharge.

The virtual origin of the velocity profiles was also calculated. This was expected to be at the boundary surface for the smooth boundary, and somewhat below the top of roughness for the rough boundary. Results showed that the virtual origin for the smooth boundary was indeed at its surface. The rough boundary virtual origin proved to be 5 mm below the top of the roughness.

Shear stresses at the boundaries were computed by two methods, as outlined in section 2.2.4. An excellent agreement between the two techniques was noted. One interesting result of this analysis was the observation that for identical slopes, discharges and bed roughnesses, at normal depth, the shear at the bed did not show a dramatic drop when a cover was placed on the flow. A theoretical solution presented in support of these results instead points to an expected drop on the order of 20%.

Covered flows were divided at the theoretical point of zero shear, determined by assuming a linear distribution of shear stress across the depth of flow, and average velocities in the two zones were computed. Average ratios of one zone to the other were 1.00 for like boundaries, as expected, and 1.16 for unlike boundaries, with the higher velocity in the smooth boundary zone. Calculations here refuted two assumptions commonly used as a basis for early analysis, namely that the hydraulic radii (i.e. depth) of the two zones were the same, and that average velocities in the two zones were identical.

Boundary roughnesses, as boundary shears, were also determined by two methods. These are detailed in section 2.2.4. A reasonable agreement between the two methods was exhibited, though there seemed to be quite a large scatter in the values of roughness computed. When converted to values of Manning's n, though, much more consistency was shown. This is likely because of sensitivity considerations, as the Chezy equation is less sensitive to the choice of k than the Manning equation is to the choice of n. The average rough boundary k_s was 0.0484 m ($n = 0.030$), while the smooth boundary values, though dependent on flow parameters, were on the order of $k_v = 0.0003$ ($n = 0.010$).

4.0 Application of Experimental Data to Previous Work

The performance of equations selected from those reviewed in sections 1.1 and 1.2 was investigated by applying the experimental data from all covered channel runs to them. First, the equations for composite roughness were examined. Then, selected empirical relations describing other aspects of covered flows had the same data applied to them.

4.1 Composite Roughness Equations

Ten equations were available to evaluate for ability to calculate a composite roughness coefficient. These included all of those from section 1.1, with the exception of those of Konovalov, Trufanov and Carey, which were not suited to calculation with the data available. It should also be noted that the equation of Dul'nev is identical to that of Lotter, so has also not been included. Additionally, the equation presented by Chee in section 1.2.8 was analyzed. In the situation where bed and cover roughnesses were equal, many of the equations yielded similar, reasonable results. However, looking at unequal boundary roughnesses, some flaws in certain equations became more readily apparent.

4.1.1 Equal Bed and Cover Roughnesses

For the situation of equal bed and cover roughnesses, six of the ten equations produce identical results. The equations of

Pavlovskiy, Lotter, Sabaneev, Shiperko, Larsen and Chee all behave identically. These all break down to $n = n_1 = n_2$ for $n_1 = n_2$.

The remaining four equations behave differently from this and from each other. The Hancu equation (1.1.2) yields results which are quite similar to the ones already noted, while the Yu equation (1.1.13) is also similar, but yields values for the composite value which are consistently lower. The Belokon equation (1.1.9), yields values substantially higher than for the Sabaneev equation which it is related to. Lastly, the Levi equation (1.1.5) yields reasonable values for the smooth boundary situation, but seems to have some problem when dealing with rough boundaries.

As to the accuracy of these equations, it appears that all of the equations, with the exception of Belokon's, behave similarly and agree well with experimental values. As noted previously, for the case of equal bed and cover roughness, Belokon's equation yields composite roughness values 58% higher than Sabaneev's. The values being compared are shown in Table 4.1 and Figure 4.1.

Equation	Run S/S/10	S/S/20	S/S/40	S/S/70	R/R/10	R/R/20	R/R/40	R/R/70
Experimental	0.026	0.015	0.016	0.014	0.029	0.029	0.024	0.023
Pavlovskiy	0.011	0.010	0.010	0.010	0.040	0.034	0.032	0.030
Belokon	0.017	0.016	0.015	0.016	0.061	0.053	0.051	0.046
Levi	0.016	0.014	0.013	0.013	-0.030	-0.044	-0.060	-0.096
Hancu	0.011	0.010	0.012	0.010	0.040	0.034	0.032	0.030
Yu	0.009	0.008	0.008	0.008	0.034	0.029	0.027	0.025

Table 4.1 - Predicted and Experimental Composite Roughnesses (Like Boundaries)

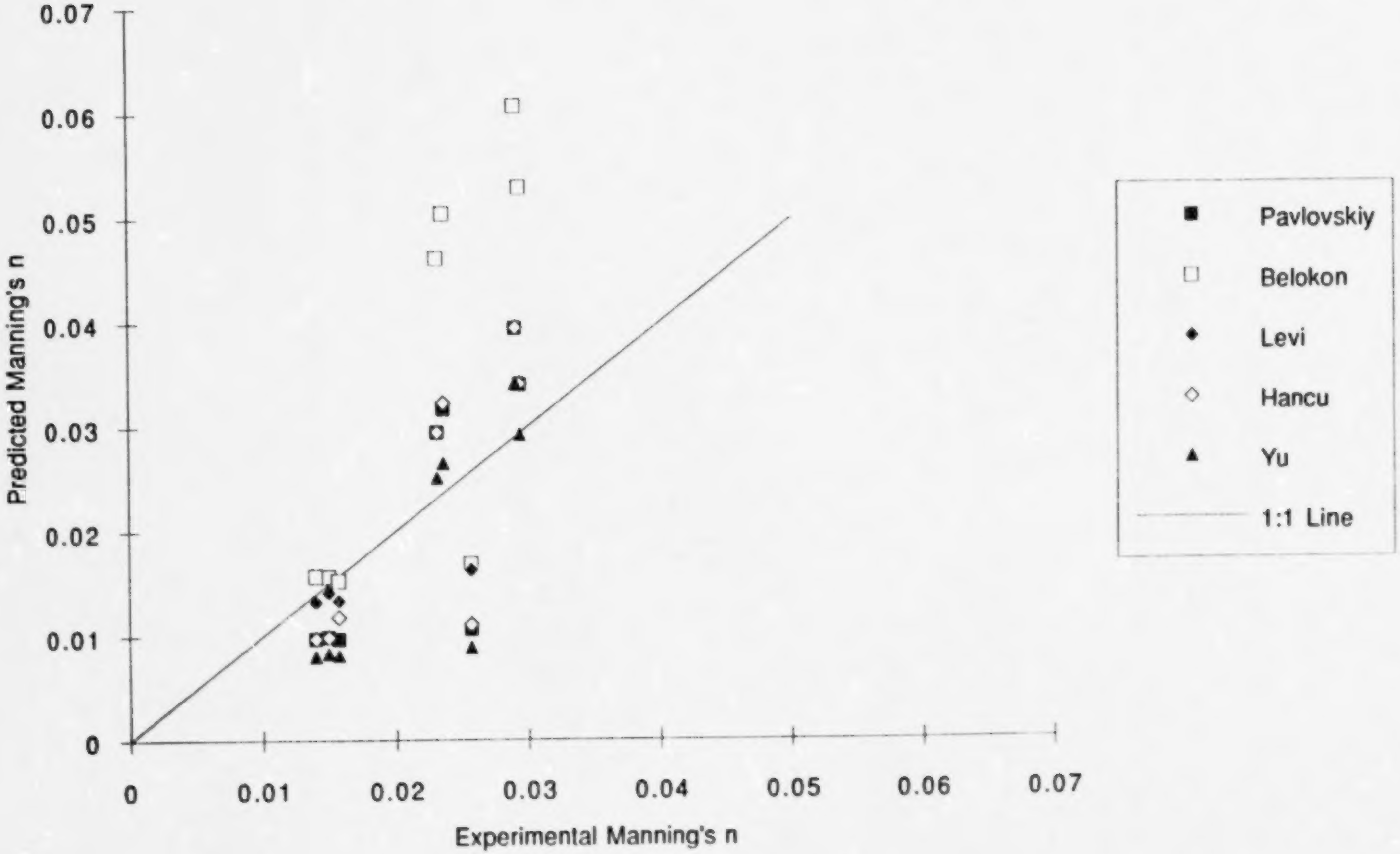

Figure 4.1 - Predicted vs. Experimental Composite Roughnesses (Like Boundaries)

4.1.2 Unequal Bed and Cover Roughnesses

For the case of unequal bed and cover roughnesses, all of the equations behave differently, except for those of Larsen and Sabaneev. These two yield virtually identical results, and along with Hancu's equation have the greatest agreement with the experimental values. Other formulas produce results of varying accuracy, with those of Belokon, Yu and Chee fairly inaccurate and that of Levi quite unreasonable. A comparison of experimental and computed values of composite Manning's n is shown in Table 4.2 and Figure 4.2.

	Run							
Equation	S/R/10	S/R/20	S/R/40	S/R/70	R/S/10	R/S/20	R/S/40	R/S/70
Experimental	0.029	0.021	0.022	0.017	0.021	0.017	0.018	0.017
Pavlovskiy	0.026	0.024	0.022	0.022	0.032	0.028	0.024	0.023
Lotter	0.016	0.015	0.015	0.0150	0.016	0.015	0.015	0.014
Belokon	0.012	0.011	0.011	0.011	0.166	0.138	0.115	0.104
Sabaneev	0.023	0.022	0.020	0.020	0.026	0.023	0.021	0.020
Levi	-0.087	-0.155	-1.706	0.590	-0.045	-0.068	-0.131	-0.390
Shiperko	0.014	0.014	0.014	0.013	0.013	0.013	0.013	0.013
Larsen	0.023	0.022	0.020	0.020	0.026	0.023	0.021	0.020
Hancu	0.022	0.021	0.020	0.020	0.025	0.022	0.023	0.020
Yu	0.081	0.077	0.064	0.064	0.011	0.010	0.009	0.009
Chee	0.011	0.011	0.011	0.012	0.010	0.010	0.010	0.010

Table 4.2 - Predicted and Experimental Composite Roughnesses (Unlike Boundaries)

Note that in Figure 4.2, values of composite Manning's n which deviate significantly from the experimental are not shown, to allow a better examination of those which are in reasonable agreement.

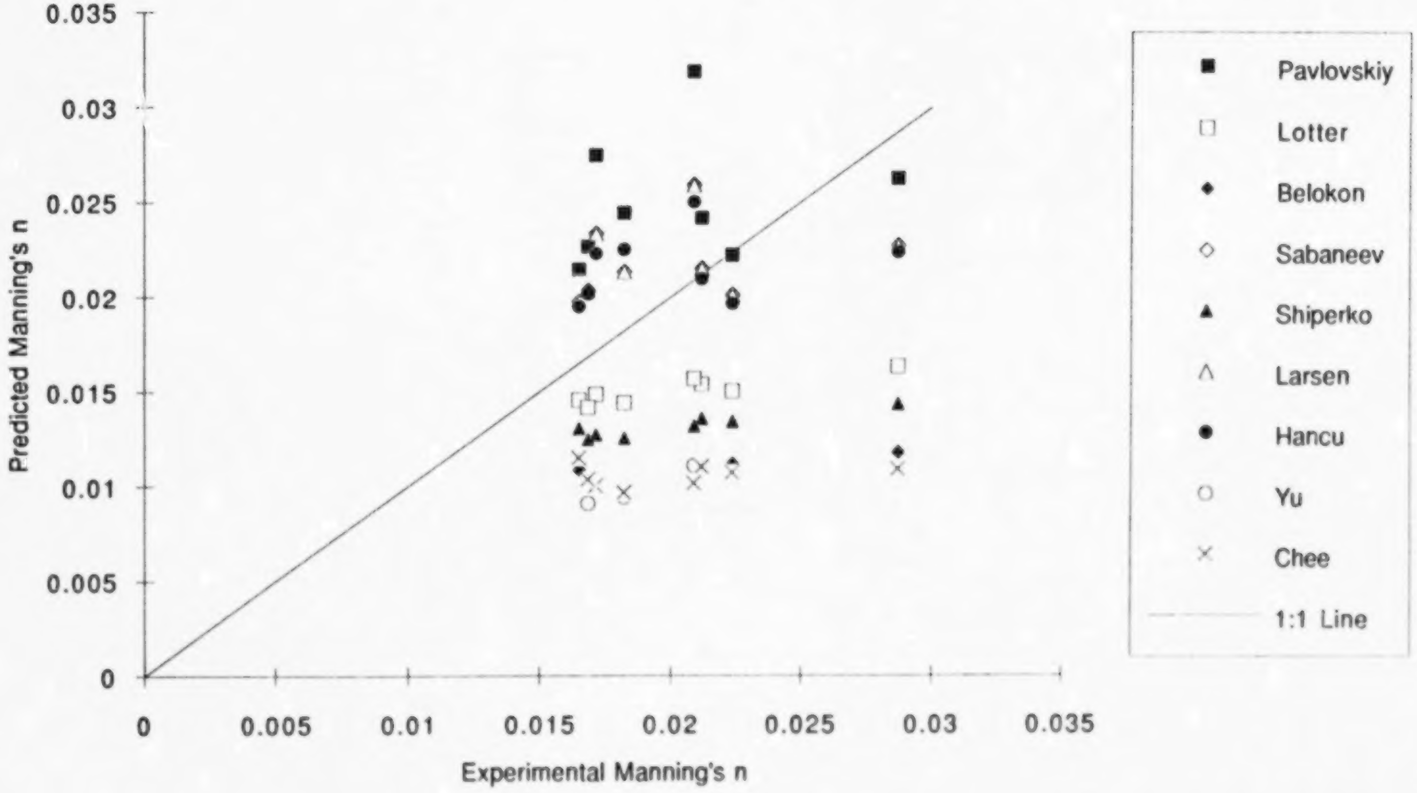

Figure 4.2 - Predicted vs. Experimental Composite Roughnesses (Unlike Boundaries)

4.1.3 Summary

Overall, it seems that the equations of Hancu and Larsen, recommended by Uzuner (1975), and that of Sabaneev, recommended by Beltaos (1983), yield the most consistently accurate results. Certainly, in practice, where input parameters tend to have a relatively high degree of uncertainty, these equations will yield reasonable results.

4.2 Comparison With Selected Empirical Equations

The work of Tatinclaux and Gogus (sections 1.2.3 and 1.2.7) provide further equations describing the form of covered flows. Several of these will be examined here. Their earlier work provides an equation which defines the average flow velocity in a zone of influence:

$$V_i = u_{max} - \frac{u_{*i}}{\kappa} \qquad (1.81)$$

as well as one which calculates the position of the plane of maximum velocity:

$$\frac{H_1}{H_e} = 0.26 \log \frac{f_1}{f_2} + 0.5 \qquad (1.83)$$

Both of these equations are applicable to all of the covered runs performed. A comparison of measured and predicted values is shown in Table 4.3 and Figure 4.3 for the former equation and Table 4.4 and Figure 4.4 for the latter.

Run	Boundary	Measured V_i (m/s)	Predicted V_i (m/s)	Difference (%)
S/S/10	Bed	0.127	0.127	-0.1
S/S/10	Cover	0.128	0.126	-1.3
S/S/20	Bed	0.230	0.231	0.3
S/S/20	Cover	0.229	0.232	1.3
S/S/40	Bed	0.332	0.331	-0.2
S/S/40	Cover	0.323	0.333	3.0
S/S/70	Bed	0.390	0.390	-0.1
S/S/70	Cover	0.397	0.390	-1.8
R/R/10	Bed	0.164	0.146	-10.8
R/R/10	Cover	0.164	0.150	-8.5
R/R/20	Bed	0.216	0.196	-9.2
R/R/20	Cover	0.214	0.207	-3.3
R/R/40	Bed	0.326	0.309	-5.2
R/R/40	Cover	0.331	0.307	-7.1
R/R/70	Bed	0.412	0.387	-6.2
R/R/70	Cover	0.407	0.394	-3.3
S/R/10	Bed	0.123	0.126	2.5
S/R/10	Cover	0.107	0.098	-8.4
S/R/20	Bed	0.195	0.201	3.3
S/R/20	Cover	0.181	0.174	-3.8
S/R/40	Bed	0.256	0.255	-0.4
S/R/40	Cover	0.218	0.209	-4.3
S/R/70	Bed	0.371	0.377	1.5
S/R/70	Cover	0.344	0.313	-9.1
R/S/10	Bed	0.184	0.161	-12.6
R/S/10	Cover	0.224	0.228	2.0
R/S/20	Bed	0.276	0.274	-0.7
R/S/20	Cover	0.336	0.332	-1.3
R/S/40	Bed	0.376	0.361	-4.0
R/S/40	Cover	0.432	0.436	0.8
R/S/70	Bed	0.485	0.437	-10.0
R/S/70	Cover	0.524	0.541	3.2

Table 4.3 - Performance of Equation 1.81

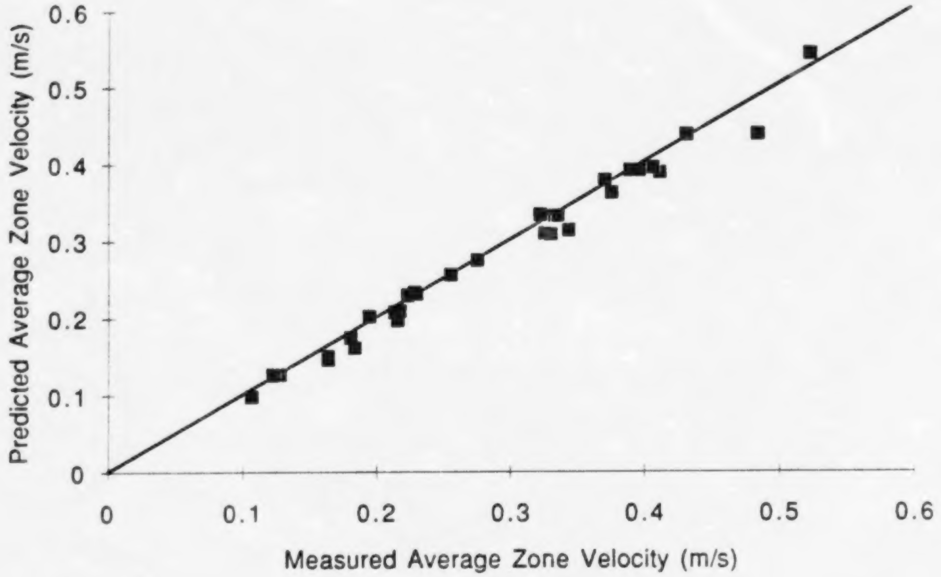

Figure 4.3 - Performance of Equation 1.81

Run	f_1	f_2	H_1 (cm)	H_e (cm)	Experimental H_1/H_e	Predicted H_1/H_e	Difference (%)
S/S/10	0.029	0.030	3.23	6.55	0.493	0.496	0.6
S/S/20	0.025	0.023	3.83	7.50	0.511	0.509	-0.4
S/S/40	0.020	0.020	5.10	10.30	0.495	0.504	1.8
S/S/70	0.017	0.018	8.90	15.25	0.584	0.497	-14.9
R/R/10	0.370	0.347	2.15	4.60	0.467	0.507	8.5
R/R/20	0.328	0.266	3.55	7.30	0.486	0.524	7.7
R/R/40	0.201	0.199	4.62	9.80	0.471	0.501	6.2
R/R/70	0.140	0.130	6.95	13.85	0.502	0.508	1.2
S/R/10	0.030	0.246	1.97	6.80	0.290	0.264	-8.9
S/R/20	0.024	0.140	3.00	9.15	0.328	0.303	-7.6
S/R/40	0.022	0.177	4.40	13.75	0.320	0.266	-17.0
S/R/70	0.019	0.139	6.15	16.50	0.373	0.275	-26.3
R/S/10	0.434	0.033	2.30	3.50	0.657	0.792	20.5
R/S/20	0.188	0.026	3.45	5.25	0.657	0.722	9.8
R/S/40	0.158	0.023	5.42	8.00	0.678	0.719	6.2
R/S/70	0.163	0.019	7.30	11.35	0.643	0.745	15.8

Table 4.4 - Performance of Equation 1.83

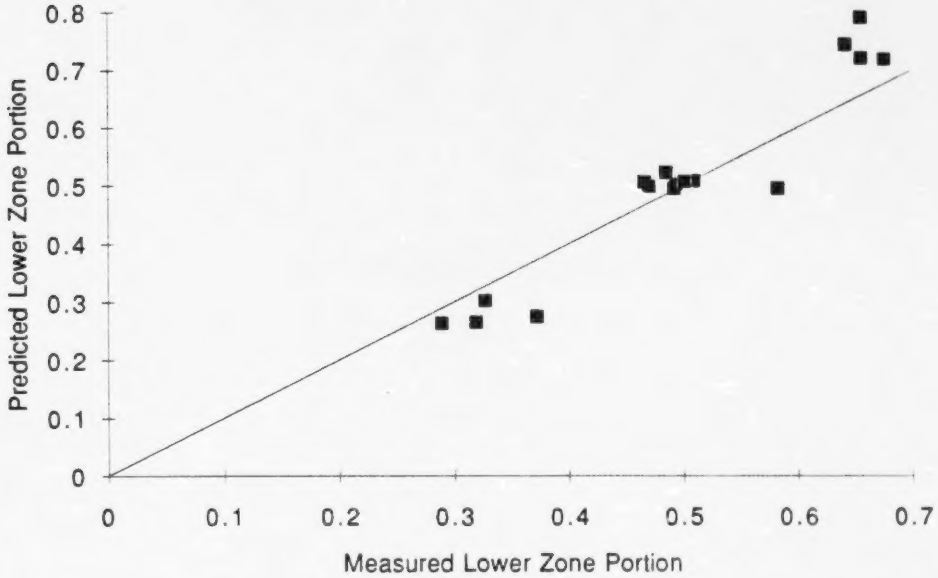

Figure 4.4 - Performance of Equation 1.83

Later work provides three more equations which calculate the size of the zones of influence in an ice covered flow. Unfortunately, two of the these, equations (1.93) and (1.94), which define the sizes of the zones of influence for the case of two rough boundaries, are not applicable here. This is because they are meant to be applied to flows where the two roughnesses are unequal, but still both hydraulically rough. Another equation (1.95), though, is available for analysis:

$$\left(1 - 2\eta\right)^{5/8} - \frac{\left(1 + 2\eta\right)^{1/2}}{R_H^{1/8}}\left[1.06 \log\left(1 + 2\eta\right) - 1.06 \log\left(\frac{k_r}{H}\right) + 0.90\right] = 0$$

$$\text{where} \qquad R_H = \frac{2VH}{\nu} \qquad (1.95, 1.97)$$

This formula predicts the relative sizes of the zones of influence for the case of one rough and one smooth boundary. A comparison of measured and predicted values for this equation is shown in Table 4.5 and Figure 4.5.

Run	H_r (cm)	H (cm)	k_r (m)	R_H	Measured η	Predicted η	Difference (%)
S/R/10	4.83	6.80	0.0484	12000	0.210	0.334	58.8
S/R/20	6.02	9.15	0.0484	23000	0.158	0.335	112.1
S/R/40	9.66	13.75	0.0484	45000	0.202	0.325	60.5
S/R/70	11.58	16.50	0.0484	78000	0.202	0.330	63.5
R/S/10	2.96	4.00	0.0484	12000	0.240	0.374	55.8
R/S/20	3.95	5.75	0.0484	24000	0.187	0.366	95.8
R/S/40	5.92	8.50	0.0484	47000	0.196	0.356	81.2
R/S/70	8.56	11.85	0.0484	80000	0.222	0.350	57.4

Table 4.5 - Performance of Equation 1.95

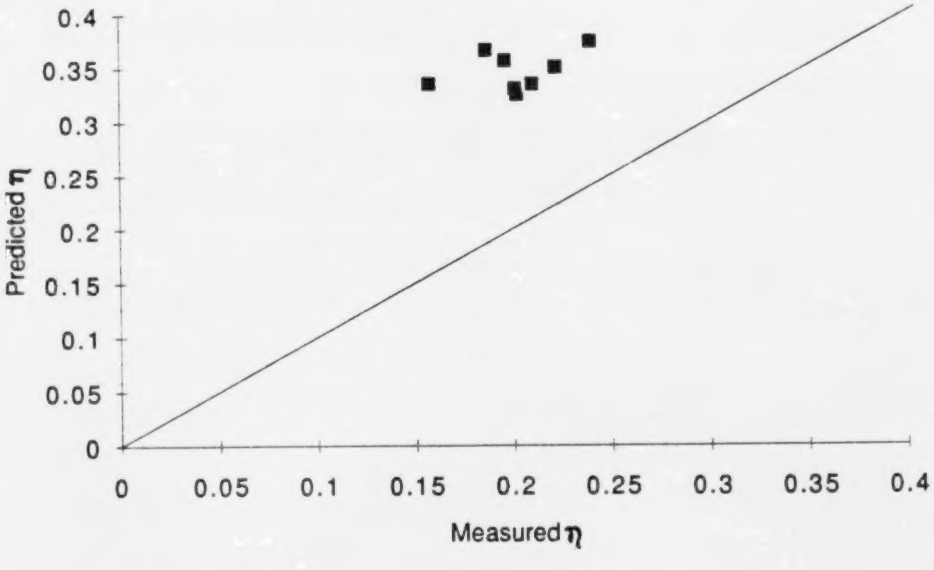

Figure 4.5 - Performance of Equation 1.95

Measured and predicted values of η both appear to be grouped quite closely within their respective group, as would be expected for a set of runs using identical smooth and rough boundaries, but the two groups have a mean difference of almost 75%. It is difficult say exactly why this difference exists without a better understanding of how the equation was developed. The logarithmic terms in the equation reduce the sensitivity to values of depth and roughness, so these would have to change significantly (by an order of magnitude) to produce matching results. It is noted that this equation is only meant to be applied to situations where $R_H < 5x10^4$, where only half of the experimental runs here fall below this value.

4.3 Summary

In examining the theoretical equations which have historically been used to describe flows in ice covered channels, it has been seen that though many of these relations have been based on false assumptions, they often provide results which are practically useful. Advances in theory in the fields of fluid mechanics and hydraulics, complemented with experimental work, have led to the development of a collection of equations. Many of these can predict flow parameters to a reasonable level of accuracy, especially considering the fact that field data often comes with its own sources of uncertainty. In particular, the equations presented by Sabaneev (1948), Larsen (1966) and Hancu (1967) all provide excellent estimates of the composite roughness of an ice covered channel. Other work, including that of Tatinclaux and Gogus in the early 1980's which is examined here, goes further towards describing the structure of an ice covered flow.

5.0 Conclusions and Recommendations

Early attempts at describing the phenomenon of ice covered flow with mathematical equations were hindered by a lack of precise experimental data. This necessitated making assumptions which were sometimes false. Subsequent theoretical developments in the fields of hydraulics and fluid mechanics aided later experimental investigations in furthering the state of knowledge in this area.

Experiments performed as the basis of this study examined flows under a flexible cover, involving combinations of rough and smooth boundaries, as well as open channel flows. Runs were performed over a range of discharges, all fully turbulent. Velocity profiles were taken using a Preston tube apparatus, allowing boundary shears to be determined by two methods. Likewise, boundary roughnesses were computed by two methods, ensuring confidence in results.

5.1 Conclusions

The Preston tube technique for measuring boundary shear was found to be quite accurate for both smooth and rough boundaries. Both smooth and rough boundary bed shears varied by less than two percent from those determined from velocity profiles.

For all covered flows, the ratio of boundary shears was computed. By assuming a linear distribution of shear stress across the depth of the flow, this can provide the location of the theoretical plane of zero shear. For like boundaries, the average cover to bed ratio was 0.97, which means that the plane of zero shear was essentially at the center of the velocity profile, coincident with the plane of maximum velocity. This result was expected. For unlike boundaries, the average ratio of rough to smooth boundary shear was 2.39. This indicates that for the combination of this specific roughness and a smooth boundary, the zero shear plane lies a distance of approximately 30% of the depth of flow from the smooth boundary. This plane, which is often used as a boundary to divide the flow into two independent elements, was found to be closer to the smooth boundary than the plane of maximum velocity, though the difference was not great. The plane of zero shear has been used as the dividing point in all calculations here. It should be recognized that in nature, roughnesses may range over orders of magnitude for both beds and covers. Ice covers may range from hydraulically smooth to roughnesses on the order of metres for ice jam accumulations, while bed material may range from silt to boulders. Thus, many combinations of bed and cover roughnesses are possible. A temporal variation in roughness is also often seen, with ice roughnesses varying over the course of a winter.

The effect of the shear redistribution due to the introduction of a cover on bed shear was noted as being tempered by the increase in stage and drop in conveyance which also resulted. It was shown, experimentally and theoretically, that for flows at normal depth, bed shears did not drop as dramatically as was expected, though some drop did result.

The average velocities in each zone of influence were calculated by averaging the five velocity profiles measured for each run. Scatter in these profiles, appearing to be more significant for runs at higher discharges, point to the existence of secondary flows. Visual observations of dye patterns also support this observation. It is felt that the averaging of five profiles yields a better result than the use of a single profile taken at the channel centreline, as has been done by previous researchers. The computed ratio of zone velocities was 1.00 for similar boundaries, as expected. For dissimilar boundaries, the ratio was 1.16, with the higher velocity in the smooth boundary zone, as expected. This shows that the common assumption of equal zone velocities is in fact flawed, though the end result in a composite roughness calculation does not appear to be overly sensitive to this.

The virtual origins of the two surfaces were also determined from velocity profile data, and these results were quite accurate and precise. For the smooth boundary, it was found to be at the surface of the boundary, as expected, with very little deviation over the range of runs. For the rough boundary, it was found to consistently lie 5 mm below the surface of the roughness.

Rough boundary equivalent sand grain roughnesses were determined both from velocity profiles and from bulk flow measurements. A fair agreement between the two techniques was seen, with an average difference of 7%. The equivalent sand grain roughness was calculated as 0.0484 m, considerably greater than the actual physical roughness of the material. For the smooth boundary, which was determined to be hydraulically smooth, a viscous roughness was calculated by the same methods, as well as by a method based on the shear velocity. Of course, this value is dependent on the flow characteristics, so no one value can describe it. A good agreement between values obtained for each run by the three techniques was obtained, but values of viscous roughness are so small that minor differences seem great. No variation of roughness with R/k ratio was seen, but it is felt that no runs had a low enough value for it to influence the measured roughness.

The experimental value was applied to a number of equations for composite roughness as well as to several describing other aspects of ice covered flows. Three equations for calculating composite roughness, those of Hancu, Larsen and Sabaneev, demonstrated the best agreement with the experimental data, and appear to be the most accurate for the range of parameters seen here. The latter equation is commonly used in practice in North America.

Certain equations describing the structure of ice covered flows, presented by Tatinclaux and Gogus in the early 1980's, were also examined. The first two of these, which calculated average velocity, based on a maximum velocity and bed shear, and the position of the plane of maximum velocity, based on zone friction factors, fit the experimental data quite well. A third equation, for computing the position of the zero shear plane between a smooth and rough boundary, did not provide such a good fit.

5.2 Recommendations

Many questions related to flow under ice covers still remain unanswered, though a sufficient level of knowledge has perhaps been reached to permit accurate, practical calculations of such things as rating and backwater curves. However, many practical calculations lose sight of the actual physics of the problem and instead use flow parameters as calibration tools. An example of this is how unrealistically high values of Manning's n may be used to account for flow constrictions resulting from frazil accumulations under ice covers.

A knowledge of the structure of the flow under a cover is essential in examining mixing processes and sediment transport in ice covered flows. The question of the degree, if any, of interaction between the two layers has implications for both topics. Though it has been assumed here that the theoretical plane of zero shear exists at the point defined by a linear shear distribution, and in fact exists, this is by no means a closed issue. Evidence does indicate that the independent zones examined in this study do exert an influence on each other, and this is certainly one area that bears further investigation.

References

Bayazit, M., 1976. "Free Surface Flow in a Channel of Large Relative Roughness", IAHR Journal of Hydraulic Research, Vol. 14, No. 2, pp 115-126.

Beltaos, S., 1983. "River Ice Jams: Theory, Case Studies, and Applications", Journal of Hydraulic Engineering, Vol. 109, No. 10, pp 1338-1359.

Beltaos, S. and J. Wong, 1986. "Downstream Transition of River Ice Jams", Journal of Hydraulic Engineering, Vol. 112, No. 2, pp 91-110.

Beltaos, S. and R. Gerard, 1987. "Discussion and Reply - River Ice Jams: Theory, Case Studies, and Applications", Journal of Hydraulic Engineering, Vol. 113, No. 2, pp 241-255.

Bray, D.I. and K.S. Davar, 1987. "Resistance to Flow in Gravel-Bed Rivers", Canadian Journal of Civil Engineering, Vol. 14, No. 1, pp 77-86.

Calkins, D.J., et al, 1982. "Resistance Coefficients from Velocity Profiles in Ice-Covered Shallow Streams", Canadian Journal of Civil Engineering, Vol. 9, pp 236-247.

Carey, K.L., 1966. "Observed Configuration and Computed Roughness of the Underside of River Ice, St. Croix River, Wisconsin", United States Geological Survey Professional Paper No. 550B, pp 192-198.

Chee, S.P. and M.R. Haggag, 1982. "Theoretical Velocity Patterns in Ice Covered Stream Channels",Proceedings of the Workshop on Hydraulics of Ice Covered Rivers, June 1 and 2, Edmonton, Alberta, pp 222-231.

Chee, S.P., 1985. "Floating Boundary River Mechanics", Advances in Water Engineering, Elsevier Applied Science Publishers, New York, pp 325-331.

Chee, S.P. and S. Ray, 1986. "Multiple Roughness Ice Covered Channels", IAHR Ice Symposium, Iowa City, Iowa, pp 53-62.

Davis, R.E., et al, 1966. "Surveying Theory and Practice", McGraw-Hill, New York, 1096 p.

Gerard, R., 1982. "Flow in Ice Covered Channels - Some Fundamentals", Proceedings of the Workshop on Hydraulics of Ice Covered Rivers, June 1 and 2, Edmonton, Alberta, pp 8-22.

Gerard, R. and D. Andres, 1982. "Hydraulic Roughness of Freeze-Up Ice Accumulations: North Saskatchewan River Through Edmonton", Proceedings of the Workshop on Hydraulics of Ice Covered Rivers, June 1 and 2, Edmonton, Alberta, pp 62-87.

Gerard, R., 1989. "Flow Along Ice Sheets", Course Notes for Civ E 636: Ice Engineering, Unpublished Material, The University of Alberta, 20 p.

Gogus, M. and J.C. Tatinclaux, 1980. "Characteristics of Flow Below a Rough Floating Cover", Workshop on Hydraulic Resistance of River Ice, Burlington, Ontario, pp 122-142.

Gogus, M. and J.C. Tatinclaux, 1981. "Mean Characteristics of Asymmetric Flows: Application to Flow Below Ice Jams", Canadian Journal of Civil Engineering, Vol. 8, pp 342-350.

Gogus, M. and J.C. Tatinclaux, 1981. "Flow Characteristics Below Floating Covers with Application to Ice Jams", Iowa Institute of Hydraulic Research, Report No. 233, 167 p.

Hanjalic, K. and B.E. Launder, 1972. "Fully Developed Asymmetric Flow in a Plane Channel", Journal of Fluid Mechanics, Vol. 51, Part 2, pp 301-335.

Haritonidis, J.H., 1989. "The Measurement of Wall Shear Stress", Lecture Notes in Engineering, Vol. 45: Advances in Fluid Mechanics Measurements, M. Gad-el-Hak, Editor, Springer-Verlag, pp 229-261.

Hendriksen, F. and K.S. Davar, 1986. "Estimation of Resistance to Flow in Ice Covered Channels Using Binary Velocity Distributions", IAHR Ice Symposium, Iowa City, Iowa, pp 41-52.

Hollingshead, A.B. and N. Rajaratnam, 1980. "A Calibration Chart for the Preston Tube", Journal of Hydraulic Research, Vol. 18, No. 4, pp 313-326.

Ismail, E. and K.S. Davar, 1978. "Resistance to Flow Under a Very Rough Top Boundary", Proceedings of the IAHR Symposium on Ice Problems, Part 2, Lulea, Sweden, pp 435-447.

Jasek, M.J., 1992. "Entrance Length and Boundary Layer Development in Open Channels", Thesis Presented in Partial Fulfillment of Degree of Master of Science, The University of Alberta, 282 p.

Kamphuis, J.W., 1974. "Determination of Sand Roughness for Fixed Beds", IAHR Journal of Hydraulic Research, Vol. 12, No. 2, pp 193-203.

Komora, J. and J. Sumbal, 1967. "Head Losses in Channels with Ice Cover", Twelfth Congress of the International Association for Hydraulic Research, Fort Collins, September 11-14, pp 270-274.

Larsen, P.A., 1966. "Head Losses Caused by an Ice Cover on Open Channels", Journal of the Boston Society of Civil Engineers, Vol. 56, pp 45-67.

Larsen, P.A., 1973. "Hydraulic Roughness of Ice Covers", Journal of the Hydraulics Division, ASCE, Vol. 99, No. HY1, pp 111-119.

Lau, Y.L. and B.G. Krishnappan, 1981. "Ice Cover Effects on Stream Flows and Mixing", Journal of the Hydraulics Division, ASCE, Vol. 107, No. HY10, pp 1225-1242.

Lau, Y.L., 1982. "Velocity Distributions Under Floating Covers", Canadian Journal of Civil Engineering, Vol. 9, No. 1, pp 76-83.

Majewski, W., et al, 1986. "Determination of Roughness Coefficients for Ice-Covered Rivers by means of Direct Measurements of Velocity Distribution", Proceedings of the International Symposium on Measuring Techniques in Hydraulic Research, IAHR, Delft, pp 237-252.

Majewski, W., et al, 1988. "Determination of Roughness Coefficient of the Underside of Ice Cover", IAHR Ice Symposium, Sapporo, pp 122-130.

Miller, D.S., 1990. "Internal Flow Systems", BHRA (Information Services), Cranfield, U.K., 396 p.

Nezhikhovskiy, R.A., 1964. "Coefficients of Roughness of Bottom Surface of Slush-Ice Cover", Soviet Hydrology: Selected Papers No. 2, American Geophysical Union, pp 127-150.

Patel, V.C., 1965. "Calibration of the Preston Tube and Limitations on its Use in Pressure Gradients", Journal of Fluid Mechanics, Vol. 23, Part 1, pp 185-208.

Preston, J.H., 1954. "The Determination of Turbulent Skin Friction by Means of Pitot Tubes", Journal of the Royal Aeronautical Society, Vol. 58, pp 109-121.

Shen, H.T. and P.D. Yapa, 1986. "Flow Resistance of River Ice Cover", Journal of Hydraulic Engineering, Vol. 112, No. 2, pp 142-156. x

Tang, T.C.C. and K.S. Davar, 1982. "Resistance to Flow in Partially-Covered Channels",Proceedings of the Workshop on Hydraulics of Ice Covered Rivers, June 1 and 2, Edmonton. Alberta, pp 232-252.

Tatinclaux, J.C. and M. Gogus, 1983. "Asymmetric Plane Flow with Application to Ice Jams", Journal of Hydraulic Engineering, ASCE, Vol. 109, No. 11, pp 1540-1554.

Uzuner, M.S., 1975. "The Composite Roughness of Ice Covered Streams", IAHR Journal of Hydraulic Research, Vol. 13, No. 1, pp 79-102.

Vedula, S. and R.R. Achanta, 1985. "Bed Shear From Velocity Profiles: A New Approach", Journal of Hydraulic Engineering, ASCE, Vol, 111, No. 1, pp 131-143.

Wuebben, J.L., 1986. "A Laboratory Study of Flow in an Ice-Covered Sand Bed Channel", IAHR Ice Symposium, Iowa City, Iowa, pp 3-14.

Yu, K-H., et al, 1968. "The effect of Ice on the Roughness Coefficient of the St. Clair River", Proceedings of the 11th Conference on Great Lakes Research, pp 668-680.

Additional Reading

Alam, A.M.Z., and J.F. Kennedy, 1969. "Friction Factors for Flow in Sand-Bed Channels", Journal of the Hydraulics Division, ASCE, Vol. 95, No. HY6, pp 1973-1992.

Alger, G.R. and H.S. Santeford, 1984. "A Procedure for Calculating River Flow Rate Under an Ice Cover", IAHR Ice Symposium, Hamburg, Vol. 1, pp 389-398, Vol. 3, pp 443-450.

Ashton, G.D., 1979. "River Ice", American Scientist, Vol. 67, pp 38-45.

Gavor, A. and E. Ratomski, 1988. "Roughness Coefficient in River Channels", Hydrotechnical Construction, August, pp 124-125.

Hanjalic, K. and B.E. Launder, 1972. "A Reynolds Stress Model of Turbulence and its Application to Thin Shear Flows", Vol. 52, Part 4, pp 609-638.

Santeford, H.S. and G.R. Alger, 1984. "Predicting Flow Rates in an Ice Covered Stream", Proceedings of the Cold Regions Specialty Conference, CSCE/ASCE, Edmonton, pp 1031-1043.

Shen, H.T. and R.W. Ruggles, 1982. "Analysis of Ice Cover Roughness", Proceedings of the Conference on Applying Research to Hydraulic Practice, ASCE, Jackson, MS, pp 160-168.

Starosolszky, O., 1985. "Ice and River Engineering", Developments in Hydraulic Engineering - 3, P. Novak, Ed., Chapter 5, pp 175-219.

Vanoni,V.A., 1977. "Sedimentation Engineering", ASCE, pp 84, 152.

APPENDIX A

THE PRESTON TUBE TECHNIQUE FOR BOUNDARY SHEAR MEASUREMENT

The ability to determine the turbulent skin friction on a surface such as a channel bed, pipe wall or airplane wing is very important when analyzing flows adjacent to such a surface. Before the latter half of this century, it was only possible to determine average shear stresses by measuring energy losses along pipes or channels or locally by direct force measurements on small surface elements. With any of these techniques, though, it was either tedious or impossible to determine enough local shear stresses to produce an accurate shear stress distribution [Preston,1954]. Other techniques such as heat transfer or Stanton tube methods can also prove difficult to calibrate and use [Haritonidis, 1989].

In a laboratory investigation of flow in an open or ice-covered channel, the Preston tube is ideally suited for determining the boundary shear. Often, it is already being used to gather velocity profiles at a section, so it is convenient to simply use the measured value of velocity at the wall. Also, the velocity profiles themselves may be analyzed to yield a measure of boundary shear, allowing one to check and compare values. The Preston tube is relatively easy to use and is sufficiently portable for these purposes. It is also relatively insensitive to misalignment, with a maximum error of approximately one percent, given a skew to the flow direction of no more than three percent in any direction [Haritonidis, 1989].

J. H. Preston, at Cambridge University, based his research on work done by Ludwieg and Tillman, which determined that there exists a region near the boundary where:

$$\frac{u}{u_*} = f\left(\frac{y\ u_*}{\nu}\right)$$

only. Here u* is defined as the shear velocity, the square root of the boundary shear divided by the fluid density. This region makes up approximately ten percent of the entire boundary layer thickness. It is much thicker than, and in fact includes, the viscous sublayer which lies immediately adjacent to the wall. In the viscous sublayer,

$$\frac{u}{u_*} = \frac{y\ u_*}{\nu}$$

and further out, according to Preston, the turbulent law of the wall for a flat plate applies:

$$\frac{u}{u_*} = 5.5 \log\left(\frac{y\ u_*}{\nu}\right) + 5.8$$

Later researchers have defined the first constant as 5.6 due to the use of a slightly lower value of von Karman's constant (0.41 as opposed to 0.42), and the second constant as 5.0.

Preston, seeking to relate the Pitot tube stagnation pressure at the wall to the boundary shear stress, developed the following relation through dimensional analysis:

$$\frac{\Delta P\ D_p^2}{\rho\ \nu^2} = f\left(\frac{\tau_0\ D_p^2}{\rho\ \nu^2}\right)$$

where ΔP = difference between Pitot and static pressures (i.e. Preston tube reading);

D_p = outside diameter of round Pitot tube;

ρ = density of fluid;

ν = kinematic viscosity of fluid;

τ_0 = boundary shear stress.

This relation may also be derived from the law of the wall in a turbulent boundary layer. Neglecting exact values for the constants, this is done as follows:

$$\frac{\overline{u}}{u_*} = A \log\left(\frac{y\, u_*}{\nu}\right) + B$$

$$\overline{u} = u_*\left[A \log\left(\frac{y\, u_*}{\nu}\right) + B\right]$$

Now, $\Delta P = \dfrac{\rho\, \overline{u^2}}{2}$ and $u_* = \sqrt{\dfrac{\tau_0}{\rho}}$, so:

$$\Delta P = \left(\frac{\tau_0}{2}\right)\left[A \log \frac{y}{\nu}\sqrt{\frac{\tau_0}{\rho}} + B\right]^2$$

The equation may now be nondimensionalized:

$$\frac{\Delta P\, y^2}{\rho\, \nu^2} = \frac{1}{2}\left(\frac{\tau_0\, y^2}{\rho\, \nu^2}\right)\left[A \log \sqrt{\frac{\tau_0\, y^2}{\rho\, \nu^2}} + B\right]^2$$

Given that the Pitot tube is flush against the boundary, the elevation of the streamline terminating in the tube is one-half of the Pitot tube diameter, so:

$$\frac{\Delta P\, D_p^2}{4\,\rho\,\nu^2} = \frac{1}{2}\left(\frac{\tau_0\, D_p^2}{4\,\rho\,\nu^2}\right)\left[A \log \sqrt{\frac{\tau_0\, D_p^2}{4\,\rho\,\nu^2}} + B\right]^2$$

And thus it is proven that:

$$\frac{\Delta P\, D_p^2}{4\,\rho\,\nu^2} = f\left(\frac{\tau_0\, D_p^2}{4\,\rho\,\nu^2}\right)$$

With this knowledge, an experimental investigation was undertaken to determine the exact form of the equation. This was determined to be:

$$\log\left(\frac{\tau_0\, D_p^2}{4\,\rho\,\nu^2}\right) = -1.39 + \frac{7}{8}\log\left(\frac{\Delta P\, D_p^2}{4\,\rho\,\nu^2}\right)$$

Experiments were performed using air flows through both a pipe and a wind tunnel over a range of velocities. Only aerodynamically smooth boundaries were used in the development of this equation, and it is not valid for rough turbulent flows. Four different Pitot tubes were used, and all had a ratio of internal to external diameter of approximately 0.60 [Preston, 1954]. Later experiments performed by Rechenberg proved that this ratio has no effect as long as it falls between 0.35 and 0.85 [Haritonidis, 1989].

V. C. Patel, also at Cambridge, presented a refinement of Preston's work. He showed that instead of one equation, there were actually three, valid over three distinct ranges. To aid in clarity, three new variables were introduced:

$$x^* = \log\left(\frac{\Delta P\, D_p^2}{4\,\rho\,\nu^2}\right);$$

$$y^* = \log\left(\frac{\tau_0\, D_p^2}{4\,\rho\,\nu^2}\right); \text{ and}$$

$$D^+ = \frac{u_*\, D_p}{\nu}$$

Patel's three equations, with their respective ranges, were:

a) $0 < y^* < 1.5$ and $D^+ < 11.2$:

$$y^* = 0.037 + 0.5\, x^*$$

b) $1.5 < y^* < 3.5$ and $11.2 < D^+ < 110$:

$$y^* = 0.8287 - 0.1381\, x^* + 0.1437\, x^{*2} - 0.0060\, x^{*3}$$

c) $3.5 < y^* < 5.3$ and $110 < D^+ < 1600$:

$$x^* = y^* + 2.0 \log\left(1.95\, y^* + 4.10\right)$$

Patel also investigated the use of Preston tubes in pressure gradients. It was determined that in both severe favorable and adverse pressure gradients, the law of the wall, which has been the basis for this work, is deviated from. Therefore, in both of these cases the Preston tube overestimates skin friction, with the error being more severe in the case of favorable pressure gradients [Patel, 1965].

So far, the discussion of the use of the Preston tube technique has been limited to applications involving smooth boundaries. A. B. Hollingshead and N. Rajaratnam have applied the technique to uniformly rough boundaries as well. Here the Karman-Prandtl equation for the turbulent flow velocity distribution is used as its basis:

$$\frac{u}{u_*} = 5.75 \log \frac{y}{k_s} + B$$

Values of B change over the range from smooth to fully rough turbulent flow:

a) $\frac{u_* k_s}{\nu} < 3.5, \; B = 5.75 \log \left(\frac{u_* k_s}{\nu} \right) + 5.5$;
b) $3.5 < \frac{u_* k_s}{\nu} < 7.1, \; B = 3.5 \log \left(\frac{u_* k_s}{\nu} \right) + 6.59$;
c) $7.1 < \frac{u_* k_s}{\nu} < 14.1, \; B = 9.58$;
d) $14.1 < \frac{u_* k_s}{\nu} < 70, \; B = 1.5 - 1.62 \log \left(\frac{u_* k_s}{\nu} \right)$; and
e) $70 < \frac{u_* k_s}{\nu}, \; B = 8.5$

Using the equations:

$$\Delta P = \frac{\rho u^2}{2} ; \text{ and}$$

$$\frac{u}{u_*} = 5.75 \log\left(\frac{D_p/2 + y_0}{k_s}\right) + B$$

where y_0 is the depth of virtual boundary beneath top of roughness, it is possible to solve iteratively for the unknown shear velocity. A calibration chart is included in the paper by Hollingshead and Rajaratnam to aid in this computation.

This paper also suggests that the velocity profile, if one has been measured, may be used to determine the shear velocity. This may be done using the equation:

$$u_* = \sqrt{\frac{\tau_0}{\rho}} = \frac{1}{5.75}\left(\frac{u_2 - u_1}{\log(y_2/y_1)}\right)$$

where y is measured from the virtual boundary. This is also based on the Karman-Prandtl equation.

The Preston tube technique is not without its drawbacks, however. One of the earliest noted problems with the technique is that the geometric center of the tube does not necessarily coincide with the effective center. Therefore, the streamline stagnating in the tube is also not the one at the elevation of the geometric center. Preston's original work, as well as Patel's, does compensate for this, though [Preston, 1954].

Other inaccuracies may result from low Reynolds number effects with small Preston tubes. The most worrisome, though, is due to the effect of high turbulence intensities near the boundary. As is shown below, the measured velocity (or pressure) is potentially somewhat higher than the actual:

$$\overline{\Delta P} = \frac{1}{2}\rho\,\overline{u^2} \text{ and } u = \overline{u} + u'$$

$$\overline{\Delta P} = \frac{1}{2}\rho\,\overline{(\overline{u} + u')^2}$$

$$\overline{\Delta P} = \frac{1}{2}\rho\,\overline{u}^2\left(1 + \frac{\overline{u'^2}}{\overline{u}^2}\right)$$

$$\overline{u_{meas}} = \overline{u}\left(1 + \frac{\overline{u'^2}}{\overline{u}^2}\right)$$

Note that the second last step drops higher order terms. The error in velocity measurement here varies with the turbulence intensity, but is generally in the range of 0.5 to 8% [Haritonidis, 1989].

Overall, the Preston tube technique is sufficiently accurate for most purposes. Its relative simplicity and portability make it invaluable for fluid mechanics research.

APPENDIX B

VELOCITY PROFILE DATA

AFTER AVERAGING

Data sheets containing experimental measurements are contained on the following pages. All "y" distances are measured from the top of the bed roughness. Values at the boundaries were not measured but are included to aid in computations. Only data for the averaged profiles (of the five taken) are provided. Later runs tend to contain fewer measurements as the author realized during the course of the experiments that matching distances from the bed between individual profiles would simplify their averaging.

Other calculated parameters on the data sheets include bed and cover zone zverage velocities with the dividing plane at both the location of maximum velocity and of zero shear, the locations of these planes, the bed and cover shear velocity (see section 2.2.4), the bed and energy (Appendix C) slopes, calculated discharge (section 2.2.1), Reynolds number (section 2.2) and aspect ratio (section 2.2.2). The date of measurement and the water temperature (where measured) are also supplied. In all calculations a temperature of 20°C was used as the measured value never varied more than one degree from this.

The last two data sheets included are those used in judging whether the flow was fully developed (section 3.1).

Run:	S/O/10	Bed Shear:	0.00905 m/s	Bed Zone V:	0.166
Date:	16/10/91	Cover Shear:	n/a	Cover Zone V:	n/a
Temp.:		Zero Shear y:	n/a	(divided at zero shear)	
Discharge:	10.9 L/s	Bed Slope:	0.00094	Bed Zone V:	0.166
Reynolds No.:	23000	Piezo. Slope:	0.00016	Cover Zone V:	n/a
Aspect Ratio:	23	Max Velocity y:	n/a	(divided at max velocity)	

y (cm)	u (m/s)	y (cm)	u (m/s)	y (cm)	u (m/s)
0.00	0.000				
0.15	0.106				
0.20	0.107				
0.30	0.122				
0.40	0.131				
0.50	0.139				
0.60	0.143				
0.80	0.148				
1.00	0.152				
1.20	0.156				
1.50	0.160				
1.80	0.164				
2.10	0.168				
2.40	0.171				
2.80	0.175				
3.30	0.178				
3.80	0.182				
4.30	0.186				
4.80	0.190				
5.37	0.190				

Run:	S/O/20	Bed Shear:	0.01251 m/s	Bed Zone V:	0.252
Date:	29/08/91	Cover Shear:	n/a	Cover Zone V:	n/a
Temp.:		Zero Shear y:	n/a	(divided at zero shear)	
Discharge:	20.9 L/s	Bed Slope:	0.00094	Bed Zone V:	0.252
Reynolds No.:	45000	Piezo. Slope:	0.00023	Cover Zone V:	n/a
Aspect Ratio:	18	Max Velocity y:	n/a	(divided at max velocity)	

y (cm)	u (m/s)	y (cm)	u (m/s)	y (cm)	u (m/s)
0.00	0.000				
0.15	0.162				
0.20	0.173				
0.25	0.178				
0.35	0.189				
0.45	0.197				
0.55	0.202				
0.65	0.207				
0.75	0.212				
0.85	0.217				
0.95	0.221				
1.15	0.224				
1.25	0.227				
1.45	0.234				
1.55	0.236				
1.95	0.242				
2.05	0.244				
2.45	0.249				
2.55	0.251				
2.95	0.256				
3.05	0.257				
3.45	0.262				
3.55	0.263				
4.45	0.269				
4.55	0.270				
5.45	0.276				
5.55	0.277				
6.45	0.291				
6.55	0.297				
6.70	0.303				
6.82	0.303				

Run:	S/O/40	Bed Shear:	0.01227 m/s	Bed Zone V:	0.264
Date:	29/08/91	Cover Shear:	n/a	Cover Zone V:	n/a
Temp.:		Zero Shear y:	n/a	(divided at zero shear)	
Discharge:	41.1 L/s	Bed Slope:	0.00094	Bed Zone V:	0.264
Reynolds No.:	83000	Piezo. Slope:	0.00012	Cover Zone V:	n/a
Aspect Ratio:	10	Max Velocity y:	n/a	(divided at max velocity)	

y (cm)	u (m/s)	y (cm)	u (m/s)	y (cm)	u (m/s)
0.00	0.000	10.55	0.282		
0.15	0.158	10.60	0.282		
0.20	0.170	11.55	0.285		
0.25	0.177	11.60	0.285		
0.30	0.182	12.40	0.291		
0.35	0.187	12.55	0.290		
0.40	0.191	12.60	0.309		
0.45	0.194	12.74	0.309		
0.55	0.199				
0.60	0.202				
0.75	0.209				
0.80	0.211				
0.95	0.215				
1.00	0.216				
1.25	0.224				
1.30	0.225				
1.55	0.229				
1.60	0.230				
2.05	0.240				
2.10	0.241				
2.55	0.248				
2.60	0.249				
3.05	0.255				
3.10	0.256				
3.55	0.261				
3.60	0.262				
4.55	0.269				
4.60	0.269				
5.55	0.274				
5.60	0.275				
6.55	0.280				
6.60	0.280				
7.55	0.280				
7.60	0.280				
8.55	0.282				
8.60	0.282				
9.55	0.281				
9.60	0.281				

Run:	S/O/70	Bed Shear:	0.01475 m/s	Bed Zone V:	0.337
Date:	16/10/91	Cover Shear:	n/a	Cover Zone V:	n/a
Temp.:		Zero Shear y:	n/a	(divided at zero shear)	
Discharge:	70.4 L/s	Bed Slope:	0.00094	Bed Zone V:	0.337
Reynolds No.:	138000	Piezo. Slope:	0.00013	Cover Zone V:	n/a
Aspect Ratio:	7	Max Velocity y:	n/a	(divided at max velocity)	

y (cm)	u (m/s)	y (cm)	u (m/s)	y (cm)	u (m/s)
0.00	0.000				
0.15	0.199				
0.20	0.214				
0.30	0.232				
0.40	0.239				
0.60	0.251				
0.80	0.261				
1.10	0.272				
1.40	0.281				
1.80	0.291				
2.30	0.302				
2.80	0.309				
3.30	0.316				
3.80	0.320				
4.80	0.331				
5.80	0.336				
6.80	0.341				
7.80	0.347				
8.80	0.349				
9.80	0.353				
10.80	0.355				
11.80	0.359				
12.80	0.361				
13.80	0.364				
14.80	0.367				
15.80	0.370				
16.80	0.375				
17.13	0.385				

Run:	R/O/10	Bed Shear:	0.03306 m/s	Bed Zone V:	0.225
Date:	22/08/92	Cover Shear:	n/a	Cover Zone V:	n/a
Temp.:		Zero Shear y:	n/a	(divided at zero shear)	
Discharge:	10.3 L/s	Bed Slope:	0.00303	Bed Zone V:	0.225
Reynolds No.:	34000	Piezo. Slope:	0.00298	Cover Zone V:	n/a
Aspect Ratio:	33	Max Velocity y:	n/a	(divided at max velocity)	

y (cm)	u (m/s)	y (cm)	u (m/s)	y (cm)	u (m/s)
-0.50	0.000				
0.15	0.158				
0.20	0.164				
0.25	0.170				
0.35	0.182				
0.45	0.189				
0.65	0.205				
0.85	0.216				
1.15	0.236				
1.65	0.262				
2.15	0.282				
2.65	0.296				
3.15	0.315				
3.24	0.315				

Run:	R/O/20	Bed Shear:	0.04492 m/s	Bed Zone V:	0.329
Date:	22/8/1992	Cover Shear:	n/a	Cover Zone V:	n/a
Temp.:		Zero Shear y:	n/a	(divided at zero shear)	
Discharge:	22.6 L/s	Bed Slope:	0.00303	Bed Zone V:	0.329
Reynolds No.:	74000	Piezo. Slope:	0.00365	Cover Zone V:	n/a
Aspect Ratio:	22	Max Velocity y:	n/a	(divided at max velocity)	

y (cm)	u (m/s)	y (cm)	u (m/s)	y (cm)	u (m/s)
-0.50	0.000				
0.15	0.194				
0.20	0.202				
0.25	0.211				
0.35	0.225				
0.45	0.238				
0.65	0.261				
0.85	0.278				
1.15	0.301				
1.65	0.327				
2.15	0.355				
2.65	0.375				
3.15	0.394				
3.65	0.409				
4.15	0.425				
4.65	0.433				
5.14	0.433				

Run:	R/O/40	Bed Shear:	0.06405 m/s	Bed Zone V:	0.434
Date:	23/8/1992	Cover Shear:	n/a	Cover Zone V:	n/a
Temp.:		Zero Shear y:	n/a	(divided at zero shear)	
Discharge:	40.7 L/s	Bed Slope:	0.00303	Bed Zone V:	0.434
Reynolds No.:	133000	Piezo. Slope:	0.00544	Cover Zone V:	n/a
Aspect Ratio:	16	Max Velocity y:	n/a	(divided at max velocity)	

y (cm)	u (m/s)	y (cm)	u (m/s)	y (cm)	u (m/s)
-0.50	0.000				
0.15	0.196				
0.20	0.213				
0.25	0.224				
0.35	0.245				
0.45	0.266				
0.65	0.303				
0.85	0.328				
1.15	0.357				
1.65	0.396				
2.15	0.425				
2.65	0.448				
3.15	0.467				
4.15	0.501				
5.15	0.536				
6.15	0.559				
6.65	0.569				
7.19	0.569				

Run:	R/O/70	Bed Shear:	0.07287 m/s	Bed Zone V:	0.561
Date:	23/08/92	Cover Shear:	n/a	Cover Zone V:	n/a
Temp.:		Zero Shear y:	n/a	(divided at zero shear)	
Discharge:	66.9 L/s	Bed Slope:	0.00303	Bed Zone V:	0.561
Reynolds No.:	219000	Piezo. Slope:	0.00553	Cover Zone V:	n/a
Aspect Ratio:	12	Max Velocity y:	n/a	(divided at max velocity)	

y (cm)	u (m/s)	y (cm)	u (m/s)	y (cm)	u (m/s)
-0.50	0.000				
0.15	0.244				
0.20	0.261				
0.25	0.272				
0.35	0.297				
0.45	0.318				
0.65	0.353				
0.85	0.388				
1.15	0.425				
1.65	0.467				
2.15	0.499				
2.65	0.535				
3.15	0.559				
4.15	0.601				
5.15	0.638				
6.15	0.666				
7.15	0.693				
8.15	0.722				
9.15	0.736				
9.28	0.736				

Run:	S/S/10	Bed Shear:	0.00765 m/s	Bed Zone V:	0.127
Date:	21/10/91	Cover Shear:	0.00784 m/s	Cover Zone V:	0.128
Temp.:		Zero Shear y:	3.23 cm	(divided at zero shear)	
Discharge:	9.8 L/s	Bed Slope:	0.00084	Bed Zone V:	0.127
Reynolds No.:	12000	Piezo. Slope:	0.00019	Cover Zone V:	0.128
Aspect Ratio:	19	Max Velocity y:	3.23 cm	(divided at max velocity)	

y	u	y	u	y	u
(cm)	(m/s)	(cm)	(m/s)	(cm)	(m/s)
0.00	0.000				
0.15	0.084				
0.20	0.086				
0.30	0.099				
0.40	0.107				
0.60	0.116				
0.80	0.123				
1.10	0.128				
1.40	0.132				
1.80	0.137				
2.30	0.142				
2.80	0.146				
3.23	0.146				
3.30	0.146				
3.80	0.145				
4.30	0.142				
4.80	0.136				
5.20	0.131				
5.50	0.126				
5.80	0.121				
6.00	0.114				
6.20	0.104				
6.30	0.098				
6.40	0.087				
6.55	0.000				

Run:	S/S/20	Bed Shear:	0.01294 m/s	Bed Zone V:	0.230
Date:	26/08/91	Cover Shear:	0.01239 m/s	Cover Zone V:	0.229
Temp.:		Zero Shear y:	3.83 cm	(divided at zero shear)	
Discharge:	21.0 L/s	Bed Slope:	0.00084	Bed Zone V:	0.230
Reynolds No.:	24000	Piezo. Slope:	0.00044	Cover Zone V:	0.229
Aspect Ratio:	16	Max Velocity y:	3.83 cm	(divided at max velocity)	

y (cm)	u (m/s)	y (cm)	u (m/s)	y (cm)	u (m/s)
0.00	0.000	3.50	0.263	7.15	0.186
0.15	0.169	3.60	0.263	7.20	0.182
0.20	0.170	3.65	0.263	7.25	0.177
0.25	0.176	3.83	0.263	7.30	0.172
0.30	0.182	3.95	0.263	7.35	0.160
0.35	0.186	4.00	0.263	7.50	0.000
0.40	0.189	4.10	0.262		
0.45	0.192	4.15	0.262		
0.50	0.196	4.45	0.259		
0.60	0.202	4.55	0.258		
0.65	0.204	4.60	0.258		
0.70	0.206	4.65	0.257		
0.80	0.210	4.95	0.255		
0.85	0.213	5.05	0.253		
0.90	0.215	5.10	0.253		
1.00	0.219	5.15	0.252		
1.05	0.221	5.45	0.246		
1.10	0.222	5.55	0.244		
1.20	0.225	5.60	0.243		
1.25	0.226	5.65	0.241		
1.30	0.227	5.85	0.236		
1.40	0.230	5.95	0.234		
1.45	0.232	6.00	0.233		
1.50	0.233	6.05	0.231		
1.60	0.236	6.15	0.229		
1.65	0.237	6.25	0.226		
1.80	0.240	6.30	0.225		
1.90	0.242	6.35	0.223		
1.95	0.244	6.45	0.220		
2.10	0.247	6.55	0.217		
2.20	0.248	6.60	0.215		
2.25	0.248	6.65	0.213		
2.50	0.252	6.80	0.208		
2.60	0.254	6.85	0.205		
2.65	0.254	6.95	0.200		
3.00	0.259	7.00	0.197		
3.10	0.260	7.05	0.194		
3.15	0.260	7.10	0.190		

Run:	S/S/40	Bed Shear:	0.01671 m/s	Bed Zone V:	0.332
Date:	24/08/91	Cover Shear:	0.01606 m/s	Cover Zone V:	0.323
Temp.:	21.0 °C	Zero Shear y:	5.25 cm	(divided at zero shear)	
Discharge:	41.1 L/s	Bed Slope:	0.00083	Bed Zone V:	0.331
Reynolds No.:	47000	Piezo. Slope:	0.00053	Cover Zone V:	0.324
Aspect Ratio:	12	Max Velocity y:	5.10 cm	(divided at max velocity)	

y (cm)	u (m/s)	y (cm)	u (m/s)	y (cm)	u (m/s)
0.00	0.000	2.95	0.355	8.40	0.322
0.15	0.232	3.00	0.356	8.45	0.321
0.20	0.242	3.10	0.358	8.60	0.317
0.25	0.250	3.40	0.361	8.80	0.310
0.30	0.256	3.45	0.362	8.85	0.309
0.35	0.262	3.50	0.362	9.00	0.303
0.40	0.267	3.60	0.363	9.10	0.299
0.45	0.270	3.90	0.367	9.15	0.297
0.50	0.273	3.95	0.367	9.30	0.291
0.60	0.279	4.00	0.368	9.40	0.287
0.65	0.283	4.10	0.368	9.45	0.285
0.70	0.286	4.40	0.370	9.60	0.278
0.80	0.293	4.45	0.370	9.65	0.275
0.85	0.295	4.50	0.371	9.80	0.265
0.90	0.298	4.60	0.371	9.85	0.261
1.00	0.302	4.90	0.372	9.90	0.257
1.05	0.305	4.95	0.372	9.95	0.253
1.10	0.307	5.00	0.373	10.00	0.248
1.20	0.311	5.10	0.373	10.05	0.243
1.25	0.312	5.25	0.372	10.10	0.236
1.30	0.314	5.40	0.372	10.15	0.221
1.40	0.317	5.45	0.371	10.30	0.000
1.45	0.318	5.60	0.370		
1.50	0.320	5.90	0.367		
1.60	0.322	5.95	0.367		
1.70	0.325	6.10	0.365		
1.75	0.326	6.40	0.361		
1.80	0.328	6.45	0.361		
1.90	0.331	6.60	0.359		
2.00	0.334	6.90	0.354		
2.05	0.335	6.95	0.353		
2.10	0.336	7.10	0.350		
2.20	0.339	7.40	0.345		
2.40	0.343	7.45	0.344		
2.45	0.344	7.60	0.341		
2.50	0.345	7.90	0.334		
2.60	0.348	7.95	0.333		
2.90	0.354	8.10	0.329		

Run:	S/S/70	Bed Shear:	0.01849 m/s	Bed Zone V:	0.390
Date:	14/08/91	Cover Shear:	0.01843 m/s	Cover Zone V:	0.397
Temp.:		Zero Shear y:	7.64 cm	(divided at zero shear)	
Discharge:	73.2 L/s	Bed Slope:	0.00083	Bed Zone V:	0.397
Reynolds No.:	78000	Piezo. Slope:	0.00046	Cover Zone V:	0.390
Aspect Ratio:	8	Max Velocity y:	8.90 cm	(divided at max velocity)	

y (cm)	u (m/s)	y (cm)	u (m/s)	y (cm)	u (m/s)
0.00	0.000	2.90	0.394	7.55	0.435
0.15	0.261	3.00	0.396	7.64	0.435
0.20	0.275	3.05	0.397	7.85	0.435
0.25	0.284	3.35	0.402	7.90	0.435
0.30	0.291	3.40	0.403	8.00	0.435
0.35	0.297	3.50	0.404	8.05	0.435
0.40	0.302	3.55	0.405	8.35	0.436
0.45	0.306	3.85	0.408	8.40	0.436
0.50	0.311	3.90	0.409	8.50	0.436
0.55	0.315	4.00	0.410	8.55	0.436
0.60	0.318	4.05	0.410	8.85	0.436
0.70	0.324	4.35	0.414	8.90	0.436
0.75	0.326	4.40	0.414	9.00	0.436
0.80	0.329	4.50	0.415	9.05	0.436
0.90	0.335	4.55	0.416	9.35	0.436
0.95	0.338	4.85	0.419	9.40	0.436
1.00	0.340	4.90	0.420	9.50	0.436
1.10	0.343	5.00	0.421	9.55	0.435
1.15	0.345	5.05	0.421	9.85	0.434
1.20	0.347	5.35	0.423	10.05	0.433
1.30	0.351	5.40	0.424	10.30	0.432
1.35	0.354	5.50	0.424	10.35	0.431
1.40	0.356	5.55	0.425	10.55	0.429
1.50	0.359	5.85	0.428	10.75	0.427
1.55	0.361	5.90	0.428	10.85	0.426
1.65	0.364	6.00	0.429	11.05	0.425
1.70	0.365	6.05	0.429	11.30	0.422
1.80	0.368	6.35	0.431	11.35	0.422
1.85	0.369	6.40	0.431	11.55	0.420
1.95	0.372	6.50	0.431	11.75	0.416
2.00	0.373	6.55	0.431	11.80	0.415
2.10	0.376	6.85	0.433	11.85	0.414
2.15	0.378	6.90	0.433	11.95	0.412
2.35	0.383	7.00	0.434	12.05	0.410
2.40	0.384	7.05	0.434	12.15	0.409
2.50	0.386	7.35	0.435	12.30	0.406
2.55	0.387	7.40	0.435	12.35	0.405
2.85	0.393	7.50	0.435	12.55	0.401

y (cm)	u (m/s)	y (cm)	u (m/s)	y (cm)	u (m/s)
12.75	0.396				
12.80	0.394				
12.95	0.390				
13.05	0.386				
13.25	0.382				
13.30	0.381				
13.35	0.379				
13.55	0.372				
13.65	0.369				
13.70	0.367				
13.75	0.365				
13.95	0.358				
14.00	0.355				
14.15	0.347				
14.30	0.338				
14.35	0.335				
14.50	0.328				
14.55	0.325				
14.70	0.315				
14.75	0.311				
14.80	0.306				
14.85	0.301				
14.90	0.295				
14.95	0.290				
15.00	0.282				
15.05	0.273				
15.10	0.262				
15.25	0.000				

Run:	R/R/10	Bed Shear:	0.03547 m/s	Bed Zone V:	0.164
Date:	23/09/91	Cover Shear:	0.03395 m/s	Cover Zone V:	0.164
Temp.:		Zero Shear y:	2.11 cm	(divided at zero shear)	
Discharge:	10.2 L/s	Bed Slope:	0.00284	Bed Zone V:	0.165
Reynolds No.:	12000	Piezo. Slope:	0.00482	Cover Zone V:	0.163
Aspect Ratio:	24	Max Velocity y:	2.15 cm	(divided at max velocity)	

y (cm)	u (m/s)	y (cm)	u (m/s)	y (cm)	u (m/s)
-0.50	0.000	2.15	0.235		
0.15	0.125	2.20	0.235		
0.20	0.130	2.25	0.235		
0.25	0.137	2.30	0.234		
0.30	0.144	2.45	0.231		
0.35	0.149	2.50	0.230		
0.40	0.153	2.60	0.227		
0.45	0.158	2.65	0.225		
0.50	0.163	2.70	0.223		
0.55	0.167	2.80	0.218		
0.60	0.171	2.85	0.215		
0.65	0.174	2.90	0.212		
0.70	0.177	3.00	0.207		
0.75	0.181	3.05	0.205		
0.80	0.184	3.10	0.202		
0.85	0.188	3.20	0.196		
0.90	0.191	3.25	0.193		
0.95	0.194	3.30	0.189		
1.00	0.197	3.40	0.183		
1.05	0.199	3.45	0.179		
1.10	0.202	3.50	0.176		
1.15	0.204	3.60	0.168		
1.20	0.207	3.65	0.163		
1.25	0.210	3.70	0.158		
1.30	0.213	3.75	0.153		
1.35	0.216	3.80	0.148		
1.40	0.218	3.85	0.143		
1.45	0.220	3.90	0.136		
1.50	0.222	3.95	0.132		
1.55	0.225	4.60	0.000		
1.60	0.226				
1.70	0.230				
1.75	0.231				
1.80	0.232				
1.85	0.233				
1.90	0.234				
2.10	0.235				
2.11	0.235				

Run:	R/R/20	Bed Shear:	0.04352 m/s	Bed Zone V:	0.216
Date:	14/09/91	Cover Shear:	0.03920 m/s	Cover Zone V:	0.214
Temp.:		Zero Shear y:	3.60 cm	(divided at zero shear)	
Discharge:	20.5 L/s	Bed Slope:	0.00284	Bed Zone V:	0.215
Reynolds No.:	24000	Piezo. Slope:	0.00448	Cover Zone V:	0.215
Aspect Ratio:	16	Max Velocity y:	3.55 cm	(divided at max velocity)	

y (cm)	u (m/s)	y (cm)	u (m/s)	y (cm)	u (m/s)
-0.50	0.000				
0.15	0.120				
0.20	0.125				
0.25	0.132				
0.35	0.143				
0.45	0.159				
0.55	0.169				
0.75	0.188				
0.95	0.205				
1.15	0.217				
1.35	0.234				
1.55	0.244				
1.85	0.258				
2.15	0.272				
2.55	0.287				
3.05	0.300				
3.55	0.305				
3.60	0.301				
4.05	0.297				
4.55	0.284				
4.95	0.266				
5.25	0.251				
5.55	0.234				
5.75	0.221				
5.95	0.208				
6.15	0.190				
6.35	0.170				
6.45	0.153				
6.55	0.144				
6.65	0.129				
7.30	0.000				

Run:	R/R/40	Bed Shear:	0.05164 m/s	Bed Zone V:	0.326
Date:	19/09/91	Cover Shear:	0.05225 m/s	Cover Zone V:	0.331
Temp.:	19.5 °C	Zero Shear y:	4.62 cm	(divided at zero shear)	
Discharge:	40.5 L/s	Bed Slope:	0.00284	Bed Zone V:	0.326
Reynolds No.:	47000	Piezo. Slope:	0.00534	Cover Zone V:	0.331
Aspect Ratio:	12	Max Velocity y:	4.62 cm	(divided at max velocity)	

y (cm)	u (m/s)	y (cm)	u (m/s)	y (cm)	u (m/s)
-0.50	0.000	2.95	0.403	7.80	0.336
0.15	0.183	3.00	0.405	7.85	0.332
0.20	0.193	3.10	0.409	7.90	0.328
0.25	0.200	3.15	0.411	8.00	0.320
0.30	0.209	3.45	0.420	8.05	0.317
0.35	0.219	3.50	0.421	8.10	0.314
0.40	0.228	3.60	0.423	8.20	0.307
0.45	0.234	3.65	0.424	8.25	0.303
0.50	0.240	4.45	0.437	8.30	0.298
0.60	0.253	4.50	0.437	8.40	0.287
0.65	0.258	4.60	0.438	8.45	0.282
0.70	0.263	4.62	0.438	8.50	0.278
0.80	0.273	4.65	0.438	8.60	0.270
0.85	0.278	5.45	0.431	8.65	0.266
0.90	0.283	5.50	0.431	8.70	0.261
1.00	0.293	5.60	0.428	8.80	0.246
1.05	0.297	5.65	0.427	8.85	0.238
1.10	0.300	5.70	0.426	8.90	0.231
1.20	0.307	6.00	0.417	9.00	0.217
1.25	0.310	6.10	0.414	9.05	0.206
1.30	0.314	6.15	0.413	9.10	0.194
1.40	0.321	6.20	0.411	9.15	0.190
1.45	0.324	6.50	0.399	9.80	0.000
1.50	0.327	6.60	0.394		
1.60	0.334	6.65	0.392		
1.65	0.337	6.70	0.390		
1.75	0.343	6.90	0.382		
1.80	0.346	7.00	0.377		
1.90	0.352	7.05	0.375		
1.95	0.355	7.15	0.370		
2.05	0.361	7.20	0.368		
2.10	0.363	7.30	0.364		
2.20	0.369	7.35	0.362		
2.25	0.371	7.45	0.358		
2.45	0.382	7.50	0.355		
2.50	0.384	7.60	0.349		
2.60	0.389	7.65	0.346		
2.65	0.391	7.70	0.342		

Run:	R/R/70	Bed Shear:	0.05454 m/s	Bed Zone V:	0.412
Date:	18/09/91	Cover Shear:	0.05177 m/s	Cover Zone V:	0.407
Temp.:	19.5 °C	Zero Shear y:	6.86 cm	(divided at zero shear)	
Discharge:	71.7 L/s	Bed Slope:	0.00284	Bed Zone V:	0.413
Reynolds No.:	80000	Piezo. Slope:	0.00402	Cover Zone V:	0.406
Aspect Ratio:	9	Max Velocity y:	6.95 cm	(divided at max velocity)	

y (cm)	u (m/s)	y (cm)	u (m/s)	y (cm)	u (m/s)
-0.50	0.000	2.95	0.449	10.00	0.460
0.15	0.214	3.05	0.453	10.05	0.459
0.20	0.226	3.15	0.457	10.40	0.445
0.25	0.235	3.35	0.463	10.50	0.441
0.30	0.244	3.40	0.465	10.55	0.439
0.35	0.252	3.45	0.467	10.90	0.424
0.40	0.259	3.55	0.470	11.00	0.420
0.45	0.267	3.65	0.473	11.05	0.418
0.50	0.276	3.85	0.480	11.30	0.408
0.55	0.284	3.90	0.482	11.40	0.402
0.65	0.296	3.95	0.484	11.45	0.400
0.70	0.301	4.05	0.487	11.60	0.390
0.75	0.306	4.15	0.489	11.70	0.384
0.85	0.314	4.85	0.506	11.75	0.380
0.90	0.319	4.90	0.507	11.90	0.370
0.95	0.323	4.95	0.508	12.00	0.363
1.05	0.333	5.05	0.510	12.05	0.359
1.15	0.343	5.15	0.511	12.10	0.356
1.20	0.347	5.85	0.520	12.20	0.349
1.25	0.351	5.90	0.521	12.25	0.345
1.35	0.359	5.95	0.521	12.30	0.341
1.45	0.367	6.05	0.522	12.40	0.332
1.50	0.371	6.15	0.522	12.45	0.326
1.55	0.374	6.86	0.523	12.50	0.321
1.65	0.379	6.90	0.523	12.60	0.311
1.75	0.385	6.95	0.523	12.65	0.307
1.85	0.390	7.00	0.523	12.70	0.302
1.90	0.393	7.05	0.523	12.80	0.289
1.95	0.396	7.90	0.515	12.85	0.284
2.05	0.402	8.00	0.513	12.90	0.278
2.15	0.408	8.05	0.512	13.00	0.267
2.35	0.419	8.90	0.492	13.05	0.258
2.40	0.421	9.00	0.489	13.10	0.248
2.45	0.424	9.05	0.488	13.15	0.239
2.55	0.429	9.40	0.478	13.20	0.229
2.65	0.434	9.50	0.475	13.85	0.000
2.85	0.445	9.55	0.474		
2.90	0.447	9.90	0.464		

Run:	S/R/10	Bed Shear:	0.00759 m/s	Bed Zone V:	0.123
Date:	17/10/91	Cover Shear:	0.01878 m/s	Cover Zone V:	0.107
Temp.:		Zero Shear y:	1.97 cm	(divided at zero shear)	
Discharge:	9.3 L/s	Bed Slope:	0.00083	Bed Zone V:	0.123
Reynolds No.:	12000	Piezo. Slope:	0.00061	Cover Zone V:	0.107
Aspect Ratio:	18	Max Velocity y:	1.97 cm	(divided at max velocity)	

y (cm)	u (m/s)	y (cm)	u (m/s)	y (cm)	u (m/s)
0.00	0.000	5.90	0.073		
0.15	0.083	5.95	0.070		
0.20	0.086	6.00	0.066		
0.30	0.101	6.05	0.064		
0.40	0.111	6.10	0.061		
0.60	0.123	6.15	0.057		
0.80	0.130	6.80	0.000		
1.10	0.136				
1.40	0.142				
1.80	0.145				
1.97	0.145				
2.30	0.145				
2.75	0.143				
2.80	0.143				
2.85	0.142				
3.25	0.138				
3.30	0.138				
3.35	0.137				
3.75	0.132				
3.80	0.131				
3.85	0.130				
4.25	0.122				
4.30	0.121				
4.35	0.120				
4.75	0.112				
4.80	0.111				
4.85	0.109				
5.15	0.101				
5.20	0.099				
5.25	0.098				
5.45	0.092				
5.50	0.090				
5.55	0.088				
5.65	0.083				
5.70	0.081				
5.75	0.080				
5.80	0.078				
5.85	0.075				

Run:	S/R/20	Bed Shear:	0.01184 m/s	Bed Zone V:	0.195
Date:	27/08/91	Cover Shear:	0.02277 m/s	Cover Zone V:	0.181
Temp.:		Zero Shear y:	3.13 cm	(divided at zero shear)	
Discharge:	20.7 L/s	Bed Slope:	0.00083	Bed Zone V:	0.214
Reynolds No.:	23000	Piezo. Slope:	0.00073	Cover Zone V:	0.172
Aspect Ratio:	13	Max Velocity y:	3.00 cm	(divided at max velocity)	

y (cm)	u (m/s)	y (cm)	u (m/s)	y (cm)	u (m/s)
0.00	0.000	3.60	0.228	7.20	0.168
0.15	0.151	3.65	0.228	7.30	0.165
0.20	0.157	3.90	0.226	7.35	0.163
0.25	0.164	3.95	0.225	7.40	0.161
0.30	0.172	4.00	0.225	7.45	0.160
0.35	0.176	4.10	0.224	7.50	0.159
0.40	0.180	4.15	0.223	7.60	0.156
0.45	0.182	4.40	0.219	7.65	0.154
0.50	0.184	4.45	0.218	7.70	0.153
0.55	0.187	4.50	0.217	7.80	0.149
0.65	0.192	4.60	0.216	7.85	0.147
0.70	0.194	4.65	0.216	7.90	0.145
0.85	0.199	4.90	0.213	8.00	0.139
0.90	0.200	5.00	0.212	8.05	0.137
1.05	0.205	5.10	0.210	8.10	0.134
1.10	0.206	5.15	0.210	8.15	0.131
1.25	0.210	5.40	0.207	8.20	0.127
1.30	0.212	5.45	0.206	8.25	0.125
1.45	0.215	5.50	0.205	8.30	0.122
1.50	0.216	5.60	0.204	8.35	0.117
1.65	0.218	5.65	0.203	8.40	0.112
1.75	0.220	5.90	0.197	8.45	0.109
1.80	0.221	5.95	0.196	8.50	0.105
1.95	0.223	6.00	0.194	9.15	0.000
2.05	0.224	6.10	0.192		
2.10	0.225	6.15	0.192		
2.25	0.226	6.40	0.188		
2.45	0.228	6.45	0.187		
2.50	0.229	6.50	0.186		
2.65	0.230	6.60	0.184		
2.95	0.231	6.65	0.183		
3.00	0.231	6.80	0.179		
3.10	0.230	6.85	0.178		
3.13	0.230	6.90	0.176		
3.15	0.230	7.00	0.174		
3.40	0.229	7.05	0.172		
3.45	0.229	7.10	0.171		
3.50	0.229	7.15	0.169		

Run:	S/R/40	Bed Shear:	0.01360 m/s	Bed Zone V:	0.256
Date:	09/08/91	Cover Shear:	0.03213 m/s	Cover Zone V:	0.218
Temp.:	21 °C	Zero Shear y:	4.09 cm	(divided at zero shear)	
Discharge:	38.5 L/s	Bed Slope:	0.00083	Bed Zone V:	0.258
Reynolds No.:	45000	Piezo. Slope:	0.00090	Cover Zone V:	0.216
Aspect Ratio:	9	Max Velocity y:	4.40 cm	(divided at max velocity)	

y (cm)	u (m/s)	y (cm)	u (m/s)	y (cm)	u (m/s)
0.00	0.000	3.30	0.284	8.90	0.243
0.15	0.180	3.40	0.285	9.10	0.239
0.20	0.187	3.60	0.287	9.40	0.234
0.25	0.195	3.75	0.288	9.60	0.231
0.30	0.201	3.80	0.288	9.70	0.229
0.35	0.207	3.90	0.288	9.90	0.226
0.40	0.211	4.09	0.288	10.10	0.221
0.45	0.216	4.10	0.288	10.20	0.220
0.50	0.220	4.25	0.289	10.40	0.215
0.60	0.225	4.30	0.289	10.50	0.213
0.65	0.227	4.40	0.289	10.60	0.211
0.70	0.230	4.60	0.289	10.80	0.205
0.80	0.234	4.75	0.288	10.90	0.202
0.85	0.236	4.90	0.288	11.00	0.199
0.90	0.238	5.10	0.287	11.10	0.196
1.00	0.242	5.25	0.287	11.20	0.194
1.05	0.244	5.30	0.287	11.30	0.193
1.10	0.246	5.40	0.286	11.40	0.190
1.20	0.249	5.60	0.285	11.50	0.187
1.25	0.250	5.75	0.284	11.60	0.183
1.30	0.252	5.90	0.283	11.70	0.178
1.40	0.255	6.10	0.281	11.80	0.173
1.55	0.259	6.20	0.280	11.90	0.169
1.60	0.261	6.40	0.279	12.00	0.166
1.70	0.263	6.60	0.276	12.10	0.162
1.85	0.266	6.70	0.275	12.20	0.155
1.90	0.267	6.90	0.274	12.30	0.148
2.00	0.269	7.10	0.272	12.40	0.142
2.20	0.272	7.20	0.271	12.50	0.137
2.25	0.273	7.40	0.267	12.60	0.130
2.30	0.274	7.60	0.263	12.70	0.122
2.40	0.275	7.70	0.262	12.80	0.113
2.60	0.278	7.90	0.260	12.90	0.104
2.75	0.280	8.10	0.258	12.95	0.100
2.80	0.280	8.20	0.256	13.00	0.096
2.90	0.281	8.40	0.253	13.05	0.092
3.10	0.283	8.60	0.250	13.10	0.088
3.25	0.284	8.70	0.248	13.75	0.000

Run:	S/R/70	Bed Shear:	0.01855 m/s	Bed Zone V:	0.371
Date:	23/07/91	Cover Shear:	0.04409 m/s	Cover Zone V:	0.344
Temp.:	21 °C	Zero Shear y:	4.92 cm	(divided at zero shear)	
Discharge:	71.2 L/s	Bed Slope:	0.00083	Bed Zone V:	0.381
Reynolds No.:	78000	Piezo. Slope:	0.00141	Cover Zone V:	0.334
Aspect Ratio:	7	Max Velocity y:	6.15 cm	(divided at max velocity)	

y (cm)	u (m/s)	y (cm)	u (m/s)	y (cm)	u (m/s)
0.00	0.000	3.70	0.410	13.50	0.312
0.15	0.263	4.05	0.414	13.55	0.310
0.20	0.271	4.15	0.415	13.60	0.309
0.25	0.278	4.20	0.415	13.80	0.302
0.30	0.286	4.92	0.418	13.85	0.300
0.35	0.293	5.05	0.420	13.90	0.298
0.40	0.300	5.15	0.421	14.00	0.294
0.45	0.305	5.20	0.421	14.15	0.287
0.55	0.313	6.05	0.423	14.20	0.285
0.60	0.318	6.15	0.423	14.35	0.281
0.65	0.321	6.20	0.423	14.40	0.279
0.75	0.328	7.10	0.420	14.55	0.267
0.80	0.331	7.20	0.420	14.60	0.264
0.85	0.335	7.60	0.417	14.75	0.251
0.95	0.340	8.10	0.414	14.80	0.247
1.00	0.342	8.20	0.414	14.95	0.241
1.05	0.345	8.60	0.408	15.00	0.239
1.15	0.350	9.10	0.402	15.15	0.224
1.20	0.353	9.20	0.401	15.20	0.220
1.35	0.359	9.60	0.395	15.25	0.217
1.45	0.362	10.10	0.386	15.35	0.208
1.50	0.364	10.20	0.385	15.40	0.203
1.65	0.368	10.60	0.379	15.50	0.191
1.75	0.372	11.10	0.372	15.55	0.187
1.80	0.373	11.15	0.371	15.60	0.182
2.05	0.380	11.20	0.370	15.65	0.176
2.15	0.382	11.60	0.360	15.70	0.170
2.20	0.383	11.65	0.359	15.75	0.156
2.35	0.386	11.70	0.358	15.80	0.150
2.55	0.390	12.10	0.349	15.85	0.144
2.65	0.392	12.15	0.348	16.50	0.000
2.70	0.393	12.20	0.346		
2.76	0.394	12.60	0.338		
3.05	0.398	12.65	0.337		
3.15	0.400	12.70	0.336		
3.20	0.401	13.10	0.324		
3.55	0.407	13.15	0.323		
3.65	0.409	13.20	0.321		

Run:	R/S/10	Bed Shear:	0.04168 m/s	Bed Zone V:	0.184
Date:	24/09/91	Cover Shear:	0.01463 m/s	Cover Zone V:	0.224
Temp.:	19.3 °C	Zero Shear y:	2.46 cm	(divided at zero shear)	
Discharge:	9.5 L/s	Bed Slope:	0.00284	Bed Zone V:	0.179
Reynolds No.:	12000	Piezo. Slope:	0.00498	Cover Zone V:	0.229
Aspect Ratio:	31	Max Velocity y:	2.30 cm	(divided at max velocity)	

y (cm)	u (m/s)	y (cm)	u (m/s)	y (cm)	u (m/s)
-0.50	0.000				
0.15	0.121				
0.20	0.130				
0.30	0.143				
0.40	0.156				
0.60	0.176				
0.80	0.193				
1.00	0.211				
1.20	0.223				
1.40	0.234				
1.70	0.248				
2.00	0.260				
2.30	0.265				
2.46	0.264				
2.60	0.264				
2.90	0.252				
3.10	0.236				
3.20	0.225				
3.30	0.208				
3.35	0.197				
3.50	0.000				

Run:	R/S/20	Bed Shear:	0.04234 m/s	Bed Zone V:	0.276
Date:	25/09/91	Cover Shear:	0.01932 m/s	Cover Zone V:	0.336
Temp.:	19.3 °C	Zero Shear y:	3.45 cm	(divided at zero shear)	
Discharge:	21.1 L/s	Bed Slope:	0.00284	Bed Zone V:	0.276
Reynolds No.:	24000	Piezo. Slope:	0.00384	Cover Zone V:	0.336
Aspect Ratio:	21	Max Velocity y:	3.45 cm	(divided at max velocity)	

y (cm)	u (m/s)	y (cm)	u (m/s)	y (cm)	u (m/s)
-0.50	0.000				
0.15	0.185				
0.20	0.193				
0.25	0.199				
0.35	0.210				
0.45	0.220				
0.65	0.243				
0.85	0.263				
1.05	0.277				
1.25	0.293				
1.45	0.303				
1.75	0.321				
2.05	0.337				
2.35	0.351				
2.65	0.363				
2.95	0.372				
3.25	0.380				
3.45	0.380				
3.55	0.380				
3.85	0.379				
4.05	0.374				
4.25	0.366				
4.45	0.355				
4.65	0.341				
4.85	0.319				
4.95	0.302				
5.05	0.288				
5.10	0.276				
5.25	0.000				

Run:	R/S/40	Bed Shear:	0.05279 m/s	Bed Zone V:	0.376
Date:	27/09/91	Cover Shear:	0.02295 m/s	Cover Zone V:	0.432
Temp.:	19.8 °C	Zero Shear y:	5.42 cm	(divided at zero shear)	
Discharge:	38.2 L/s	Bed Slope:	0.00284	Bed Zone V:	0.376
Reynolds No.:	47000	Piezo. Slope:	0.00397	Cover Zone V:	0.432
Aspect Ratio:	14	Max Velocity y:	5.42 cm	(divided at max velocity)	

y (cm)	u (m/s)	y (cm)	u (m/s)	y (cm)	u (m/s)
-0.50	0.000				
0.15	0.214				
0.20	0.223				
0.30	0.235				
0.40	0.254				
0.50	0.269				
0.70	0.290				
0.90	0.312				
1.20	0.341				
1.50	0.360				
1.90	0.384				
2.30	0.408				
2.70	0.426				
3.10	0.442				
3.50	0.457				
4.00	0.474				
4.50	0.486				
5.00	0.493				
5.42	0.493				
5.50	0.493				
5.90	0.488				
6.30	0.477				
6.70	0.457				
7.00	0.440				
7.30	0.416				
7.50	0.396				
7.55	0.389				
7.70	0.364				
7.75	0.355				
7.80	0.347				
7.85	0.338				
8.00	0.000				

Run:	R/S/70	Bed Shear:	0.06771 m/s	Bed Zone V:	0.485
Date:	26/09/91	Cover Shear:	0.02604 m/s	Cover Zone V:	0.524
Temp.:	19.6 °C	Zero Shear y:	8.06 cm	(divided at zero shear)	
Discharge:	71.7 L/s	Bed Slope:	0.00284	Bed Zone V:	0.474
Reynolds No.:	80000	Piezo. Slope:	0.00453	Cover Zone V:	0.539
Aspect Ratio:	10	Max Velocity y:	7.30 cm	(divided at max velocity)	

y	u	y	u	y	u
(cm)	(m/s)	(cm)	(m/s)	(cm)	(m/s)
-0.50	0.000	11.20	0.391		
0.15	0.218	11.35	0.000		
0.20	0.231				
0.25	0.260				
0.30	0.269				
0.40	0.290				
0.50	0.308				
0.70	0.335				
0.90	0.357				
1.20	0.388				
1.50	0.418				
1.90	0.447				
2.30	0.475				
2.70	0.491				
3.10	0.514				
3.50	0.534				
4.00	0.553				
4.50	0.560				
5.00	0.575				
5.50	0.589				
6.00	0.597				
6.50	0.601				
6.90	0.604				
7.30	0.606				
7.70	0.604				
8.06	0.601				
8.10	0.598				
8.50	0.593				
8.80	0.585				
9.10	0.575				
9.40	0.565				
9.70	0.552				
10.00	0.539				
10.30	0.519				
10.50	0.501				
10.70	0.479				
10.90	0.451				
11.10	0.420				

Run:	S/R/70	RUN DONE AT TEST SECTION			
Date:	23/07/91	ON 5 cm LATERAL SPACING			
Temp.:	21 °C				
Discharge:					
Reynolds No.:					
Aspect Ratio:					

y	u	y	u	y	u
(cm)	(m/s)	(cm)	(m/s)	(cm)	(m/s)
0.00	0.000	2.20	0.392	6.30	0.430
0.15	0.271	2.25	0.393	6.35	0.430
0.20	0.278	2.30	0.394	7.05	0.428
0.25	0.287	2.35	0.395	7.15	0.428
0.30	0.295	2.55	0.399	7.20	0.428
0.35	0.302	2.65	0.401	7.25	0.428
0.40	0.308	2.70	0.402	7.30	0.427
0.45	0.313	2.75	0.402	7.35	0.427
0.50	0.317	2.80	0.403	7.65	0.425
0.55	0.321	2.85	0.404	8.05	0.422
0.60	0.325	3.05	0.407	8.15	0.421
0.65	0.329	3.15	0.408	8.20	0.421
0.70	0.332	3.20	0.409	8.25	0.420
0.75	0.336	3.25	0.410	8.30	0.420
0.80	0.339	3.30	0.411	8.35	0.419
0.85	0.342	3.35	0.412	8.65	0.416
0.90	0.345	3.55	0.414	9.05	0.411
0.95	0.348	3.65	0.416	9.15	0.410
1.00	0.351	3.70	0.416	9.20	0.410
1.05	0.353	3.75	0.417	9.25	0.409
1.10	0.355	3.80	0.417	9.30	0.408
1.15	0.357	3.85	0.418	9.35	0.408
1.20	0.359	4.05	0.420	9.65	0.403
1.25	0.361	4.15	0.421	10.05	0.396
1.30	0.363	4.20	0.421	10.15	0.395
1.35	0.365	4.25	0.422	10.20	0.394
1.45	0.369	4.30	0.422	10.25	0.393
1.50	0.371	4.35	0.422	10.30	0.392
1.55	0.373	5.05	0.427	10.35	0.391
1.60	0.374	5.15	0.427	10.65	0.386
1.65	0.376	5.20	0.427	11.05	0.380
1.75	0.380	5.25	0.428	11.15	0.378
1.80	0.382	5.30	0.428	11.20	0.377
1.85	0.383	5.35	0.428	11.25	0.376
1.90	0.385	6.05	0.430	11.30	0.375
1.95	0.386	6.15	0.430	11.35	0.374
2.05	0.388	6.20	0.430	11.55	0.369
2.15	0.391	6.25	0.430	11.65	0.367

y (cm)	u (m/s)	y (cm)	u (m/s)	y (cm)	u (m/s)
11.70	0.366	14.40	0.279		
11.75	0.365	14.45	0.276		
11.80	0.363	14.50	0.273		
11.85	0.362	14.55	0.269		
12.05	0.357	14.60	0.266		
12.15	0.355	14.65	0.262		
12.20	0.354	14.70	0.259		
12.25	0.352	14.75	0.255		
12.30	0.351	14.80	0.251		
12.35	0.350	14.85	0.248		
12.55	0.344	14.90	0.245		
12.65	0.341	14.95	0.242		
12.70	0.340	15.00	0.239		
12.75	0.338	15.05	0.235		
12.80	0.337	15.10	0.230		
12.85	0.335	15.15	0.225		
13.05	0.329	15.20	0.220		
13.15	0.326	15.25	0.215		
13.20	0.325	15.30	0.210		
13.25	0.323	15.35	0.205		
13.30	0.322	15.40	0.200		
13.35	0.320	15.45	0.195		
13.45	0.317	15.50	0.190		
13.55	0.314	15.55	0.184		
13.60	0.313	15.60	0.179		
13.65	0.311	15.65	0.173		
13.70	0.309	15.70	0.164		
13.75	0.307	15.75	0.156		
13.85	0.303	15.80	0.147		
13.90	0.300	15.85	0.142		
13.95	0.298	15.90	0.133		
14.00	0.295	15.95	0.155		
14.05	0.293	16.60	0.000		
14.15	0.289				
14.20	0.287				
14.25	0.286				
14.30	0.284				
14.35	0.281				

Run:	S/R/70	RUN DONE 1.0 m UPSTREAM			
Date:	30/07/91	OF TEST SECTION ON 5 cm			
Temp.:	21 °C	LATERAL SPACING			
Discharge:					
Reynolds No.:					
Aspect Ratio:					

y (cm)	u (m/s)	y (cm)	u (m/s)	y (cm)	u (m/s)
0.00	0.000	2.55	0.394	8.30	0.424
0.15	0.264	2.65	0.396	8.35	0.424
0.20	0.267	2.70	0.397	9.05	0.418
0.25	0.277	2.80	0.399	9.15	0.417
0.30	0.285	2.85	0.400	9.20	0.417
0.35	0.292	3.05	0.403	9.30	0.416
0.40	0.298	3.15	0.404	9.35	0.415
0.45	0.304	3.20	0.405	10.05	0.406
0.50	0.310	3.30	0.406	10.15	0.405
0.55	0.315	3.35	0.407	10.20	0.404
0.60	0.319	3.55	0.410	10.30	0.402
0.65	0.322	3.65	0.411	10.35	0.402
0.70	0.326	3.70	0.412	11.05	0.390
0.75	0.330	3.80	0.413	11.15	0.388
0.80	0.333	3.85	0.413	11.20	0.387
0.85	0.336	4.05	0.415	11.30	0.385
0.90	0.339	4.15	0.416	11.35	0.384
0.95	0.342	4.20	0.416	11.55	0.380
1.00	0.345	4.30	0.417	11.65	0.378
1.05	0.347	4.35	0.417	11.70	0.377
1.10	0.350	5.05	0.422	11.80	0.374
1.15	0.352	5.15	0.422	11.85	0.373
1.20	0.355	5.20	0.422	12.05	0.369
1.30	0.359	5.30	0.423	12.15	0.366
1.35	0.360	5.35	0.423	12.20	0.365
1.45	0.364	6.05	0.426	12.30	0.362
1.50	0.366	6.15	0.426	12.35	0.361
1.60	0.370	6.20	0.426	12.55	0.355
1.65	0.371	6.30	0.427	12.65	0.352
1.75	0.375	6.35	0.427	12.70	0.351
1.80	0.376	7.05	0.428	12.80	0.347
1.90	0.379	7.15	0.428	12.85	0.346
1.95	0.380	7.20	0.428	13.05	0.339
2.05	0.383	7.30	0.428	13.15	0.336
2.15	0.385	7.35	0.428	13.20	0.334
2.20	0.387	8.05	0.425	13.30	0.330
2.30	0.389	8.15	0.425	13.35	0.329
2.35	0.390	8.20	0.425	13.45	0.324

y (cm)	u (m/s)	y (cm)	u (m/s)	y (cm)	u (m/s)
13.55	0.320	15.65	0.167		
13.60	0.318	15.70	0.160		
13.70	0.314	15.75	0.153		
13.75	0.313	15.80	0.151		
13.85	0.309	15.85	0.146		
13.90	0.307	15.90	0.141		
14.00	0.302	15.95	0.134		
14.05	0.299	16.00	0.135		
14.15	0.294				
14.20	0.291				
14.25	0.289				
14.30	0.286				
14.35	0.284				
14.40	0.282				
14.45	0.280				
14.50	0.277				
14.55	0.275				
14.60	0.271				
14.65	0.268				
14.70	0.264				
14.75	0.261				
14.80	0.258				
14.85	0.255				
14.90	0.251				
14.95	0.246				
15.00	0.242				
15.05	0.237				
15.10	0.233				
15.15	0.228				
15.20	0.223				
15.25	0.217				
15.30	0.212				
15.35	0.206				
15.40	0.201				
15.45	0.195				
15.50	0.189				
15.55	0.181				
15.60	0.174				

APPENDIX C

DETERMINATION OF

BED AND ENERGY SLOPES

Detailed surveys were performed to measure bed, water surface and roughness elevations while performing the experiments. In examining the bed elevation data, it was found that the supposedly planar flume bottom not only displayed vertical imperfections but tilted slightly to the right as noted in section 3.2. Therefore, in determining the average bed profile, measurements were taken at five points laterally across each section. These points coincided with the spacing for velocity profile measurements, that is, on the centreline of the flume and both 15 and 30 cm to the left and right of it. In calculating the bed slope, a reach averaged value based on the average profile was used.

In that an attempt was made to achieve a uniform flow by visually matching bed and water surface slopes, it was hoped that these values would match and survey data would verify their closeness. However, the shallowness of the slopes used as well as the fact that the flow was developing along the cover reduced any confidence this procedure may have inspired. An alternate technique for determining the energy slope based on boundary shear measurements was thus introduced as a more accurate method for determining its value at a section. Here:

$$\frac{d\tau}{dy} = -\gamma S_f$$

describes the shear stress profile across the depth of the flow [Gerard, 1989]. Therefore, a knowledge of the boundary shears can easily provide a value for the energy slope. Bed slopes and energy slopes determined by the methods described are provided in Table C.1.

Run	Bed slope (m/m)	Energy slope Surveyed	Calculated
S/O/10	0.00094	0.00013	0.00016
S/O/20	0.00094	0.00028	0.00023
S/O/40	0.00094	0.00028	0.00012
S/O/70	0.00094	0.00028	0.00013
S/S/10	0.00094	0.00016	0.00019
S/S/20	0.00094	0.00052	0.00044
S/S/40	0.00094	0.00061	0.00053
S/S/70	0.00094	0.00053	0.00046
S/R/10	0.00094	0.00041	0.00061
S/R/20	0.00094	0.00071	0.00073
S/R/40	0.00094	0.00069	0.00090
S/R/70	0.00094	0.00069	0.00141
R/O/10	0.00303	-	0.00298
R/O/20	0.00303	-	0.00365
R/O/40	0.00303	-	0.00544
R/O/70	0.00303	-	0.00553
R/S/10	0.00303	0.00275	0.00498
R/S/20	0.00303	0.00269	0.00384
R/S/40	0.00303	0.00246	0.00397
R/S/70	0.00303	0.00239	0.00453
R/R/10	0.00303	0.00272	0.00482
R/R/20	0.00303	0.00215	0.00448
R/R/40	0.00303	0.00235	0.00534
R/R/70	0.00303	0.00242	0.00402

Table C.1 - Bed and energy slopes